DERIVATION AND APPLICATION OF CONE FACTORS IN DANISH SOILS

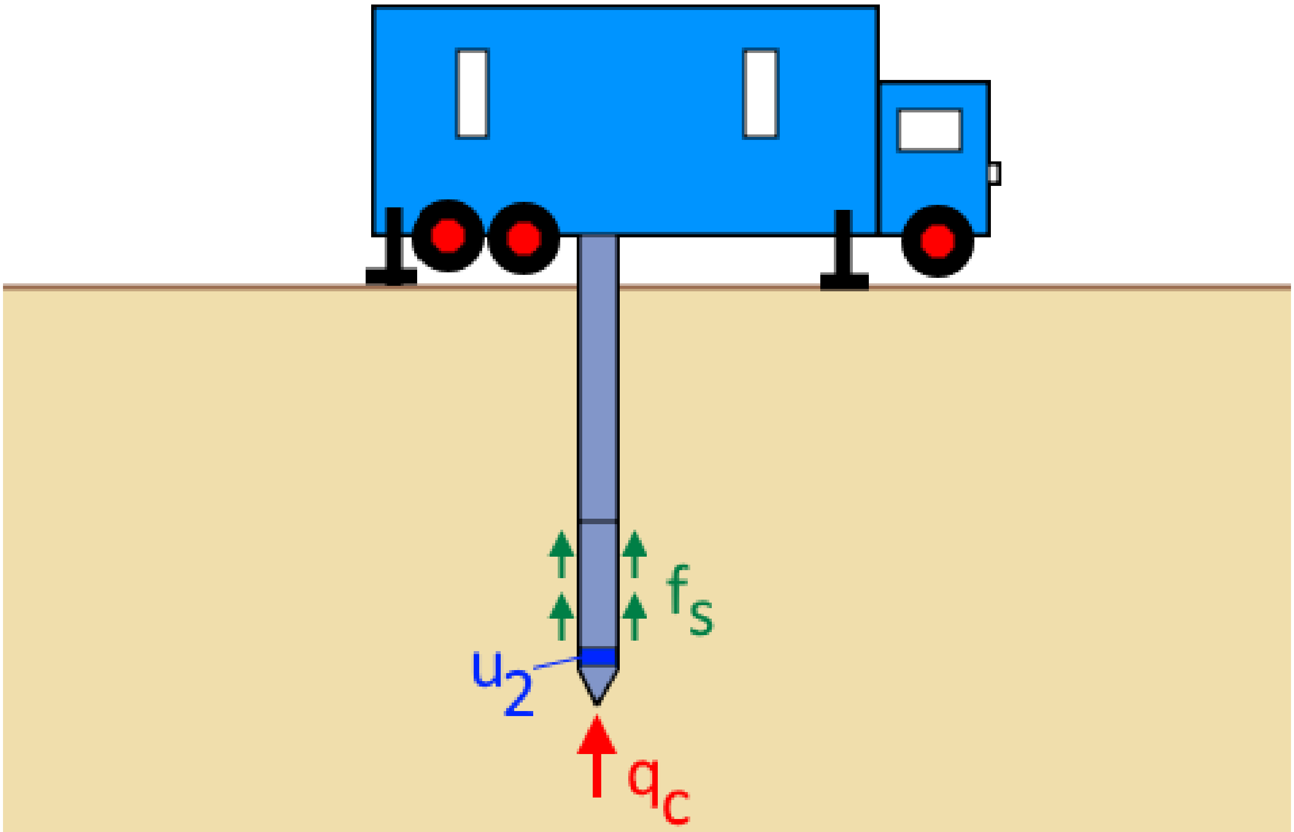

Master thesis by Jakob Lund Nadj
Aalborg University
Structural and Civil Engineering
7th June 2019

The Faculty of Engineering and Science

Structural and Civil Engineering
Thomas Manns Vej 23
9220 Aalborg Øst
https://www.byggeri.aau.dk

AALBORG UNIVERSITY
STUDENT REPORT

Title:
Derivation and application of cone factors in Danish soils

Project period:
February 2019 – June 2019

Participants:
Jakob Lund Nadj

Supervisors:
Benjaminn Nordahl Nielsen
John Dalsgaard Sørensen
Søren Dam Nielsen

Number of pages in main report:
71 pages

Number of pages including appendix:
125 pages

Date of hand in:
7th June 2019

Preface

This master thesis is made by Jakob Lund Nadj, who studied at Structural and Civil Engineering at Aalborg University, Denmark. The thesis consists of a main report and four appendices, which is developed in the period of February 2019 – June 2019.

I would like to acknowledge the supervision by my supervisors, who guided me through this thesis. Benjaminn Nordahl Nielsen and Søren Dam Nielsen has been supervising with regards to the geotechnical part of the report, while John Dalsgaard Sørensen has been supervising with regards to the statistical part of the report. Further I would like to express my gratitude to Lars Brønnum Fisker, Linea Christiansen and Dennis Nielsen from Sweco, who helped me with additional supervision of the project. Also, a great thanks goes to Jan Dannemand Andersen for supporting the project. Lastly, I would like to thank my wife for supporting me through the whole semester and keeping me motivated.

> *Psalms 121, 1-2*

Reading guide:

The Harvard method is used for referring to prior studies and references. The references are thereby presented in brackets where the last name of the author and year for publication is written. For example: "(Nadj, 2019)". The reference is placed in the end of the sentence it belongs to and if a table/ figure is borrowed from another author, the reference is mentioned in the caption of the figure/ table. Further, if the figure/ table is edited it is noted with a "-edited" after the reference.

Figures and tables are numbered after the chapter that it belonged to and hereafter the number of figure or table it is in that current chapter. For example, "Figure 2.5" is the fifth figure in chapter two. For equations the numbering is very similar, but the number of the equation is separated by a comma and everything is placed inside brackets. For example, "equation (4,5)" is the fifth equation in chapter four.

The appendices are named A, B, C etc. The figures, tables and equations are referred to as in the main report, but with a small change. Instead of only the appendix, the appendix and section number are included. For example, "Table A.1.5" is the fifth table in Appendix A.1 and "equation (A.1,5)" is the fifth equation in Appendix A.1. Each appendix belongs to a specific chapter, while Appendix E is showing detailed calculations for both chapter 4 and 5.

Resume

I indestående rapport undersøges fire empiriske modeller til at bestemme den udrænede forskydningsstyrke i ler på baggrund af CPT-forsøg. Til at undersøge de fire modeller, er der indsamlet CPT og triaxial forsøg udført i Søvindmergel, som er en fed og sprækket ler der forefindes på bl.a. Århus Havn.

De fire empiriske modeller er meget ens, men adskiller sig ved at anvende forskellige parametre fra CPT-forsøget. Ydermere anvender de hver deres empiriske keglefaktorer som er navngivet henholdsvis N_K, N_{KT}, N_{ke} og $N_{\Delta u}$. Værdierne for disse keglefaktorer bestemmes ved at sammenligne parametre fra CPT-forsøget med et triaxial forsøg.

Der er i nærværende rapport udført et todelt litteraturstudie, hvor første del bestemmer værdier for keglefaktorerne fra tidligere studier. Der er kun fundet tidligere værdier for N_K og N_{KT} i Søvindmergel. Ydermere beskrives der i den første del af litteraturstudiet også tidligere fundne sammenhænge mellem de forskellige keglefaktorer og øvrige parametre, som for eksempel poretryksforholdet eller plasticitetsindekset.

Anden del af litteraturstudiet omhandler, hvilke faktorer der har indflydelse på CPT målingerne og derved også har indflydelse på resultaterne af de anvendte fire modeller. Her præsenteres standarder for penetrationshastigheden og hældningen af kegle-penetrometeret. Det ses, at ved en afvigelse af disse standarder, vil der være risiko for at spidsmodstanden og dybden ikke måles korrekt. Ydermere er det bestemt at keglespidsen og filtrene skal mættes omhyggeligt for at sikre, at poretrykket måles korrekt.

De indsamlede data fra Århus havn præsenteres herefter, hvor to projekter med tilsammen 21 triaxial-forsøg er indsamlet. Dertilhørende er der udvalgt et enkelt repræsentativt CPT-profil til hver af projekterne. Det ene projekt er udført som en ”down the hole test” mens det andet projekt er udført som en kontinuerlig CPT. I begge projekter er der opdaget problemer med de målte poretryk, men projekterne er dog stadig anvendt på trods af dette.

Inden CPT-dataene anvendes, databehandles de for at korrigere for evt. fejl. Hvis CPT-dataene ikke korrigeres, kan fejlene blive overført, til de udledte værdier af keglefaktorerne eller den udrænede forskydningsstyrke. Ved ”Projekt 2” fjernes der op til 56 % af målepunkterne, grundet en for høj penetrationshastighed under udførslen. Ydermere grundet en betydelig hældning af kegle-penetrometeret, korrigeres 120 meter penetrationslængde til 90 meter penetrationsdybde.

Efterfølgende fjernes visuelle fejl i form af ekstremværdier gennem metoden ”peak over threshold”. Dette fjerner de ekstreme værdier som tydeligt afviger fra øvrige målinger og derved antages at være fejl. Ydermere korrigeres det målte poretryk for ”Projekt 2”, eftersom det tydeligt ses, at dette ikke er målt korrekt.

Værdier for de fire keglefaktorer udledes herved gennem de fire modeller, og det ses at værdierne varierer i intervallerne 7.0-27.2 for N_K, 7.6-31.3 for N_{KT}, 6.8-29.8 for N_{ke} og 0.9-12.1 for $N_{\Delta u}$.

Den karakteristiske udrænede forskydningsstyrke kan herefter bestemmes ved metoden angivet i Anneks D fra EN1990. De tre modeller, som anvender N_{KT}, N_{ke} og $N_{\Delta u}$, undersøges yderligere, for at bestemme den mest fordelagtige model. Det bestemmes at de tre modeller har tilnærmelsesvis den samme modelusikkerhed på omkring 0.4, hvilket er relativt højt. Modellen som anvender keglefaktoren N_{KT} er mindst påvirket af det dårlige målte poretryk fra to indsamlet projekter og denne vælges derfor til at bestemme den karakteristiske udrænede forskydningsstyrke.

Det vises at den fysiske usikkerhed i den udrænede forskydningsstyrke kan reduceres på baggrund af størrelsen af en valgt geoteknisk konstruktion. Dog bestemmes det at reduktionen er minimal, eftersom modelusikkerheden er relativ stor ift. den fysiske usikkerhed.

Content

1 Introduction

A cone penetration test (CPT) is one of the most common field tests. The test is conducted by pushing a cone penetrometer vertically through the soil with a rig that normally consist of a hydraulic jacking and a reaction system. The cone penetrometer is mounted on a string of rods that are used to push down the cone, while measuring cone resistance, q_c, sleeve friction, f_s, and pore pressure, u_2 (Lunne, et al., 1997). The location, where the parameters are measured is shown on the front page. Further, the depth and time are also registered, while the testing is conducted. The cone penetrometer is shown in Figure 1.1 and an example of the measured CPT data is shown in Figure 1.2.

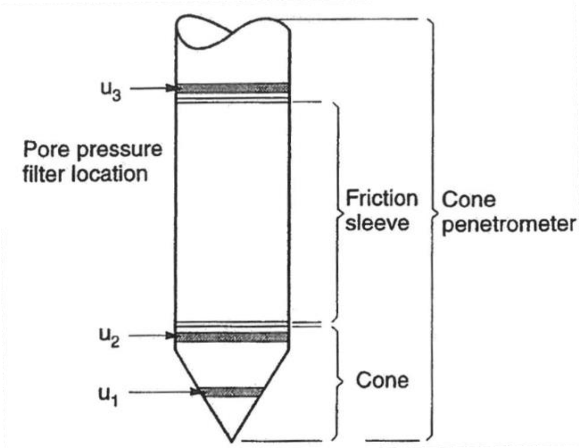

Figure 1.1: Terminology of the cone penetrometer from (Lunne, et al., 1997). u_1 and u_3 are alternative locations for measuring the pore pressure. This is explained further in Appendix A.1.

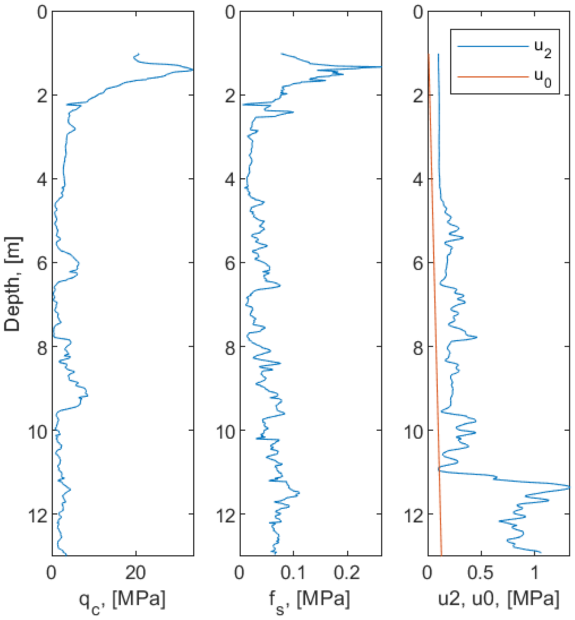

Figure 1.2: Example of measured CPT data. u_2: pore pressure; u_0: hydrostatic pressure.

The CPT has a lot of advantages compared to other field tests such as the shear vane test. The shear vane test can only estimate the undrained shear strength in cohesive soils and it is therefore not conducted in frictional soils, while the CPT is conducted in both cohesive and frictional soils. The CPT is only limited by gravely soils, since this can damage the cone. The CPT is furthermore quickly conducted, and the test produces a lot of measurements, since the cone is measuring multiple parameters continuously. Depending on the sampling frequency, the CPT approximately measures the parameters once per 2 cm. As a comparison the shear vane test measures one parameter, usually per 50-100 cm. The amount of data gathered by the CPT therefore shows more variation in the tested soil than the shear vane test. This is beneficial because it can give a better understanding of the variations through the soil, but at the same time, it gives a greater task in interpreting the CPT data.

Most of the interpretations from the CPT are empirical and the CPT should therefore not stand alone. The CPT should be supported by boreholes and simple laboratory tests to verify the empirical results and further the empirical interpretation should always be corrected with local experience for the specific soil. The CPT data can be used to estimate sub-surface stratigraphy, to estimate geotechnical parameters and to provide results for geotechnical design.

It is not possible within the scope of this report to investigate all the aspects of the test and it is therefore decided to narrow the report down to investigate the method of determining the undrained shear strength in a specific clay, which according to (Lunne, et al., 1997), is one of the most reliable parameters derived from a CPT.

1.1 Søvind Marl at the Port of Aarhus

The following investigation is decided to be carried out for Søvind Marl, which is a soft and fissured clay, found at the Port of Aarhus, Denmark. The location of the Port of Aarhus is shown in Figure 1.3.

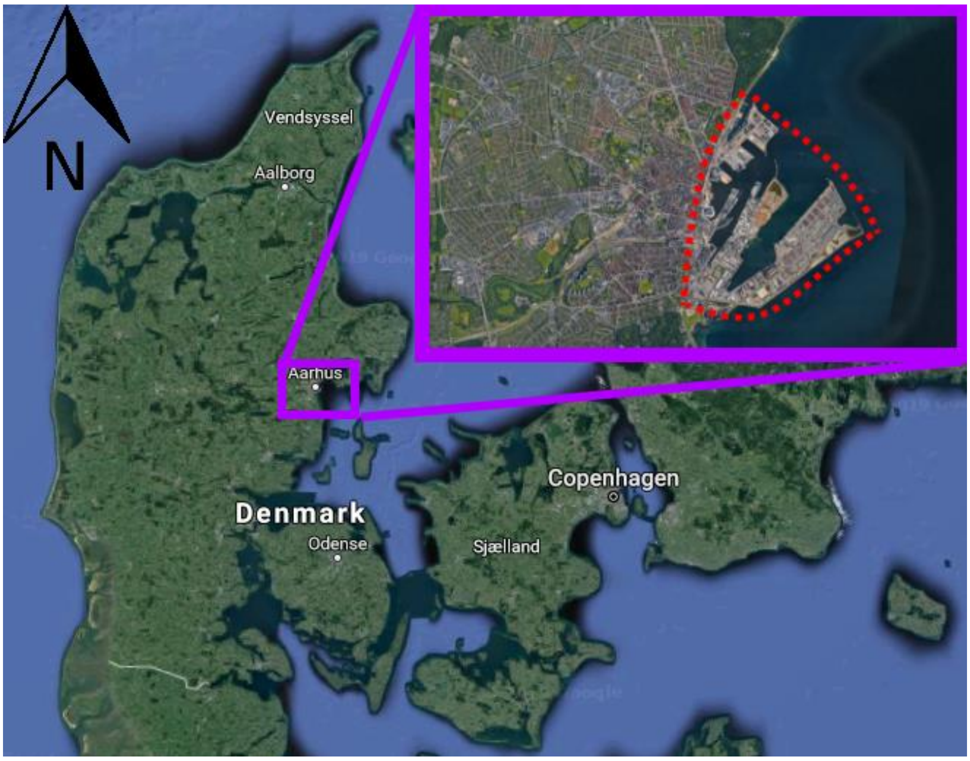

Figure 1.3: Port of Aarhus marked with red dots. Map is taken from (Google, 2019)-edited.

The stratification at the Port of Aarhus consists in general of 10 m sandy fill and hereafter Søvind Marl to greater depths than 70 m below ground surface. Underneath Søvind Marl, Lillebælt clay is found, which is roughly similar to Søvind Marl, but without any carbonate content (Nadj, 2019).

Søvind Marl is a high plasticity clay with a plasticity index ranging from 100 % to 300 %. The clay has a carbonate content varying significantly between 0-65 %, even in the same borehole. Further a linear relation has been determined between an increasing plasticity index with a decreasing carbonate content (Grønbech, et al., 2014). The total unit weight of Søvind Marl varies between 16-19 kN/m^3 with an average of 17.7 kN/m^3 and if the carbonate content is disregarded, the clay is very homogeneous.

According to (Bjerrum, 1973), the relation between the horizontal and vertical shear strength is depending on the plasticity index. This relation is shown as a function of the plasticity index in Figure 1.4. The plasticity index is explained in Appendix A.3.

It is seen that the relation between horizontal and vertical shear strength becomes close to 1, when the plasticity index is 60 %. By assuming that the relation stays at 1 with increasing plasticity index, it seems to be reasonable to also assume that the Søvind Marl is isotropic, since the plasticity index is above 100 %.

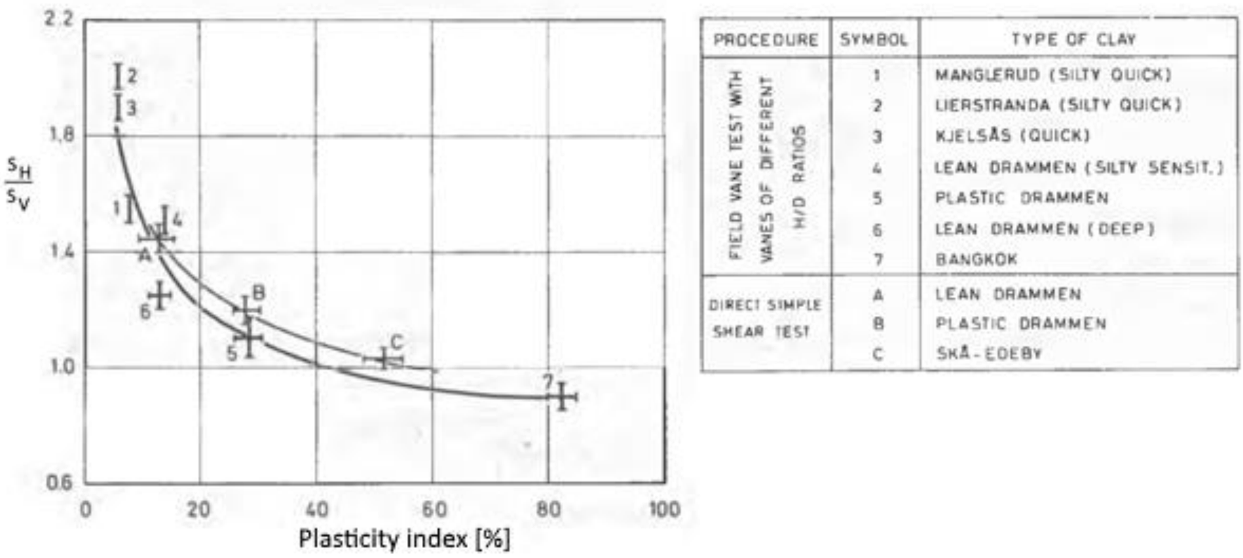

PROCEDURE	SYMBOL	TYPE OF CLAY
FIELD VANE TEST WITH VANES OF DIFFERENT H/D RATIOS	1	MANGLERUD (SILTY QUICK)
	2	LIERSTRANDA (SILTY QUICK)
	3	KJELSÅS (QUICK)
	4	LEAN DRAMMEN (SILTY SENSIT.)
	5	PLASTIC DRAMMEN
	6	LEAN DRAMMEN (DEEP)
	7	BANGKOK
DIRECT SIMPLE SHEAR TEST	A	LEAN DRAMMEN
	B	PLASTIC DRAMMEN
	C	SKÅ-EDEBY

Figure 1.4: Anisotropy decreasing with increasing plasticity index after (Bjerrum, 1973). s_H: horizontal shear strength; s_V: vertical shear strength.

1.2 The undrained shear strength estimated by a CPT

According to (Lunne, et al., 1997), a theoretical solution to estimate the undrained shear strength, from a CPT, has been developed by different theoretical considerations. By considering bearing capacity theory, cavity expansion theory, analytical and numerical approaches and strain path theory, the theoretical solution can be derived. Each theoretical proposal resulted in the same general formula shown in equation (1,1).

$$s_u = \frac{q_c - \sigma_0}{N_c} \qquad (1,1)$$

Where

s_u	Undrained shear strength	$[\mathrm{kPa}]$
q_c	Cone resistance	$[\mathrm{kPa}]$
σ_0	Depending of the method; horizontal, vertical or mean overburden stress	$[\mathrm{kPa}]$
N_c	Theoretical cone factor	$[-]$

The theoretical solution has shown a relation between the undrained shear strength and cone resistance, by taking the overburden stress into consideration. Since cone penetration is a complex problem, the solution withholds simplifying assumptions regarding, soil behavior, failure mechanism and boundary conditions. The theoretical solution is therefore primally good at giving an understanding of the solution, since the theoretical solution cannot take stress history, anisotropy, sensitivity and ageing into consideration. Empirical models are therefore preferred, since the theoretical solution must be verified with field or laboratory test. From the theoretical solution three empirical and semi-empirical models are derived. The empirical models estimate the undrained shear strength by using; the total cone resistance, the effective cone resistance and excess pore pressure (Lunne, et al., 1997).

1.2.1 Total cone resistance

The total cone resistance is a model directly taken from the theoretical solution, and the cone factor, N_K, is used instead of N_c to distinguish from the theoretical solution. The only difference between N_c and N_K is that N_K is determined empirically. The solution using N_K is shown in equation (1,2) (Lunne, et al., 1997).

$$s_u = \frac{q_c - \sigma_{v0}}{N_K} \tag{1,2}$$

Where

s_u	Undrained shear strength	[kPa]
q_c	Cone resistance	[kPa]
σ_{v0}	Vertical overburden stress	[kPa]
N_K	Empirical cone factor	[−]

It has later been discovered that the pore pressure influenced the cone resistance due to an "unequal end area effect" and the cone resistance is therefore corrected, which is shown in equation (1,3). The need for a correction of the cone resistance has been discovered at deep water investigations, where it has been observed that the cone resistance deviated from the water pressure (Lunne, et al., 1997).

$$q_t = q_c + u_2(1 - \alpha) \tag{1,3}$$

Where

q_c	Cone resistance	[kPa]
u_2	Pore pressure	[kPa]
α	Net area ratio	[−]

The net area ratio is used to account for the "unequal end area effect", which is caused by the inner geometry of the cone. This is explained in Appendix A.1 along with the different filter locations for measuring the different pore pressures u_1 and u_3.

By using the corrected cone resistance, equation (1,2) is changed to equation (1,4), which names the cone factor, N_{KT} instead.

$$s_u = \frac{q_t - \sigma_{v0}}{N_{KT}} \tag{1,4}$$

Where

q_t	Corrected cone resistance	[kPa]
σ_{v0}	Vertical overburden stress	[kPa]
N_{KT}	Empirical cone factor	[−]

The benefit of using the corrected cone resistance is greatest in soft clay, where the pore pressure can be in the same magnitude as the cone resistance and the correction is therefore significant (Lunne, et al., 1997).

1.2.2 Effective cone resistance

Another method to estimate the shear strength is by using the effective cone resistance, which is shown in equation (1,5). The effective cone resistance has been used in other geotechnical works, such as soil classification and pile capacity prediction. It therefore seems obvious to estimate the undrained shear strength with this approach (Lunne, et al., 1997).

$$s_u = \frac{q_e}{N_{ke}} = \frac{q_t - u_2}{N_{ke}} \tag{1,5}$$

Where

q_e	Effective cone resistance	[kPa]
q_t	Corrected cone resistance	[kPa]
u_2	Pore pressure	[kPa]
N_{Ke}	Empirical cone factor	[−]

In normally consolidated clay, the pore pressure can reach up to 90 % of the cone resistance and the quantity therefore becomes very small. This makes the effective cone resistance very sensitive with regards to the pore pressure and cone resistance. The model works well for some soils, but in general it is not applicable, and it is therefore not recommended (Lunne, et al., 1997).

1.2.3 Excess pore pressure

The last model is more favorable in soft clays, where the cone resistance is relatively small and therefore sensitive to small changes. Instead the excess pore pressure is used, which is shown in equation (1,6).

$$s_u = \frac{\Delta u}{N_{\Delta u}} = \frac{u_2 - u_0}{N_{\Delta u}} \tag{1,6}$$

Where

u_2	Pore pressure	[kPa]
u_0	Hydrostatic pressure	[kPa]
$N_{\Delta u}$	Empirical cone factor	[−]

Equation (1,6) is derived for normally and lightly over consolidated clays. It is not recommended to extrapolate it to heavily over consolidated clays, where the pore pressure ratio can be small or negative (Lunne, et al., 1997).

1.1 Problem statement

The empirical cone factors N_K, N_{KT}, N_{Ke} and $N_{\Delta u}$ can be determined from respectively the models presented in equation (1,2), (1,4), (1,5) and (1,6), by using a reference test. The reference test, which usually is a shear vane test or triaxial test, is used to determine the undrained shear strength, and hereby the cone factors can be determined. The undrained shear strength is not easily estimated, since several models with different cone factors exists. Further the values of the cone factors vary for different cohesive soils and even within the same soil.

The problem statement for this report hereby becomes:

"What are the values of the empirical cone factors for Søvind Marl and how can a characteristic undrained shear strength, from at least one of the models, be estimated?"

The problem statement is supported with the following bullet points as a guidance for this report:

- What measured parameters or methods of interpretations affects the calculations of empirical cone factors?
- Which empirical cone factors are the most favorable in Søvind Marl?
- What are the model uncertainties the most applicable models?
- What effect does the size of a foundation have on the estimated characteristic undrained shear strength?

2 Literature study

The literature study is separated into two parts. Section 2.1 investigates the estimated values of the empirical cone factors from prior studies in cohesive soils. Section 2.2 determines factors that affect the CPT measurements, which indirectly influences the calculations of the cone factors, since the CPT measurements are used to calculate them.

2.1 Prior values determined for the cone factors

Gathered studies with derived values of N_K are shown in Table 2.1. The gathered values of N_K are in the interval of 6-28.4, which seems to be a large interval. One study, which is conducted in Søvind Marl, estimates the value of N_K to be 6-7.6, while other studies in soft soils, such as Holocene clay, shows a large range of values for N_K. The studies from (Okkels, et al., 2008), do not specify exactly, how the values of N_K are derived. For this reason it is hard to explain why the range of N_K is so narrow in the specific study. It is therefore assumed that the studies from (Okkels, et al., 2008) are containing simplifying assumptions to present such a narrow range for Søvind Marl or even single values of N_K for the other clays.

Further a dependency is seen between the values of N_K and the used reference test. It is seen that when the shear vane test is used as reference test, the values of N_K are in general lower than the studies which uses the triaxial test. According to (Nadj, 2019), the shear vane test has the tendency to overestimate the undrained shear strength and it is therefore necessary to correct the measured values with a correction factor, μ. In case no corrections are made on these shear vane tests, the derived cone factors are underestimated. This is not only important for the derived value of N_K but also for the derived value of the other cone factors. It must therefore be secured that the derived undrained shear strengths, from the reference tests, are representable, and not overestimated due to the reference test itself.

Table 2.1: Prior determined values of N_K summarized from various authors.

N_K value range	Reference test	Comments	Reference
6-7.6	Shear vane	Søvind Marl: High plasticity, soft clay, from Port of Aarhus. (0 % < Ca < 60 %) (50 % < I_p < 200 %) (10 < OCR < 12) N_K is independent of depth, I_p and R_f N_K is of same magnitude in nearby septarian clay.	(Okkels, et al., 2008)
7.5	Shear vane	Soft moraine clay: (22 % < I_p < 27 %) (5 < OCR < 6) N_K is independent of depth Could not confirm $N_K = 10$ in moraine clay which was determined in prior study	(Okkels, et al., 2008)
8.0	Shear vane	Skive Septarian clay: (62 % < I_p < 73 %) (10 < OCR < 12)	(Okkels, et al., 2008)
17	Triaxial compression	Non-fissured clay	(Lunne, et al., 1997)
11-19	Shear vane	Normal consolidated marina clay	(Lunne, et al., 1997)

10.5-27.6	Triaxial compression	Soft Holocene clay Classified as silt and clay with varying plasticity. (12 < s_u < 124) (540 kPa < q_c < 1900 kPa) 22 triaxial tests are conducted	(Rémai, 2012)
7.6-28.4	-	German experience on different soil types	(Rémai, 2012)
5-12	-	Experience from three test sites in Malaysia	(Rémai, 2012)

NOTE: Ca: carbonate content, I_p: plasticity index, s_u: undrained shear strength, q_c : cone resistance, OCR: over consolidation ratio, R_f: friction ratio.

In Table 2.2, gathered values for N_{KT} are shown, where the values of N_{KT} are in the interval 4-32.1. Again, a study has been found on Søvind Marl that determines the value of N_{KT} to be in the interval of 20-30. For some of the studies it is seen that there is determined a dependency between the over consolidation ratio and N_{KT} and a dependency between the pore pressure ratio and N_{KT}. These dependencies are worth remembering, since the same dependency will be looked for in this report. Parameters such as the plasticity index, over consolidation ratio and pore pressure ratio are explained in Appendix A.

Table 2.2: Prior determined values of N_{KT} from (Rémai, 2012) unless else stated..

N_{KT} value range	Reference test	Comments
8-16	Triaxial compression test, triaxial extension and direct shear	For clays (3 % < I_p < 50 %) N_{KT} increases with I_p
11-18	-	Found no Correlation between N_{KT} and I_p
8-29	Triaxial compression	N_{KT} varies with *OCR*
10-20	Triaxial compression	From (Powell, et al., 1988)
6-15	Triaxial compression	N_{KT} decreases with B_q
7-20	Triaxial compression	Busan clay, Korea 25% < I_p < 40%
4-16	Vane shear	High plasticity, soft clay, 42% < I_p < 400%
11.9-32.1	Triaxial compression	Soft Holocene clay Classified as silt and clay with varying plasticity. (12 < s_u < 124) (540 kPa < q_c < 1900 kPa) 22 triaxial tests were conducted
20-30	Triaxial compression	From (Grønbech, 2015) Søvind Marl at Port of Aarhus 7 triaxial tests were conducted

NOTE: I_p: plasticity index; B_q pore pressure ratio, s_u: undrained shear strength, q_c : cone resistance, OCR: over consolidation ratio.

When the N_K and N_{KT} are determined, the negative contribution from the vertical overburden stress in equation (1,2) and (1,4) is neglected in most studies. It is assumed that it is neglected, since the cone resistance often is considerably greater than the vertical overburden stress, and therefore the effect of including the vertical overburden stress is neglectable. By neglecting the vertical overburden stress, the values of

N_K and N_{KT} are slightly overestimated than, if the overburden stress is taken into consideration. The determined values of N_K and N_{KT} are therefore sometimes derived to describe the direct relation between undrained shear strength and the cone resistance or undrained shear strength corrected cone resistance respectively.

Gathered values of N_{ke} are shown in Table 2.3. It is seen that the values are in the interval 1-37, which is the largest interval of all the cone factors. As it is explained earlier, the method of using the effective cone resistance, is not recommended, since the pore pressure and the corrected cone resistance can be in the same magnitude and thereby the calculation of N_{ke} is very sensitive. This can explain the determined values of N_{ke} as being the most varying cone factor.

No studies are gathered, which determined the values of N_{ke} in Søvind Marl. Instead the values of N_{ke} is determined in Holocene clay, which also is a soft clay, that might be comparable with Søvind Marl. In Table 2.3 it is further seen that two studies also determines a dependency between the pore pressure ratio and N_{ke}. This dependency is also worth remembering, since the same dependency will be looked for in this report.

Table 2.3: Prior determined values of N_{ke} from various authors.

N_{ke} **value range**	**Reference test**	**Comments**	**Reference**
6-12	-	For clays (3 % < I_p < 50 %)	(Rémai, 2012)
1-13	-	N_{ke} varies with B_q, for a normally consolidated clay.	(Lunne, et al., 1997)
2-10	Triaxial compression	N_{ke} decreases with B_q	(Rémai, 2012)
3-18	Triaxial compression	Busan clay, Korea 25% < I_p < 40%	(Rémai, 2012)
10.9-28.6	Triaxial compression	Soft Holocene clay Classified as silt and clay with varying plasticity. (12 < s_u < 124) (540 kPa < q_c < 1900 kPa) 22 triaxial tests were conducted	(Rémai, 2012)
7-37	Triaxial compression	Silty clay at Bookmyun area in Changwon city. 3 % < I_p < 42%	(Kim, 2009)

NOTE: I_p: plasticity index; B_q pore pressure ratio, s_u: undrained shear strength, q_c : cone resistance.

Values for $N_{\Delta u}$ are shown in Table 2.4. The values are in the interval 1-26, but by neglecting the theoretical values and the values determined in silt, it is seen that the interval narrows down to 1-13.1. $N_{\Delta u}$ thereby has the narrowest interval compared with the other cone factors. As for N_{ke}, no studies are gathered about deriving values of $N_{\Delta u}$ in Søvind Marl. The Holocene clay, which also is a soft clay, is therefore the best for comparison with values determine for Søvind Marl in this report.

Table 2.4: Prior determined values of $N_{\Delta u}$ summarized from various authors.

$N_{\Delta u}$ value range	Reference test	Comments	Reference
1.8-13.1	Triaxial compression	Soft Holocene clay Classified as silt and clay with varying plasticity. ($12 < s_u < 124$) (540 kPa < q_c < 1900 kPa) 22 triaxial tests were conducted	(Rémai, 2012)
1-26	Triaxial compression	Silty clay at Bookmyun area in Changwon city. 3 % < I_p < 42%	(Kim, 2009)
2-20	-	Theoretical value based on cavity expansion	(Lunne, et al., 1997)
4-10	Triaxial compression	North sea clays	(Lunne, et al., 1997)
7-9	Shear vane	Three Canadian clays with $1.2 < OCR < 50$	(Lunne, et al., 1997)
6-8	Triaxial compression	No clear dependency on B_q	(Lunne, et al., 1997)

NOTE: s_u: undrained shear strength; qc: cone resistance; I_p: plasticity index; OCR: over consolidation ratio; B_q: pore pressure ratio.

From the study of the three Canadian clays, it is indicated that $N_{\Delta u}$ is independent of the over consolidation ratio, since the determined values are in a very narrow interval, while the over consolidation ratio of the tested clays varied between 1.3-50.

It is also noticeable that the last study does not determine any dependency between $N_{\Delta u}$ and the pore pressure ratio. According to (Lunne, et al., 1997), studies have determined such a relation, and it can indicate that a dependency with the pore pressure ratio is depending on the soil.

2.1.1 Dependencies between the cone factors and soil parameters

According to (Rémai, 2012), studies suggest a dependency between N_{KT}, and other soil parameters (e.g. plasticity index and over consolidation ratio). These dependencies are not confirmed in later studies, which can indicate that N_{KT} is depending on several parameters. According to (Lunne, et al., 1997), N_{KT} increases when taking the effect of fissured clay and scale effect into consideration.

Figure 2.1 shows an example of the determined relation between N_{KT} and the plasticity index. The relation is relative linear with N_{KT} increasing with increasing plasticity index. The left figure used the mean value of triaxial compression test, triaxial extension test and direct simple shear test, as reference test, while the right figure used triaxial compression test as reference test. It is therefore seen, that the used reference test is important, since the left figure has approximately 50 % higher values of N_{KT}, than the right figure.

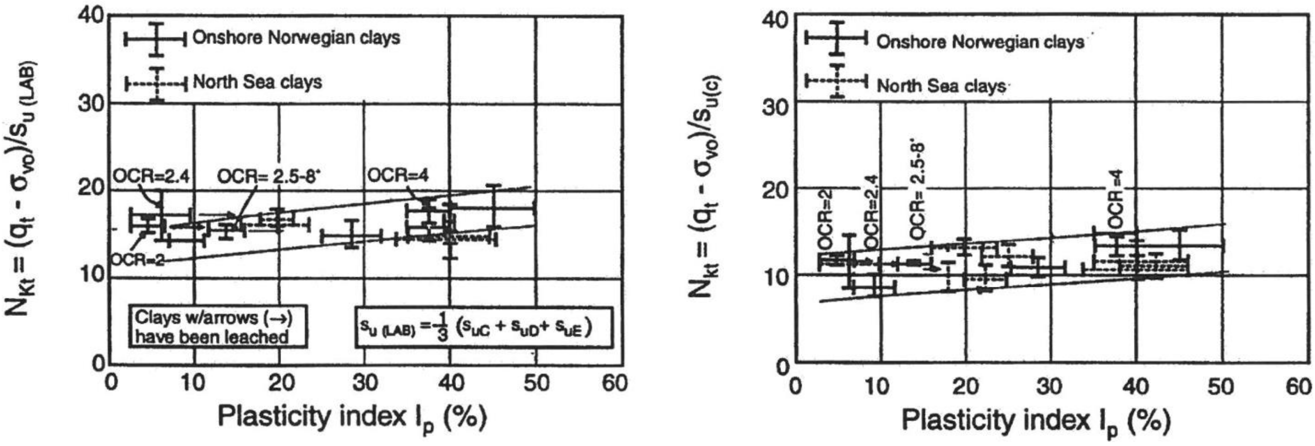

Figure 2.1: Dependency between N_{KT} and I_p. s_{uc} triaxial compression; s_{ue} triaxial extension; s_{ud} direct simple shear from (Lunne, et al., 1997)-edited.

Figure 2.2 shows three suggested relations between the plasticity index and N_K in highly over consolidated clay. It has been noted, in the current study, that the derived values of undrained shear strength should be used with care, since the effect of fissures is uncertain.

Figure 2.3 shows a study using triaxial compression test as reference test, to determine $N_{\Delta u}$. No dependency for the pore pressure ratio has been determined, but from another study it seems that the lower range is a good fit. According to (Rémai, 2012), several studies have determined at good dependency between $N_{\Delta u}$ and the pore pressure ratio. It would therefore be relevant to investigate this dependency for Søvind Marl, since $N_{\Delta u}$ has been determined to be good for soft clays.

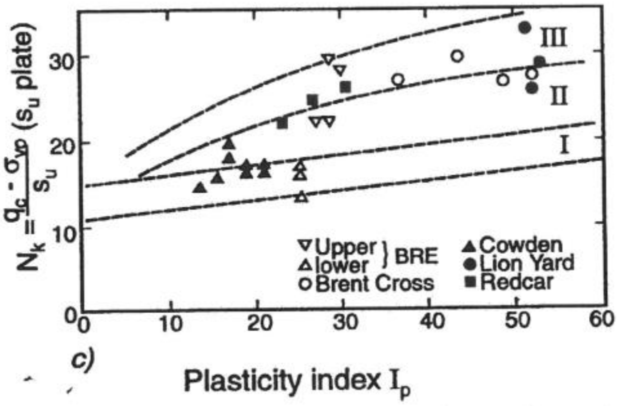

Figure 2.2: Values of N_k in fissured clay vs I_p from (Lunne, et al., 1997).

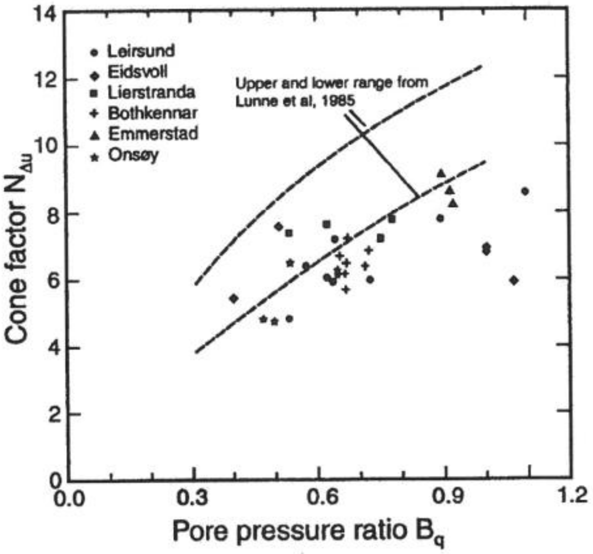

Figure 2.3: Values of $N_{\Delta u}$ vs B_q from (Lunne, et al., 1997).

According to (Lunne, et al., 1997) studies have suggested that N_{ke} is dependent on the pore pressure ratio, B_q, with a minor scatter. This dependency is derived for normally and lightly over consolidated clay and it is not recommended to extrapolate this to heavily over consolidated clays, since the pore pressure ratio can be small or even negative. Figure 2.4 (left) shows relation determined between N_{KT} vs pore pressure ratio and Figure 2.4 (right) a relation between N_{ke} and pore pressure ratio with triaxial compression tests as reference test. The left figure shows some scatter, while the right side shows a relative narrow band, which could indicate a dependency on the pore pressure ratio and N_{ke}.

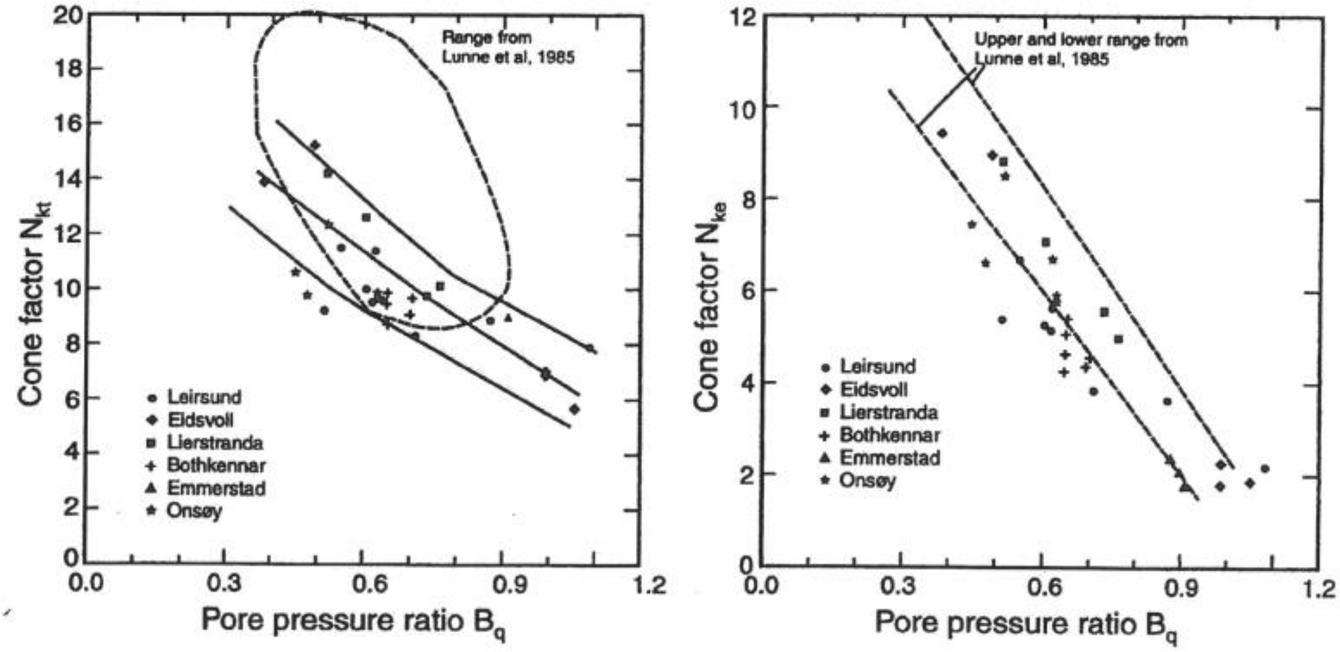

Figure 2.4: Left: Values of N_{KT} vs B_q; Right: Values of N_{ke} vs B_q from (Lunne, et al., 1997).

As seen from the studies in Table 2.1 to Table 2.4 and Figure 2.1 to Figure 2.4, a clear dependency between a certain cone factor and a soil parameter, is not always present at all times. It seems to vary from different soils and it can therefore be necessary to investigate each cone factor for each soil. Dependencies will therefore be investigated in Søvind Marl, for the for four cone factors.

2.2 Factors affecting the CPT measurements

This section covers factors that affects the CPT measurements, which indirectly influences the determined cone factors, since the CPT data is used to estimate the cone factors. This section will be based on standards from (BSI Group, 2013), where relevant standards for the CPT will be presented.

2.2.1 Saturation of the filter and cone tip

Saturation of the filter and the cone tip is important in order to achieve a good pore pressure measurement. The effect of good and poor saturation is shown in Figure 2.5. Two tests have been conducted at the same location, where “test 1” is with a poor saturation, and “test 2” is with a good saturation. It is seen that due to the poor saturation, “test 1” does not measure the peaks and troughs as “test 2”, which has a good saturation.

If the cone is pushed down in a soil that is not saturated, it is usually necessary to predrill. If the predrilling is not carried out, there is a risk of the filter and cone tip can lose the saturation. Hereafter it will take some time for the filter and cone tip to regain the saturation, which is seen in Figure 2.6 (Wong, et al., 1990). Figure 2.6 shows the pore pressure between 0-4 m is fluctuating around 0 kPa and hereafter slowly increasing until it starts to measure a realistic pore pressure.

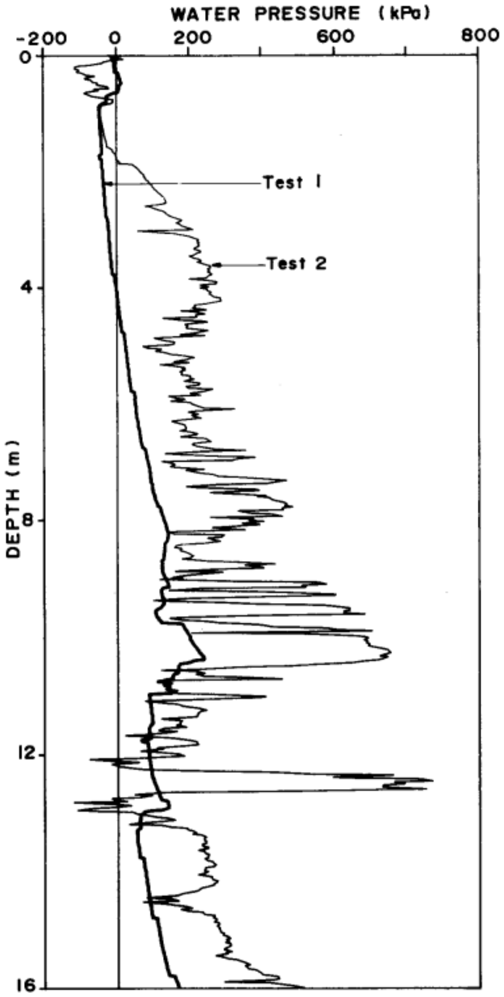

Figure 2.5: Pore pressure measured at adjacent locations but with a poorly and good saturated filter and cone tip from (Wong, et al., 1990).

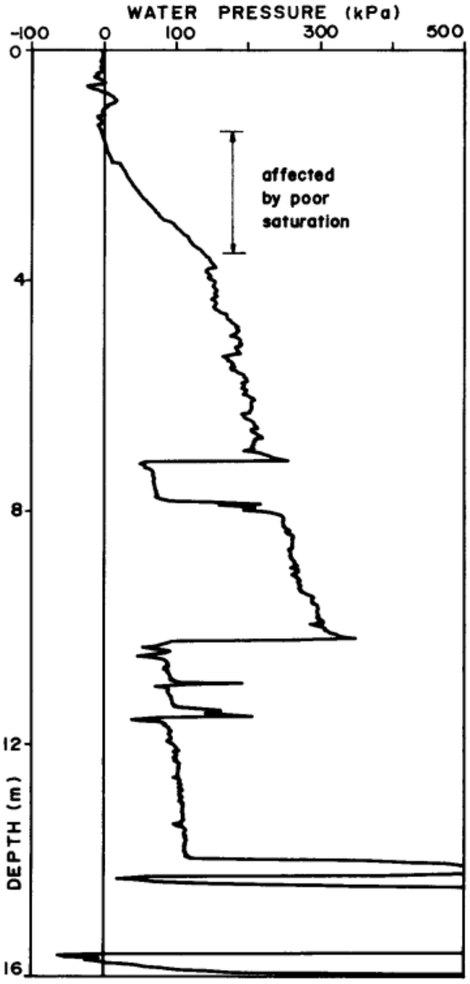

Figure 2.6: The effect of poor saturation shown in the interval 0-4 m of the measured pore pressure from (Wong, et al., 1990).

To measure the pore pressure precisely, the saturation is important. If the filter is saturated, then the pore pressure is directly transferred to the transducer, inside the cone. If an air bubble is trapped in the duct, which is seen in Figure 2.7, or the cone is poorly saturated, an increase in the pore pressure will not be transferred correctly to the transducer. The increased pore pressure will cause the air bubble to compress instead of transferring the change in pore pressure. This causes the measured pore pressure to be smoothed out and thereby not measuring the peaks and troughs, as seen for “test 1” in Figure 2.5 (Wong, et al., 1990).

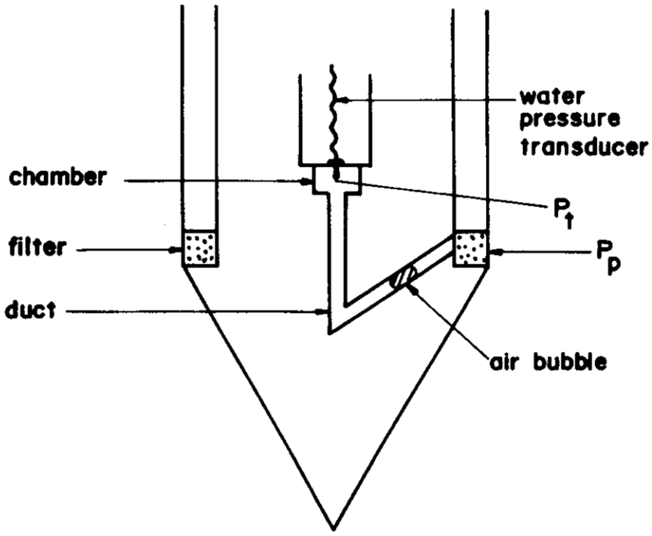

Figure 2.7: Piezocone with filter, duct, chamber and transducer from (Wong, et al., 1990).

The saturation can be done with fluids such as de-aired water or glycerin. The saturation process is not presented here but is explained in (BSI Group, 2013). De-aired water is easy to use for saturated soils and it is important to maintain a good saturation until the cone is pushed down into the saturated soil. The saturation can be maintained with a rubber membrane, placed around the cone and filter, that bursts when the penetration begins. When the cone penetrometer is pushed into a soil that is not saturated, and a predrilling is not carried out, glycerin can be more favorable due to the high viscosity, which is 10 times greater than water. The glycerin can maintain the saturation until the penetrometer reaches the saturated soil layers. The poorly measured pore pressure shown in Figure 2.6, between the depth of 0-4 m, can thereby be avoided.

2.2.2 Inclination of the cone penetrometer

Besides the cone resistance, sleeve friction and pore pressure, additional sensors can be added into the cone penetrometer to measure extra parameters. One of the most noteworthy and relevant parameters for this report is the inclination. The pushing rod and the cone penetrometer should be pushed as vertical as possible. According to (BSI Group, 2013), the CPT should be stopped, if the inclination deviates more the 15 ° from the vertical axis. If the inclination is not secured to be vertical, there is a risk that the penetration length, l, and penetration depth, z, are different from each other, which is illustrated in Figure 2.8. In case of the inclination deviating from vertical, the penetration length should be corrected to a penetration depth. Further the measured soil properties of the soil parameters, can deviate from the soil properties if measured in the vertical direction.

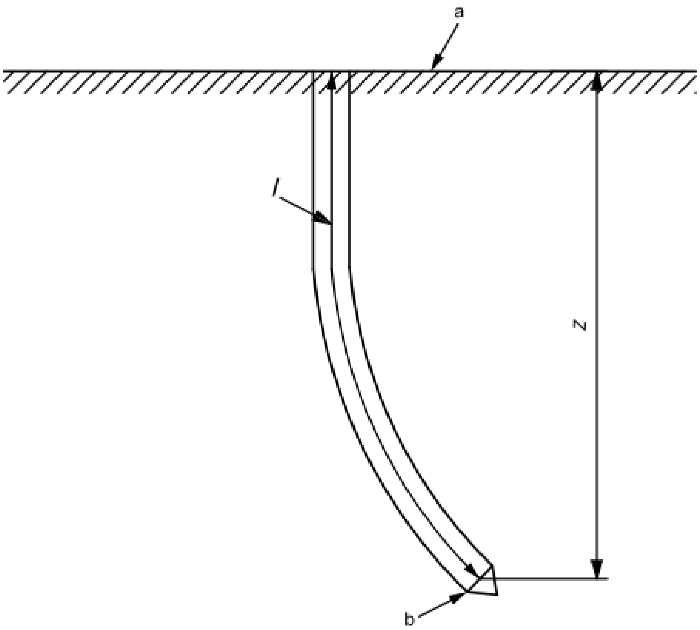

Figure 2.8: Penetration length and penetration depth defined in (BSI Group, 2013). a: fixed horizontal plane, b: base of conical part of cone, l: penetration length, z: penetration depth.

A CPT with a penetration depth less than 5 m is not required to measure the inclination. At greater depth it is required to make sure that penetration length and penetration depth are equal (BSI Group, 2013).

2.2.3 Penetration rate

The standard penetration rate is 2±0.5 cm/s. The rate is favorable since it usually measures an undrained behavior in clays and a drained behavior in sands. In silty soils and soils with a similar coefficient of consolidation, it is not always clear if it is measuring drained or undrained behavior (Martinez, et al., 2016).

The penetration rate also affects the magnitude of the cone resistance, sleeve friction and pore pressure. (Danziger, et al., 2018) observed this effect in clay which confirmed results from prior studies. The effect on the cone resistance is shown in Figure 2.9, for Connecticut river valley varved clay, which is a soft clay. At low penetration rates the behavior is predominantly drained. With increasing penetration rate, the pore pressure is generated and therefore reduces the effective stresses. At further increase of the penetration rate, viscous forces dominate the undrained behavior and thereby increase the cone resistance.

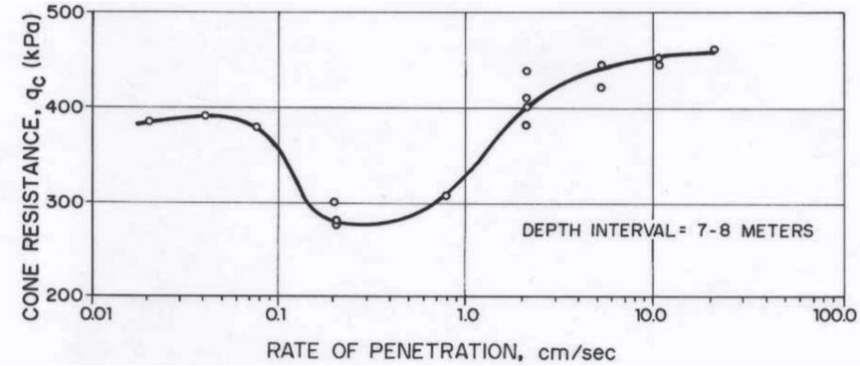

Figure 2.9: The effect of penetration rate shown in Connecticut river valley varved clay, from (Danziger, et al., 2018).

It should be kept in mind that if the penetration rate is changed, the interpretation might not be correct, since most interpretations of the CPT are empirically derived. (Lunne, et al., 1997) summarized a couple of studies that determined an increase in the measured cone resistance, sleeve friction and pore pressure, if the penetration rate is increased. The studies primarily concerned the cone resistance and from (Powell, et al., 1988) it is determined that a tenfold increase in the penetration rate, resulted in an increase of 10-20 % of the cone resistance in stiff clay and 5-10 % increase in soft clay.

3 Data from Port of Aarhus

The Søvind Marl from the Port of Aarhus has been chosen, due to a lot of construction have been conducted at this location and the amount of CPT data is assumed to be significant in Søvind Marl. Several project reports are gathered, by asking companies for them. By looking through the gathered projects, only five projects have conducted triaxial tests, which could be used as reference tests. From those five projects, two of the projects had not measured any pore pressure. This made it impossible to investigate all the cone factors for these projects, since pore pressure is necessary, and these projects are therefore discarded. One project has only very few CPT measurements, which are conducted several meters vertically away from the depth where the triaxial test specimens are taken from. It is therefore not reasonable to use these as reference tests for the CPT data, and the project is therefore discarded.

In the end two project are left, which have the CPT data and reference tests that are needed for this report. The projects are in this report referred to as “Project 1” and “Project 2”. The projects have carried out triaxial tests, shear vane tests, CPTs, oedometer tests and boreholes. Further several classifications test are conducted to determine soil parameters such as Atterberg limits, carbonate contents and the total unit weight of Søvind Marl.

3.1 CPT data from Project 1 and 2

For each project, a representative CPT is chosen to be compared with the borehole from where the triaxial test specimens are taken from. The net area ratio is determined from the manufacturer (Envi, 2019) to be 0.68 for both Project 1 and 2. For Project 1, five deep boreholes are made along with five deep CPTs. The CPTs are made as “down the hole”, which means that the CPT is conducted in the same borehole, as the soil samples are taken from. The CPTs are compared and shows similar variation down through the Søvind Marl. The representative CPT is chosen to be the one conducted in the same borehole as the triaxial test specimens are taken from. The CPT is 70 m deep and it can be seen in Figure 3.1. From the figure it is seen that the CPT is conducted in intervals varying between 1-8 m, before test is stopped, and soil samples are taken.

It is determined that water table is 1.6 m below ground surface and the Søvind Marl starts at the dept of 10 m. The friction ratio and pore pressure ratio are calculated and shown along with the CPT data. The friction ratio and pore pressure ratio are explained in Appendix A.2.

By observing Figure 3.1, it is seen at the penetration length of 22 m, the pore pressure reaches a threshold of 2.05 MPa, which is caused by the capacity of the pore pressure transducer. This is the case for all the CPTs for Project 1, which is unfortunate since most of the cone factors are depending on the pore pressure. The CPT data is still used, and the importance of the pore pressure is investigated with regards to the cone factors in section 6.1.3.

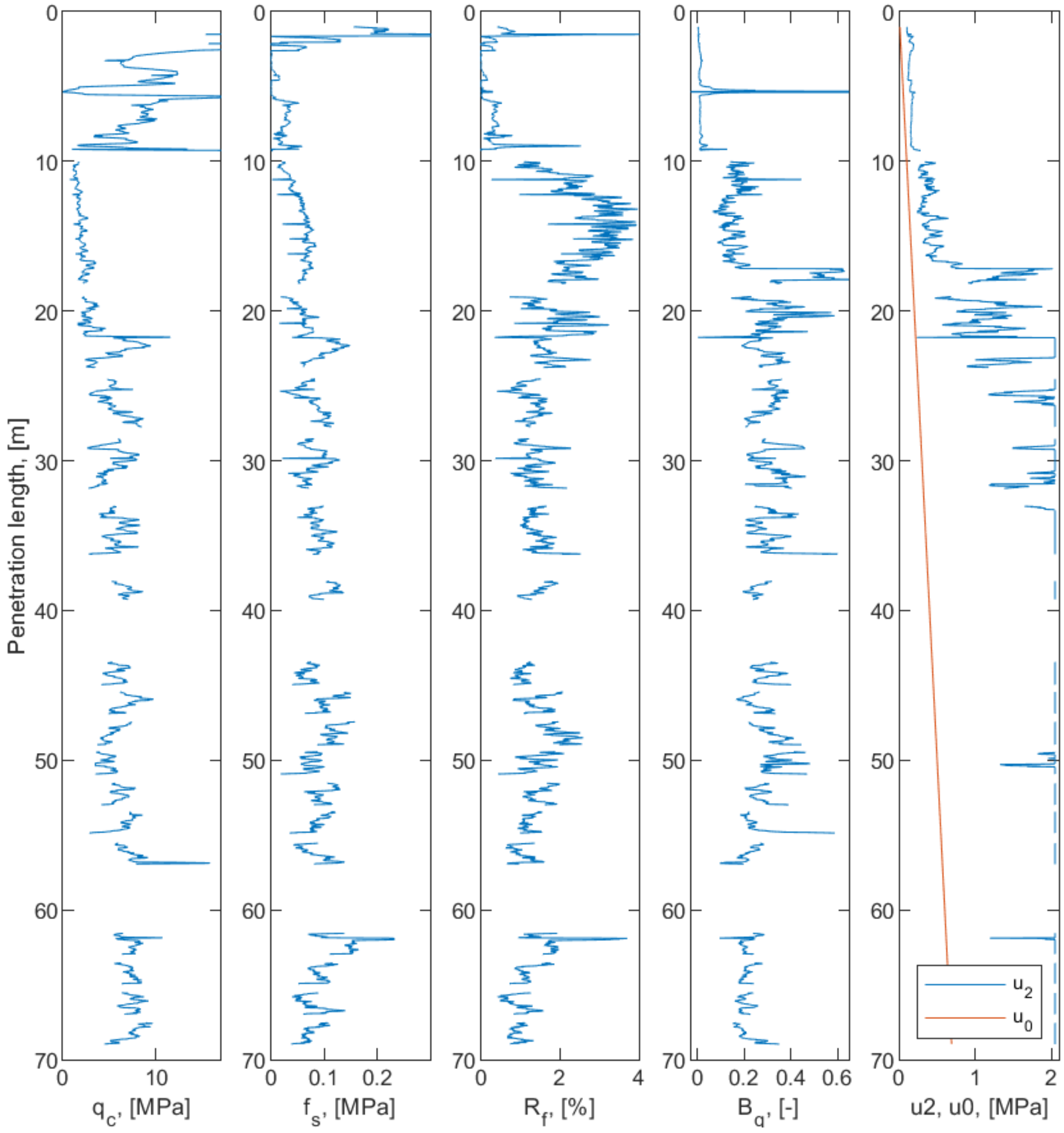

Figure 3.1: The representative CPT from Project 1.

For Project 2, three deep CPTs are conducted along with one borehole in where the triaxial test specimens are taken from. Two of the CPTs, which are measured 60 m apart, has strongly coinciding CPT measurements and one of these CPTs are the closest to the borehole. The closest CPT to the borehole is chosen as the representative CPT for Project 2, since it is the closest and because another CPT verified the measurements. The distance between the chosen CPT and the borehole is 20 m, which is a considerable distance. It is still decided to be a reasonable comparison, since the soil at the Port of Aarhus has a very similar stratigraphy. This is seen by observing a clear shift between the fill and the Søvind Marl in all the observed boreholes and CPTs from Project 1, 2 and from other projects that are discarded. According to (Nadj, 2019), Søvind Marl is determined to be very homogeneous, which is also confirmed by looking at the gathered boreholes from all the projects. As an example, the borehole of Project 2 is shown in Appendix B.2. Since the stratification is similar in the different projects, and Søvind Marl is homogeneous, it is assumed that the distance of 20 m does not have any influence when comparing the borehole and the representative CPT for Project 2.

The chosen CPT for Project 2 is shown in Figure 3.2. The CPT has a penetration length of 120 m and the whole penetration is done in one test. For Project 2, the water table is also determined to be 1.6 m below ground surface and the Søvind Marl starts at 10.2 m below ground surface.

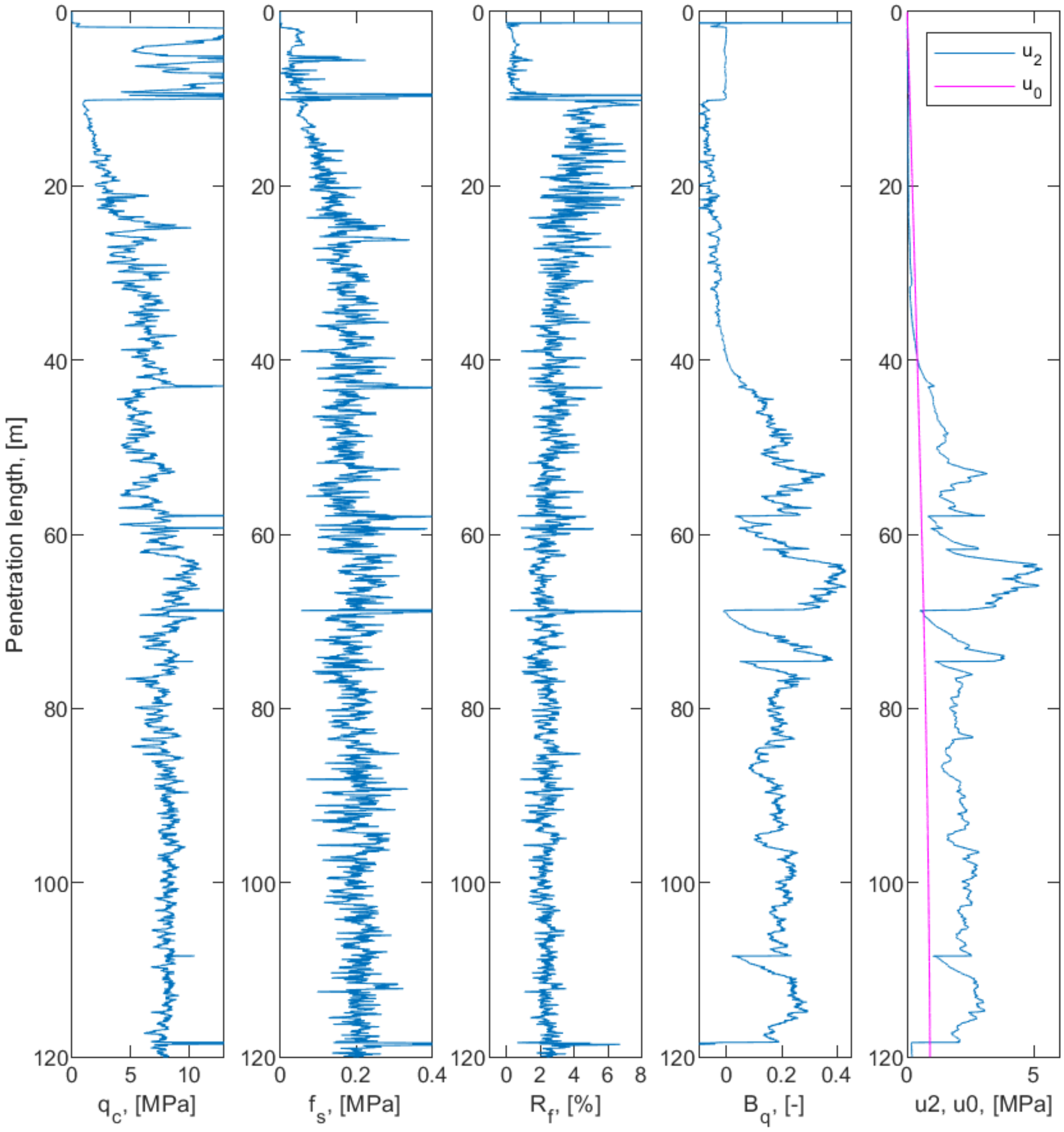

Figure 3.2: The representative CPT data from Project 2.

Again, there is observed a problem with the measured pore pressure. The pore pressure transducer has no problem measuring above 2.05 MPa, but instead there is an indication of a poor saturation of the cone tip and filter. This is seen by comparing with Project 1, where the pore pressure is above the hydrostatic pressure at 10 m below ground surface. By comparing with one of the other CPTs from Project 2, it is seen, that another measurement of the pore pressure, exceeds the hydrostatic pressure at 68 m below ground surface, which is significantly deviating from the presented CPT in Figure 3.2. Therefore, there is an indication of the pore pressure not being measured correctly, since there are such great differences in the two CPTs from Project 2. Lastly the shape of the pore pressure curve looks very similar to "test 1" from Figure 2.5, where a poor saturation has been done on purpose to investigate the effects of poorly saturated filter and cone tip. Even though there are indications of a poorly measured pore pressure, the data is still used and then the importance of the pore pressure are investigated with regards to the cone factors in section 6.1.3.

3.2 Gathered triaxial tests from Project 1 and 2

It is assumed that the determined triaxial shear strength is the true undrained shear strength in Søvind Marl. The triaxial shear strength will therefore be used as reference tests in equation (1,2), (1,4), (1,5) and (1,6) to estimate the cone factors.

From the two projects 26 triaxial test are conducted, where six tests belong to Project 1 and 20 tests belong to Project 2. A closer investigation of the triaxial tests led to a removal of three triaxial tests from Project 1 and two triaxial test from Project 2. The removal is due to strange behavior in the results of the triaxial tests, which can be caused from fissures in the clay. This is explained in Appendix B along with the derivation of the triaxial shear strength from the triaxial tests.

The triaxial shear strength with the relevant soil parameters belonging to each test are shown in Table 3.1 and Table 3.2. For information about the laboratory test used to determining the soil parameters in Table 3.1, it is recommended to read (DGF's Laboratoriekomitet, 2001).

Table 3.1: Triaxial tests with depth and relevant soil parameters.

Project	**Depth**	**Level**	s_u*	I_p	w_L	w_p	w	Ca
	[m]	DVR90	[kPa]	[%]	[%]	[%]	[%]	[%]
Project 1	17.2	-15.4	105	190.6	240	49.4	43.5	22
	31.2	-29.4	213	185.2	230.5	45.3	41.9	29
	67.2	-65.4	413	218.3	263.5	45.2	43	5
Project 2	21.6	-19.8	245	114	161	47	45	23.4
	23.6	-21.8	303	-	-	-	39	43.1
	25.0	-23.2	197	76	115	39	42.4	-
	30.8	-29.0	359	95	135	40	36	30.1
	35.5	-33.7	281	75	109	34	40.4	40.2
	38.8	-37.0	280	114	152	38	39.3	27.4
	43.6	-41.8	411	152	196	44	46.2	23
	47.5	-45.7	292	-	-	-	50.2	-
	51.3	-49.5	479	-	-	-	41.5	-
	51.8	-50.0	718	151	200	49	45.6	15.4
	55.8	-54.0	346	-	-	-	43.5	27
	60.5	-58.7	338	-	-	-	42	-
	60.9	-59.1	718	123	163	40	35.4	36.5
	64.7	-62.9	276	138	181	43	41	2.4
	69.2	-67.4	325	-	-	-	48.2	3.2
	75.5	-73.7	878	149	206	57	47.1	1.8
	78.0	-76.2	412	-	-	-	48.8	4.9
	82.1	-80.3	453	126	180	54	49.3	1.9

NOTE: * Project 1 used CIU triaxial tests and Project 2 used UU triaxial test to determine the shear strength. I_p: Plasticty index, w_L: liquid limit, w_p: plastic limit, w: water content, Ca: carbonate content, -: data not gathered.

Table 3.2: Extra data belonging to the triaxial tests from Table 3.1.

Project	**Depth**	**Level**	$\boldsymbol{\sigma_{v0}}$	$\boldsymbol{\sigma_{pc}}$*	$\boldsymbol{OCR}$
	$[\mathbf{m}]$	$\mathbf{DVR90}$	$[\mathbf{kPa}]$	[%]	[%]
Project 1	17.2	-15.4	277	500	1.8
	31.2	-29.4	520	5500	10.6
	67.2	-65.4	1168	6200	5.3
Project 2	21.6	-19.8	350	4000	11.4
	23.6	-21.8	386	4000	10.4
	25	-23.2	412	4000	9.7
	30.8	-29.0	516	4000	7.8
	35.5	-33.7	600	5000	8.3
	38.8	-37.0	660	5000	7.6
	43.6	-41.8	745	5000	6.7
	47.5	-45.7	815	5000	6.1
	51.3	-49.5	883	5000	5.7
	51.8	-50.0	892	5000	5.6
	55.8	-54.0	963	5000	5.2
	60.5	-58.7	1048	5000	4.8
	60.9	-59.0	1054	5000	4.7
	64.7	-62.9	1122	5000	4.5
	69.2	-67.4	1204	5000	4.2
	75.5	-73.7	1316	5000	3.8
	78.0	-76.3	1362	5000	3.7
	82.1	-80.3	1434	5000	3.5

NOTE: *$\boldsymbol{\sigma_{pc}}$ is only a minimum value determined for Project 2.
$\boldsymbol{\sigma_{pc}}$: preconsolidation stress, $\boldsymbol{\sigma_{v0}}$: vertical overburden stress, $\boldsymbol{OCR}$: over consolidation ratio.

The Atterberg limits and carbonate content belonging to each triaxial test are determined by looking at the borehole at the depts of where the triaxial test specimens are taken from. If any Atterberg limits or carbonate content is determined within a vertical distance of 1 m, the closest values are assumed to be the same for the triaxial test specimen. For this reason, some of the triaxial tests in Table 3.1 do not have any determined Atterberg limits or carbonate, since no classifications tests has been conducted within a vertical distance of 1 m. The Atterberg limits are explained in Appendix A.2.

The vertical overburden stress in Table 3.2, is calculated with the assumption that the sandy fill has a total unit weight of 20 kN/m^3, which is assumed from (Jensen, 2013). Further 17.7 kN/m^3 is used as total unit weight of Søvind Marl, since this is the mean value determined at the Port of Aarhus.

It is seen that the preconsolidation pressure is not determined precisely, but only a minimum value is determined. This explains the decreasing over consolidation ratio, with depth, which is incorrect. Since the over consolidation ratio is not determined correctly, it cannot be used for determining a dependency with any of the cone factors. Further it is a limitation of the model in equation (1,6) to be used in heavily over consolidated soil, which is the case for Søvind Marl. It is seen in Table 3.2 that Søvind Marl has an over consolidation ratio up to 11.4. This limitation is neglected, but it can indicate that the values of $N_{\Delta u}$ might not be applciable.

4 Determination of cone factors

In this chapter, the cone factors N_K, N_{KT}, N_{ke} and $N_{\Delta u}$ are determined from the CPT data and the triaxial tests. Dependencies among the cone factors and soil parameters are investigated, and hereafter the best cone factor(s) are chosen for further calculations of the undrained shear strength.

4.1 Data processing

Before the CPT data is used, it is processed in four steps, which are shown in Figure 4.1.

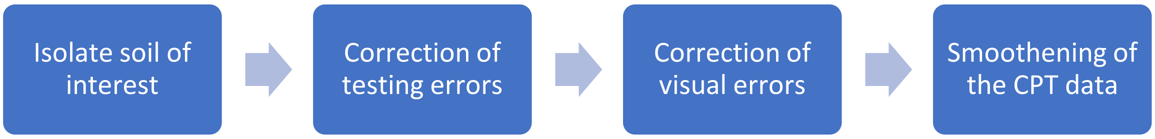

Figure 4.1: Four steps of data processing before the CPT data is used.

The purpose of the data processing is to modify the CPT data to compensate for the errors arose during testing. If these data is not modified or removed, the errors could affect the value of the derived cone factors. The data processing is done for both projects but since Project 2 had the most noticeable modifications, this project is the only one presented in this report. The data processing for Project 1 is presented in Appendix C.1.

4.1.1 Isolate soil of interest

The data processing is conducted in one soil layer at a time and hereafter repeated for the each of the other soil layers which are relevant for a specific project. It is therefore necessary to remove the CPT data that is not relevant for this report, which in this case is the sandy fill. The Søvind Marl is the only soil layer of interest for this report, and since it has been determined to be homogeneous and isotropic, it is treated as one layer. The CPT data from the Søvind Marl is shown in Figure 4.2.

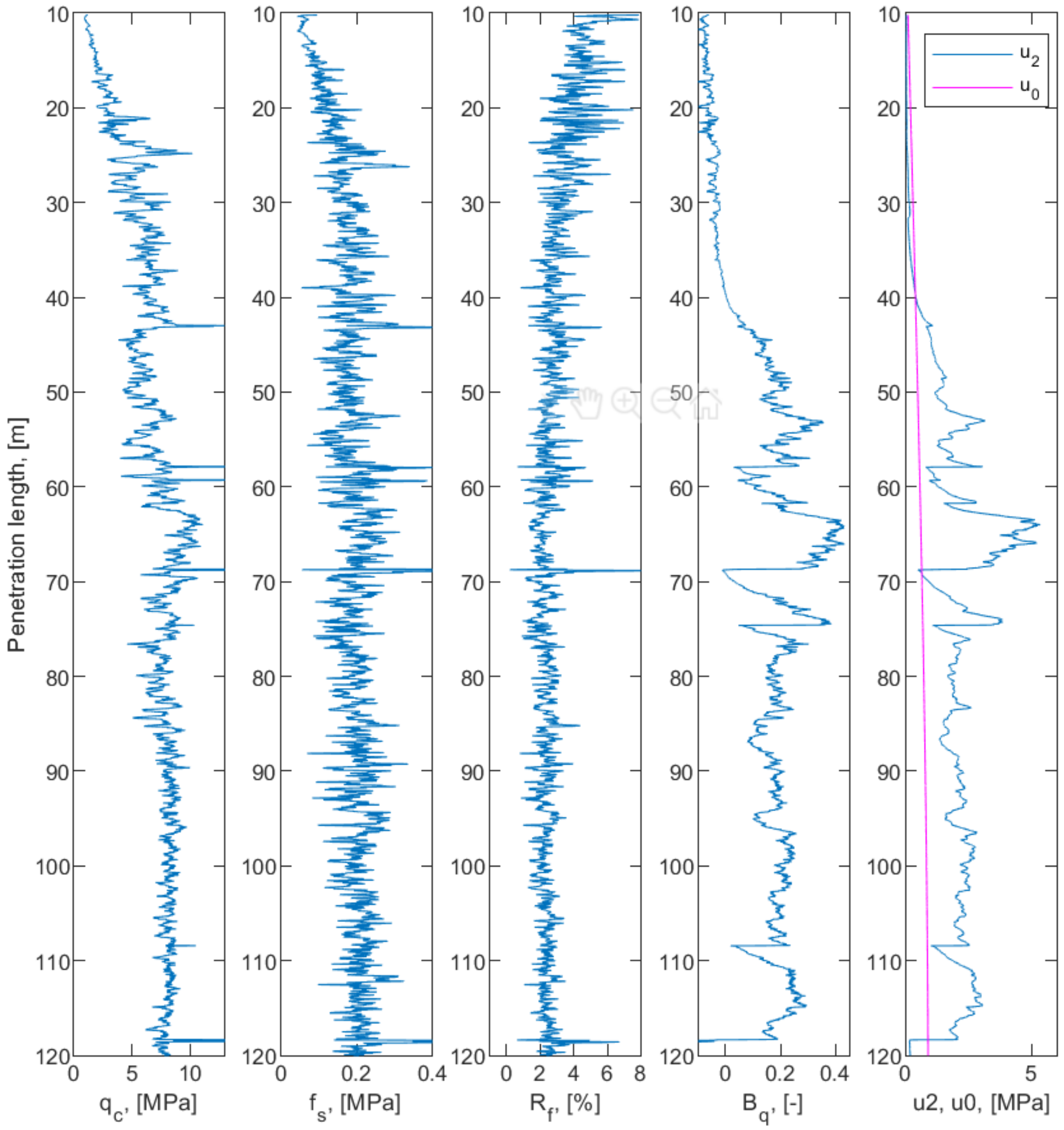

Figure 4.2: CPT data with the sandy fill layer removed for Project 2

4.1.2 Correction of testing errors

Next step is to investigate the CPT data for testing errors. These includes inclination and penetration rate of the cone penetrometer, that deviates from the standard. As determined in the second part of the literature study, these factors could affect the CPT data, and they should therefore be accounted for.

Inclination

The inclination measured for Project 2 is deviating considerable from the vertical axis. The inclination is plotted against the penetration length in Figure 4.3, where it is seen that the inclination is increasing considerably. From (BSI Group, 2013) it is recommended to stop the CPT if the inclination is deviating more than 15 °, from the vertical axis, but this is not done for Project 2. From Figure 4.3 it is seen that the inclination is 15 ° at a penetration length of 35 m and hereafter the inclination is seen to roughly increase linearly.

By knowing the inclination and penetration length, the penetration depth can be calculated. This is already calculated in the given CPT data for Project 2 and the penetration depth is therefore used instead of the penetration length, due to the large inclination. The penetration length of 120 m is therefore corrected to a penetration depth of 90 m.

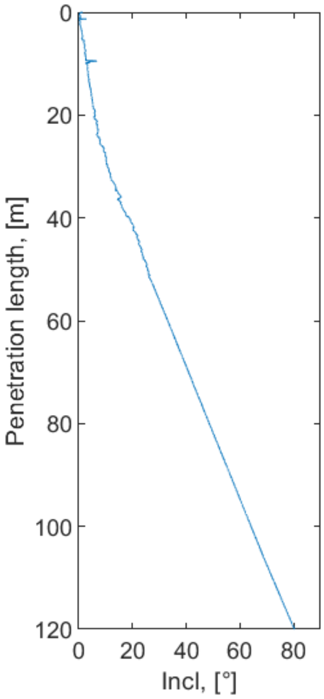

Figure 4.3: The developed inclination, of the cone penetrometer, over the penetration length for Project 2.

Even though the penetration length is corrected to the penetration depth, the measured CPT data could be affected by the inclination. Firstly, the anisotropy of the soil could affect the cone resistance, since soils does not always have the same physical properties in horizontal and vertical direction. Further the sleeve friction is usually only affected by the horizontal earth pressure but since the cone penetrometer has not been vertical, it must be assumed that a combination of the horizontal and the vertical earth pressure affected the sleeve friction.

The CPT data from Project 2 is still used because it is decided to be reasonable, since Søvind Marl is determined to be an isotropic soil. This means that the effect of the inclination on the cone resistance is neglectable. Further the sleeve friction is not used to determine the cone factors, so the parameter is not important for this report. The CPT data is plotted with the penetration dept in Figure 4.4. Hereafter the penetration depth, is only referred to as “depth”.

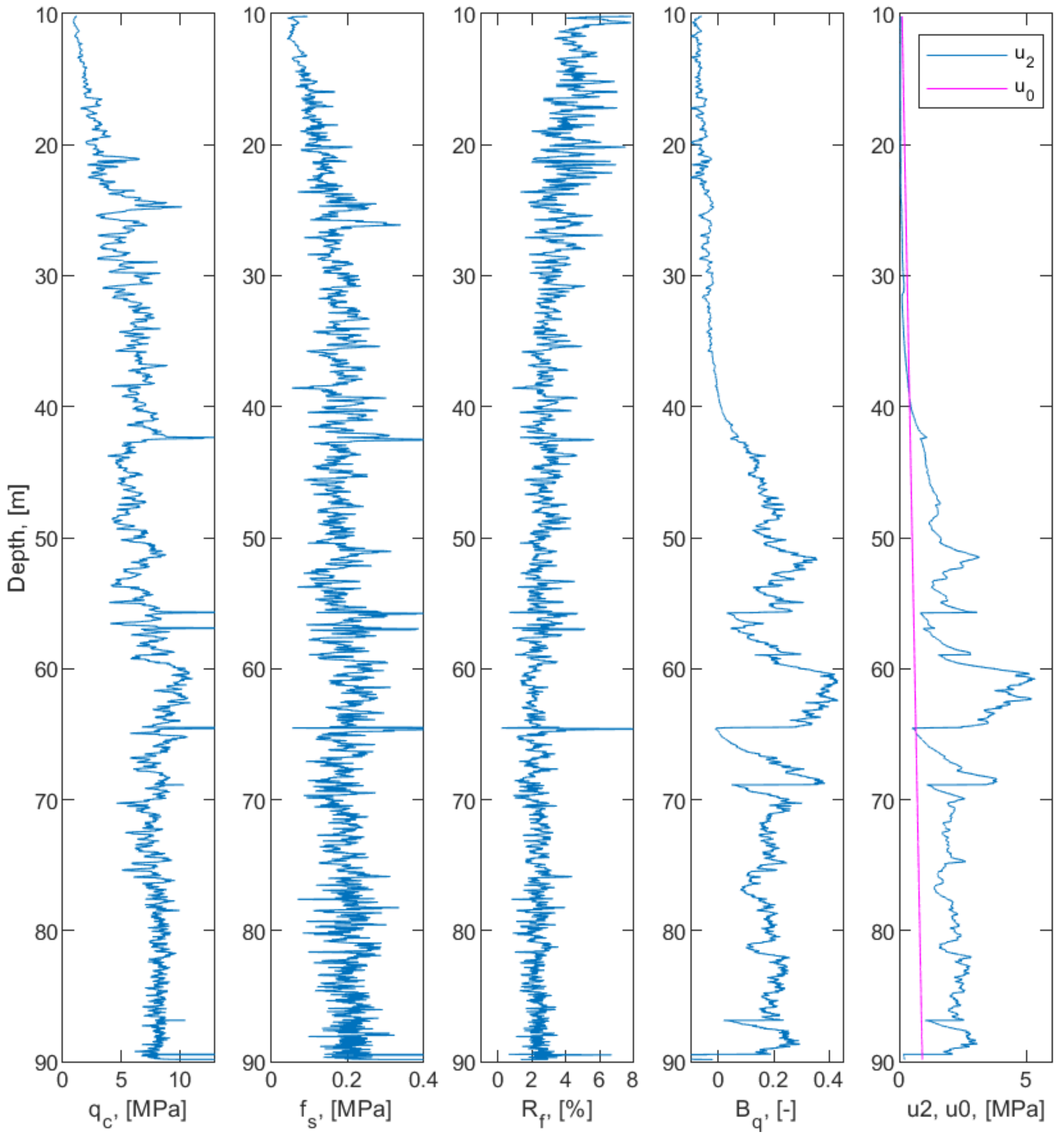

Figure 4.4: CPT data from Project 2 with corrected depth instead of penetration length.

Penetration rate

Project 2 did not have any measurements of the time or the penetration rate. The penetration rate is therefore approximated from the measured penetration length and an assumed sampling frequency. The CPT data is measured per 1.1-1.6 cm with most of the measurements being less than 1.3 cm. By assuming that the contractors tried to penetrate with a rate close to 2 cm/s, an assumed sampling frequency of twice per second, results in a penetration rate of 2.2-3.2 cm/s. The standard allowed the penetration rate to deviate with ±0.5 cm/s, and the CPT data with penetration rates greater than 2.5 cm/s are therefore removed (BSI Group, 2013).

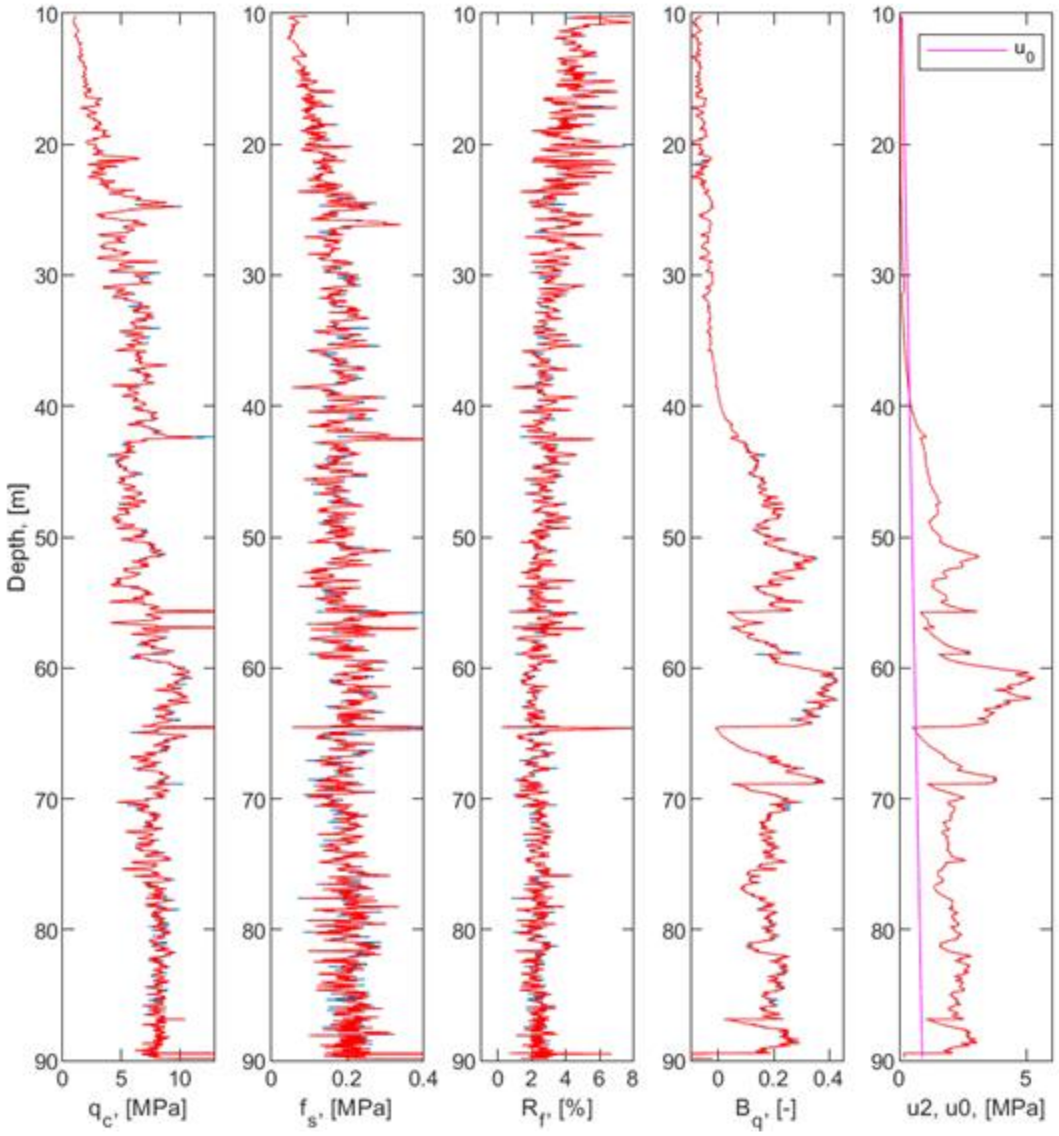

Figure 4.5: CPT data from Project 2 before and after removal of the CPT data with penetration rates greater than 2.5 cm/s. Blue: before removal, red: after removal.

Before the CPT data with penetrations rates above 2.5 cm/s is removed, there are 8664 measurements of each parameter. After the removal, only 3778 measurements are left of each parameter. Thereby approximately 56 % of the CPT data is discarded due to a greater penetration rate than given by the standard. In Figure 4.5 it is seen that a lot of small peaks are reduced, and the before and after measurement in general still coincides. It therefore seems fair to discard 56 % of the measurements, since no greater change is seen in the CPT data.

4.1.3 Correction of visual errors

After removing the CPT data with penetration rates greater than 2.5 cm/s, there are still major peaks and troughs in the cone resistance, sleeve friction and pore pressure. The peaks and troughs deviated considerably from the rest of the measurements, and they are therefore assumed to be errors. It is further seen that, there is a dependency between the peak and troughs. It is seen in Figure 4.5 that when a peak is measured in the cone resistance, the sleeve friciton also peaks, while the pore pressure drops instead. This tendency is for example observed at the depths of 56 m and 65 m. Further a few peaks are observed at the depths of 42 m and 57 m, where no major change is observed in the pore pressure. Since not all peaks and troughs are dependent on each other, these are handled differently. To account for the peaks in the cone resistance and sleeve friction, a threshold is set to 11.2 MPa and 0.33 MPa respectively. If any of the measurements reached the thresholds, the CPT data is removed.

The pore pressure is more challenging to account for, since it is not possible to correct these measurements with a threshold. At the depth intervals of 56-60 m, 64-68 m and 69-70 m it is see that the pore pressure drops drastically. These drops in pore pressure seems to be related to the peaks in the cone resistance and sleeve friction, but unfortunately the drops in the pore pressure are not recovered as quickly as the peaks in the cone resistance and sleeve friction. Instead it takes several meters to recover the drops, which is seen in Figure 4.5. The pore pressure is therefore corrected manually in intervals 56-60 m, 64-68 m and 69-70 m to a constant value.

In the depth interval of 56-60 m, it is seen that the pore pressure dropped twice. Before the first drop, the pore pressure had a value of 2.6 MPa. After each drop, the pore pressure started to recover and reached both times the value of 2.6 MPa or greater. Since the pore pressure reached the value of 2.6 MPa, after each drop, the pore pressure is corrected to a constant value 2.6 MPa in the depth interval of 56-60 m.

In the depth interval of 64-68 m, similar tendency happened as before. The pore pressure dropped and hereafter recovered to 3.5 MPa before it dropped again. The pore pressure is therefore again set to a constant value of 3.5 MPa, since this is the value that the pore pressure recovered to after each drop.

In the last considered depth interval of 69-70, a minor drop is shown. In the interval the pore pressure is set to the constant value of 2 MPa, since the mean value of the pore pressure after the depth of 70 m is relatively close to 2 MPa. The value of the greater pore pressure measured just before the drop is therefore neglected.

The corrections of the peaks and trough in CPT data is shown before and after in Figure 4.6 with blue and red respectively.

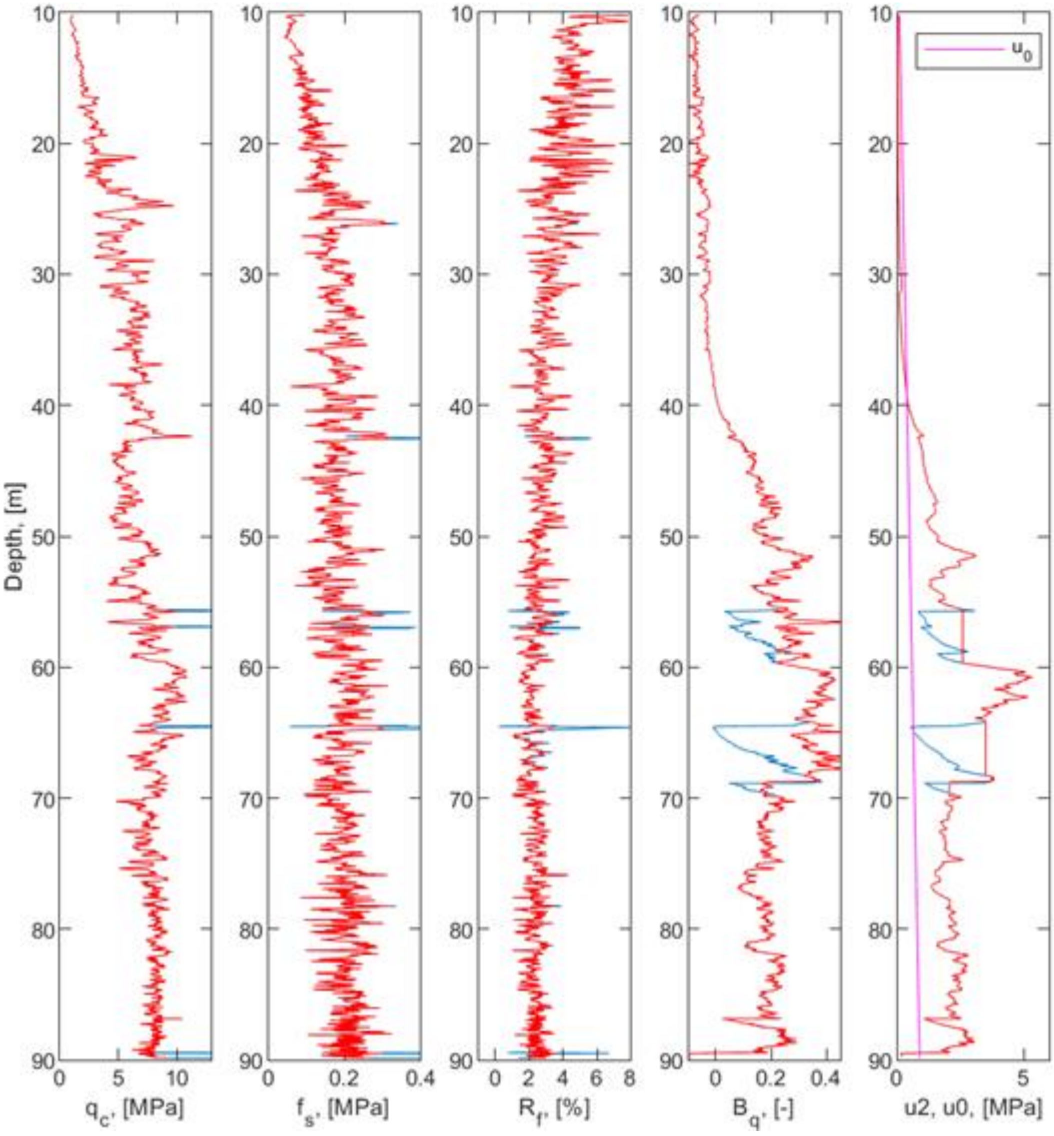

Figure 4.6: Removal of major peaks in CPT data from Project 2. Blue: before removal, red: after removal.

Before the removal of the peaks, there has been 3778 measurements of each parameter and after the removal, there is 3722 measurements. This means that 0.6 % of all the gathered CPT data in Søvind Marl is discarded due to peaks, which is considerably less than the CPT data removed due to greater penetration rate.

In the gathered CPT data, no time is measured, or at least this has not been handed out with the CPT data. For the same reason the penetration rate is not calculated but only assumed. The time is an important measurement to use for explaining the errors that is seen in Figure 4.6. It could have been relevant to investigate the time measurements at the depth between 56- 70 m, where a lot of the peaks and troughs occurs in the cone resistance, sleve friction and pore pressure. It could be assumed, that the CPT is stopped for some time and afterwards started again. During these breaks, the pore pressure could have drained away, and when testing is ressumed, these troughs occurred in the pore pressure, while the cone resistance and sleeve friction peaked. For exploring such errors, messurements of the time is critical.

4.1.4 Smoothening of the CPT data

Prior studies like (Holmsgaard, et al., 2011) and (Alshibli, et al., 2011) smoothens (or averages) the CPT data to account for "unnecessary scatter". The scatter consists of local variations but also great peaks, which has been processed as a separate step in this report. The peaks and troughs are taken care of before the smoothening, since it does not seem reasonable to let the peak values influence the adjacent measurements, when smoothening. The smoothening will therefore only smoothen out the local variations in this report, since the peaks already are removed.

According to (Lunne, et al., 1997), the measurement of the cone is influenced by the soil behind and in front of the cone. The distance in which the soil influenced the cone, is depending on the stiffness of the soil. For soft clays the soil within a sphere with a diameter of 2-3 cone diameters will affect the cone, while in sand the sphere diameter can reach up to 10 or 20 cone diameters.

Since the cone is affected by the soil before and after the cone, within a sphere, it is decided to also smoothen out the variations in the CPT data within the same interval. Søvind Marl is a soft clay and the smoothening is therefore conducted by using a sphere with a diameter of three cone diameters. According to (BSI Group, 2013), the standard diameter of a cone is 35.7 mm, which results in a sphere diameter of approximately 107 mm.

The CPT data is smoothened as it is shown for the cone resistance in Figure 4.7. Two vectors are defined for the cone resistance. The first one is called $q_{c,before}$, which contains all the measured values of the cone resistance. The second vector is called $q_{c,after}$ and this vector contains all the smoothened values of the cone resistance. In Figure 4.7 an example is shown, how the smoothened values are calculated for $q_{c,after}$. To determine a smoothened value in the vector $q_{c,after}$, the center of the sphere is placed at the depth of an observed value, V_i. The averaged value of all the measurements within the sphere, V_{i-3} to V_{i+3}, is placed in the vector $q_{c,after}$ at the same location in the vector, as the value V_i had in $q_{c,before}$. This method is carried out through all the measurements of the cone resistance, and a vector containing all the values of the smoothened cone resistance is hereby obtained. The process is repeated for the sleeve friction and pore pressure.

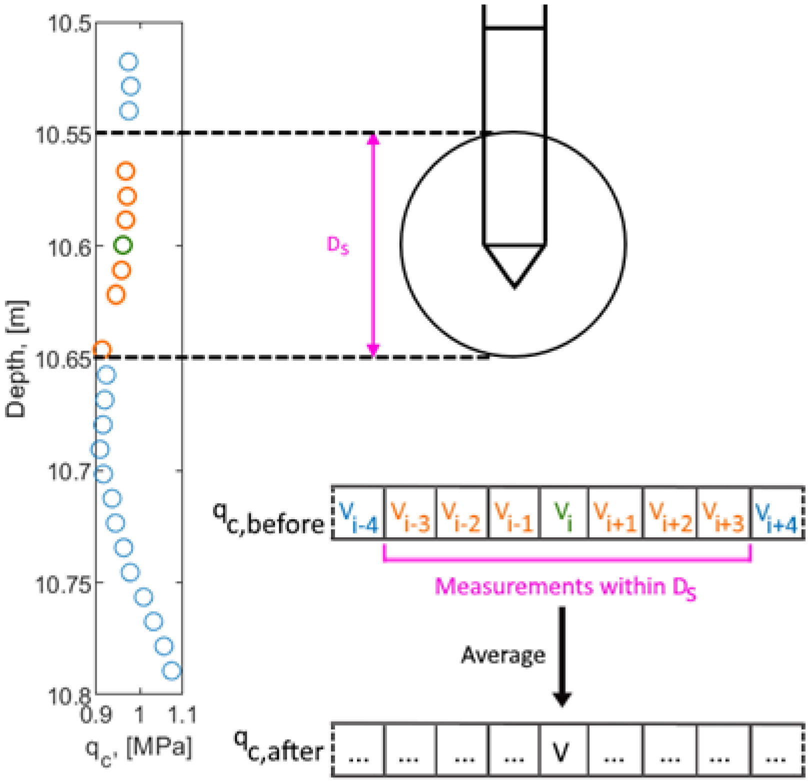

Figure 4.7: Smoothening of the measured cone resistance within the sphere diameter.

In Figure 4.8 the CPT data before and after smoothing is shown with respectively blue and red. It is seen that the smoothening only reduced the variations in the cone resistance and sleeve friction, while no noticeable change is seen in the pore pressure. This makes sense, since the pore pressure does not have as many local variations as the cone resistance and sleeve friction.

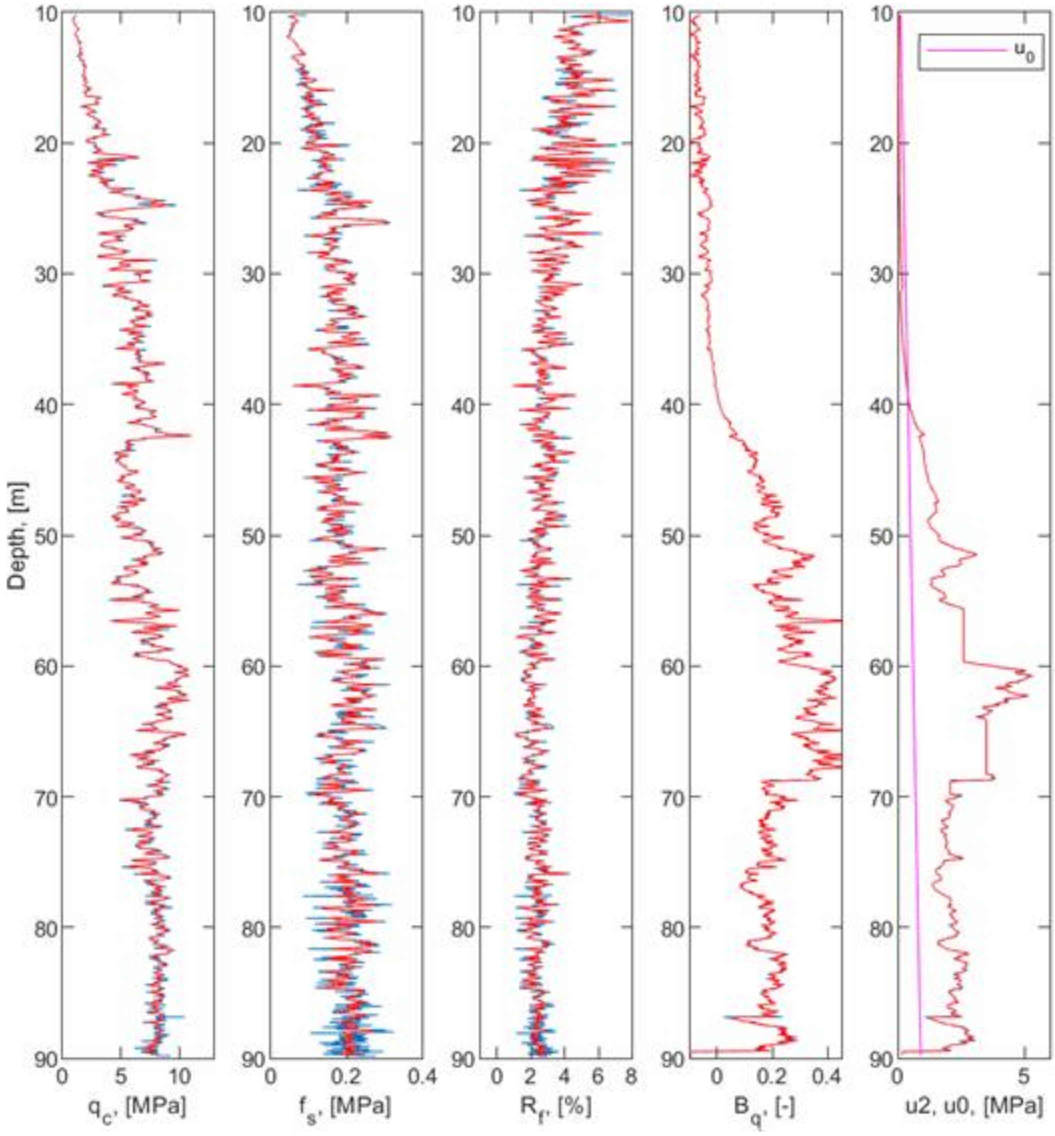

Figure 4.8: Smoothened CPT data from Project 2. Blue: Before smoothing, red: after smoothing.

The smoothening is the last step in the data processing and hereby the modifications in the CPT data can be evaluated. two things are noticeable from correcting the testing errors. The influence of the inclination can be great, which is seen in the difference between the penetration length and penetration depth. Further it is surprising that about 56 % of the CPT data has been removed due to great penetration rates, and no greater changes are seen in the CPT data.

In Appendix C.2, each step of the modified CPT data is shown separately instead of a before and after plot, which has been shown in Figure 4.5, Figure 4.6 and Figure 4.8. After the data processing, the cone factors can be determined.

4.2 Determined values of the cone factors

The cone factors is determined by equation (1,2), (1,4), (1,5) and (1,6) by using a triaxial test as reference test. The CPT data for Project 1 and 2, are shown in Figure 4.9 and Figure 4.10 along with the associated depth of each triaxial test which are shown with horizontal green lines.

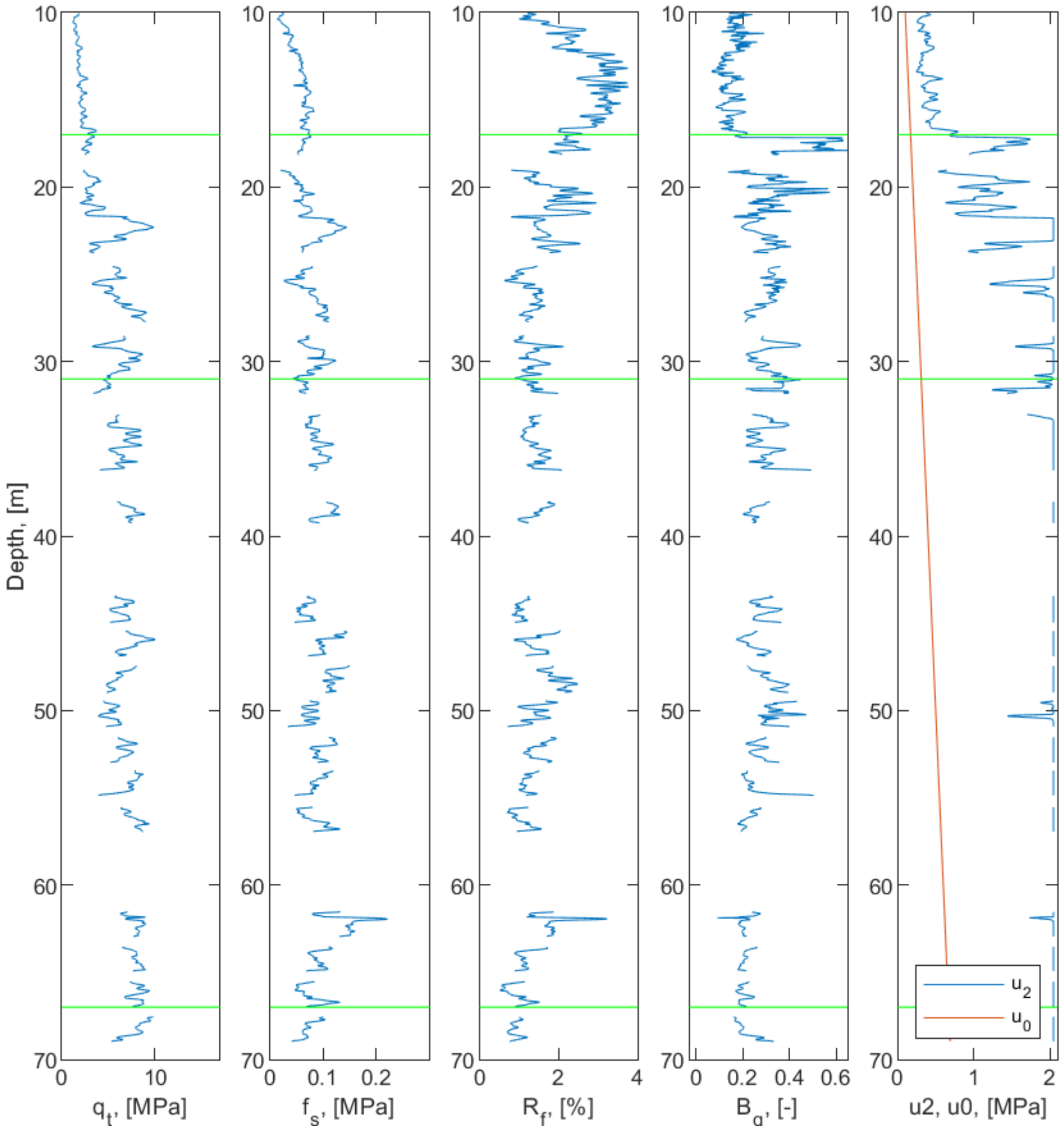

Figure 4.9: Modified CPT data from Project 1, plotted with the associated depth of each triaxial test. Horizontal green line: triaxial test.

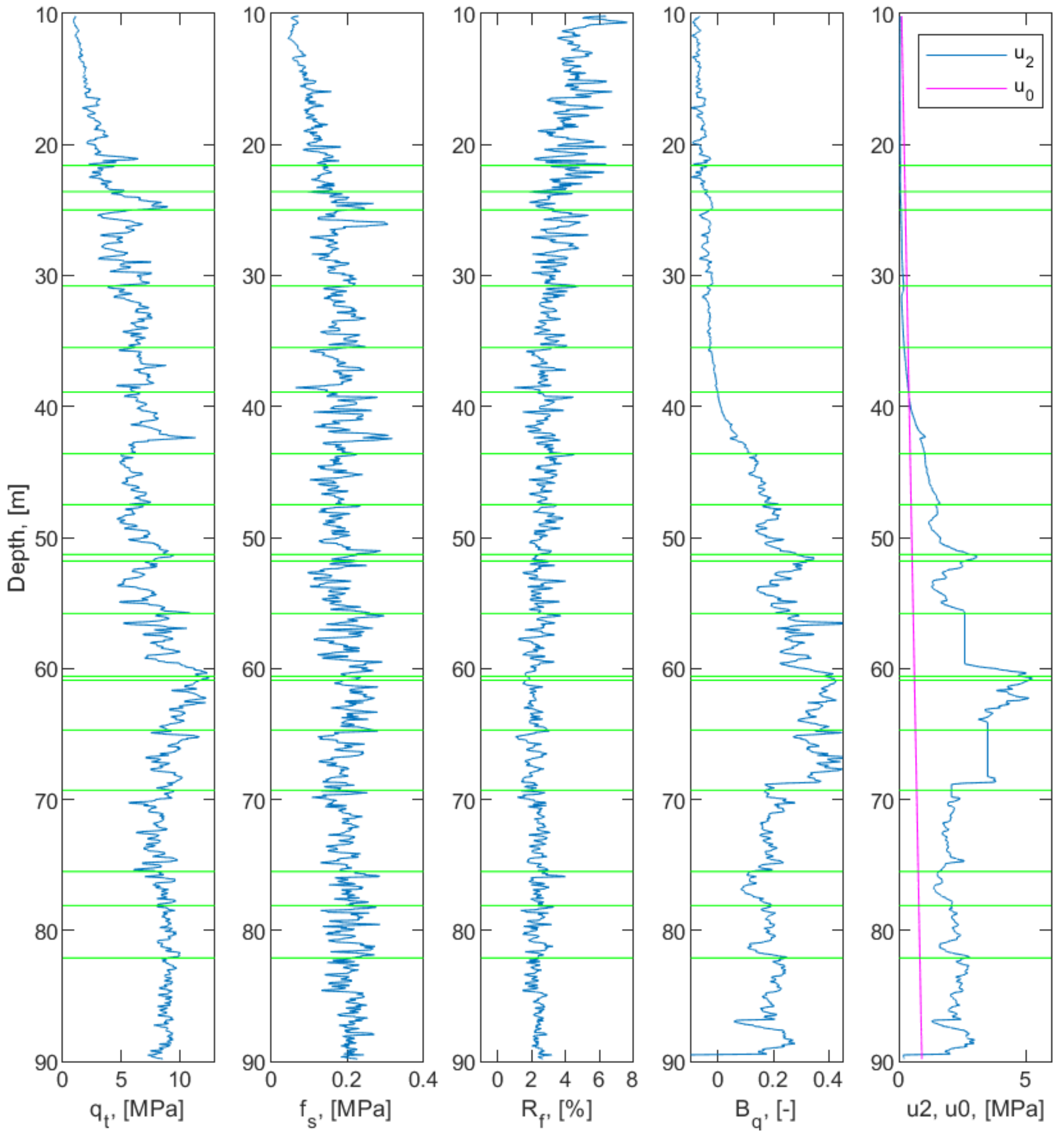

Figure 4.10: Modified CPT data from Project 2, plotted with the associated depth of each triaxial test. Horizontal green line: triaxial test.

Even though the CPT data is smoothened, there are still some variations in the CPT data. It is therefore investigated if these variations affects the derivation of the cone factors. For this investigation, N_K is estimated by using the first triaxial test from Project 2, at the depth of 21.6 m. In Figure 4.11 the measured cone resistance is shown along with the placement of the triaxial test. It is seen that the cone resistance is varying between 2-4.5 MPa, within a vertical distance of around 15 cm.

Five measurements are numbered, and the corresponding cone resistance and vertical overburden stress is given in Table 4.1 along with the mentioned triaxial test that had a triaxial shear strength of 245 kPa. By inserting these values into equation (1,2), a value of N_K is determined by using the corresponding values of each numbered point in Figure 4.11. The respectively determined values of N_K is also shown in Table 4.1 and it is seen that the value varies between 7-17.

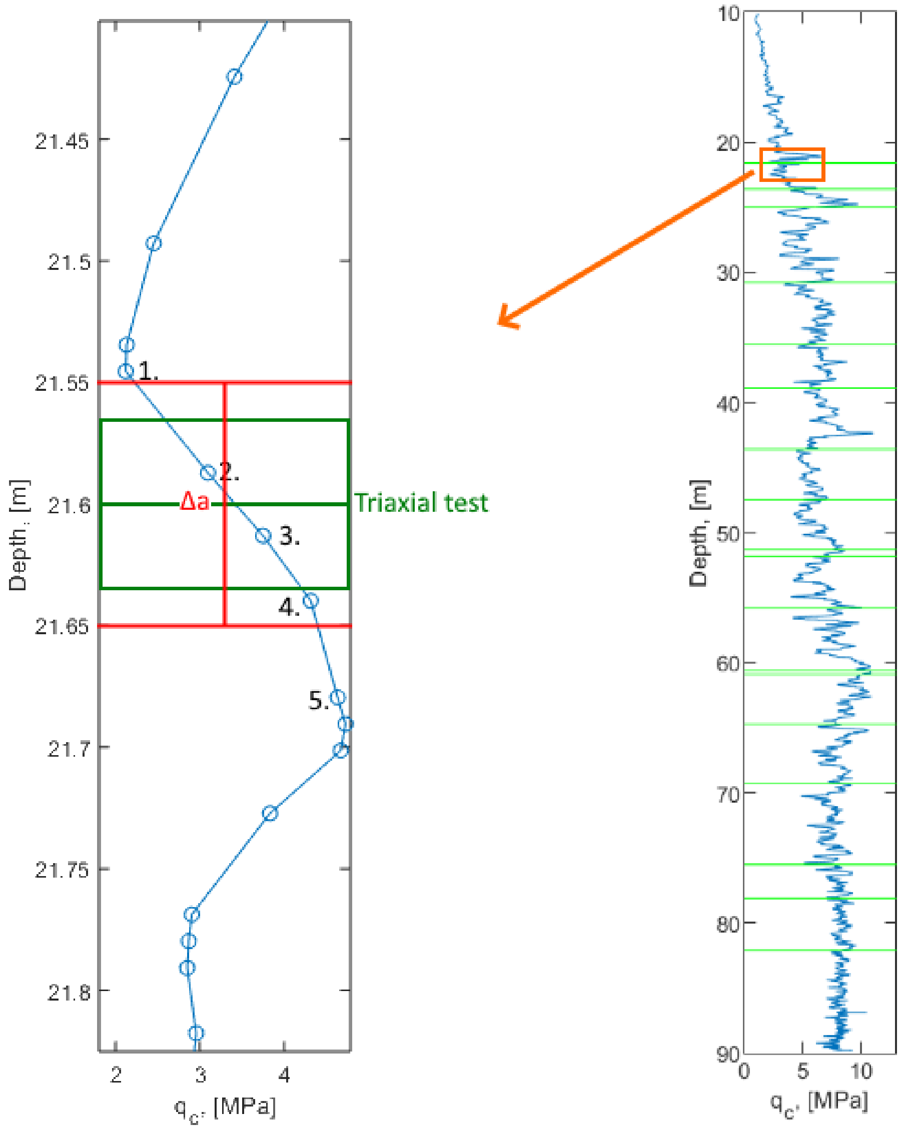

Figure 4.11: The triaxial test from the depth of 21.6 m from Project 2, shown along with nearby measurements of the cone resistance, the interval Δa and the height of the triaxial specimen. In the figure Δa is set with a value of 10 cm, which is an example.

Table 4.1: Estimated values of N_K using the data from each numbered point in Figure 4.11 and the corresponding triaxial strength determined from the depth of 21.6 m in Project 2.

Nr.	q_c [kPa]	σ_{v0} [kPa]	s_u [kPa]	N_K [-]
1.	2121	405	245	7
2.	3097	406	245	11
3.	3751	406	245	14
4.	4317	407	245	16
5.	4637	407	245	17

It does not seem reasonable to insert one measured value of the cone resistance with the corresponding vertical overburden stress into equation (1,2), since the cone resistance can vary with more than 100 % over a 15 cm distance. Further the triaxial test specimen has a height of 7 cm and to have a reasonable comparison between the CPT data and the triaxial test in equation (1,2), several measurements should be included for representing the cone resistance.

It is therefore decided to use an averaged value of the cone resistance for determining N_K. A vertical interval, Δa, is introduced to determine the number of measurements that should be averaged before inserted into equation (1,2). The center of the interval, Δa, coincides with the center of the triaxial test specimen, which is shown in Figure 4.11.

By looking through the gathered triaxial test in Table 3.1, it is seen that the triaxial shear strength gathered for Project 2, are varying considerably over small distances. By looking at the triaxial strength determined at the depths of 51.3 m and 51.8 m, the triaxial shear strength goes from 479 kPa to 718 kPa. That is an increase of about 50 % over a 50 cm distance. By looking at the determined shear strength at the depths of 60.5 m and 60.9 m, it is seen that the triaxial shear strength goes from 338 kPa to 718 kPa, which is an increase of more than 100 % over a 40 cm distance. The interval Δa should therefore not have a size close to 40 cm, since it is seen that the triaxial tests, can vary considerably over such short distances. Δa is investigated in Appendix C.3, where the size of the interval is varied. From the appendix, it is determined that the cone factors are least affected by the used CPT measurements when Δa is equal to 16 cm. This seems reasonable, since the height of Δa should not be much greater than the height of the triaxial test specimen in order to have a reasonable comparison between the triaxial test and CPT data.

The method of using Δa for averaging the cone resistance is also used for the corrected cone resistance and the pore pressure before inserting the measurements into equation (1,2), (1,4), (1,5) and (1,6),. The values of the vertical overburden stress and hydrostatic pressure are the ones belonging to the depths of the triaxial tests. By using Δa for the CPT measurements, the cone factors determined through equation (1,2), (1,4), (1,5) and (1,6), are less sensetive towards variations in the used parameters. It is hereafter possible to derive the cone factors, and these are shown in Table 4.2. An example of calculating each cone factor is shown in Appendix E.1.

Due to the poorly measured pore pressure between the depth of 10-40 m in Project 2, the six derived values of $N_{\Delta u}$ becomes negative. These values are neglected, since they are influenced by the poor measurements and they are therefore not representable. Further it is assumed that the first six values of N_{ke}, determined for Project 2, are influenced by the poorly measured pore pressure. This is assumed since, the pore pressure is directly used in equation (1,5) as it is for $N_{\Delta u}$ in equation (1,6). The six values of N_{ke} determined between 10-40 m are therefore also neglected. The neglected values are marked in Table 4.2 with orange.

No values of N_K and N_{KT} are neglected, since the pore pressure is not included in equation (1,2) and it is only partly included through the corrected cone resistance in equation (1,3). It is therefore assumed that the pore pressure only has a minor effect on the derived values of N_{KT}.

Table 4.2: Cone factors determined for Project 1 and 2.

	Depth	N_K	N_{KT}	N_{ke}	$N_{\Delta u}$
	[m]	**[-]**	**[-]**	**[-]**	**[-]**
Project 1	17.2	23.6	26.2	22.6	5.1
	31.2	16.6	19.8	12.9	8.1
	67.2	13.8	15.8	13.8	3.3
Project 2	21.6	12.0	13.8	15.3	-0.7
	23.6	15.7	14.1	15.4	-0.6
	25.0	27.2	28.6	30.5	-0.9
	30.8	11.6	12.3	13.4	-0.4
	35.5	19.1	18.0	19.6	-0.5
	38.8	20.3	20.0	21.2	-0.0
	43.6	10.6	11.4	10.9	1.4
	47.5	16.1	19.7	17.4	3.6
	51.3	15.3	16.9	13.0	4.8
	51.8	8.0	9.1	6.9	2.9
	55.8	21.4	21.9	17.4	5.8
	60.5	26.9	31.4	20.6	12.3
	60.9	12.5	14.9	9.4	6.3
	64.7	24.5	26.3	17.9	10.3
	69.2	22.4	24.1	21.5	4.3
	75.5	7.0	7.3	7.1	0.9
	78.0	15.5	17.2	15.6	3.1
	82.1	14.5	16.9	14.6	3.8

The interval for each cone factor is summarized in Table 4.3 along with cone factors determined from prior studies, which has been presented in the literature study. It is seen that the determined values of the cone factors within this report, varies considerably more than the prior studies conducted in Søvind Marl. The prior values of N_K has been determined by using the shear vane test as reference test, and this is assumed to be the reason of the low values of N_K. Further if not many reference tests are conducted, it is not possible, to determine several values of N_K and thereby the interval is narrower.

For N_{KT} the prior determined values are in a narrower interval than the values determined within this report. Seven triaxial test are conducted in the study and compared to 21 triaxial test used in this report, it can be expected to determine a narrower interval of N_{KT}. No prior values of N_{ke} and $N_{\Delta u}$ are determined in Søvind Marl, so no comparison can be made.

The determined cone factors seem to lay within a wide interval compared to prior studies in Søvind Marl, but by comparing with another study conducted in Holocene clay, it is seen that such a wide interval of values for the cone factors has been determined before. From the literature study, the cone factors have been determined in Holocene clay from 22 triaxial test. From Table 4.3 it is seen that the values of the cone factors, determined in this report, coincide well with the intervals determined for Holocene clay. The only difference is that cone factors in this report have slightly lower values than the determined values in Holocene clay. The determined intervals of the cone factors in this report therefore seems reasonable, since similar intervals are determined in another soft clay.

Table 4.3: Summery of determined interval of cone factors in this report and prior studies of Søvind Marl and Holocene clay.

Cone factor	**Søvind Marl**	**Prior studies in Søvind Marl**	**Prior studies in Holocene clay**
N_K	7-27.2	6.0-7.6*	10.5-27.6
N_{KT}	7.3-31.4	20-30	11.9-32.1
N_{ke}	6.9-22.6	-	10.9-28.6
$N_{\Delta u}$	0.9-12.3	-	1.8-13.1

*Shear vane test is used as reference test

4.2.1 Dependencies between the cone factors and other parameters

From Table 4.2 it is seen that each cone factor varies considerably in the soil. This is the reason, why determination of a cone factor for calculating the undrained shear strength is problematic, since only one value can be calculation. An example of calculating the undrained shear strength with different values are shown in Appendix E.2. From the example in Appendix E.2, it is seen that the chosen value of the cone factor, has a great impact on the calculated value of the undrained shear strength and it is therefore important to determine a representable value.

An alternative of choosing one value, is to determine a dependency between the cone factors and a parameter. The value of the cone factor can hereby be varied, if a dependency is found. An example is that the values of the cone factors can increase with dept, or it is dependent on the plasticity index of the soil. If one dependency is determined between a cone factor and another parameter, that does not mean that the same dependence is applicable for the other cone factors.

From the literature study, prior dependencies have been determined between some of the cone factors and parameters such as the pore pressure ratio and plasticity index. These are therefore relevant to investigate, along with several other parameters. This is done by plotting the cone factors from Project 2 against different parameters. In Figure 4.12 and Figure 4.13 the pore pressure ratio and friction ratio are plotted against the cone factors, while several other parameters are plotted against the cone factors in Appendix C.4.

In Figure 4.12, it is seen that there is a linear dependency between the pore pressure ratio and $N_{\Delta u}$. This is also expected since earlier studies had determined such a relation in other soft clays. Besides this dependency, no other has been determined with regards to the friction ratio or the other parameters shown in Appendix C.4.

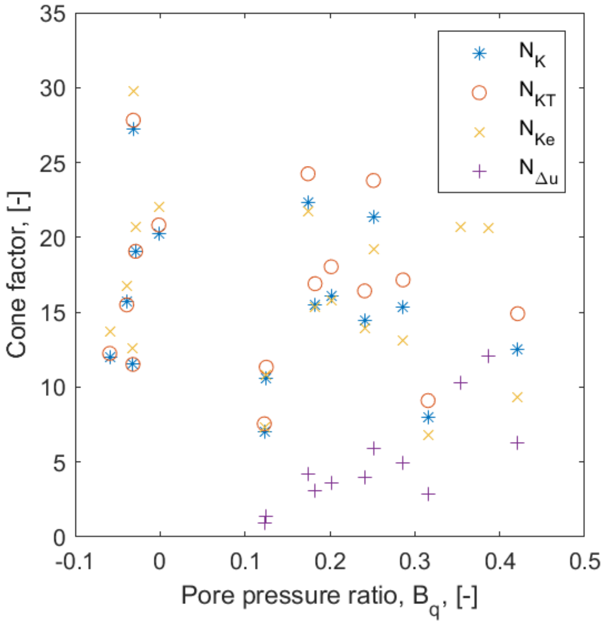

Figure 4.12: Relation between cone factors and pore pressure ratio for Project 2

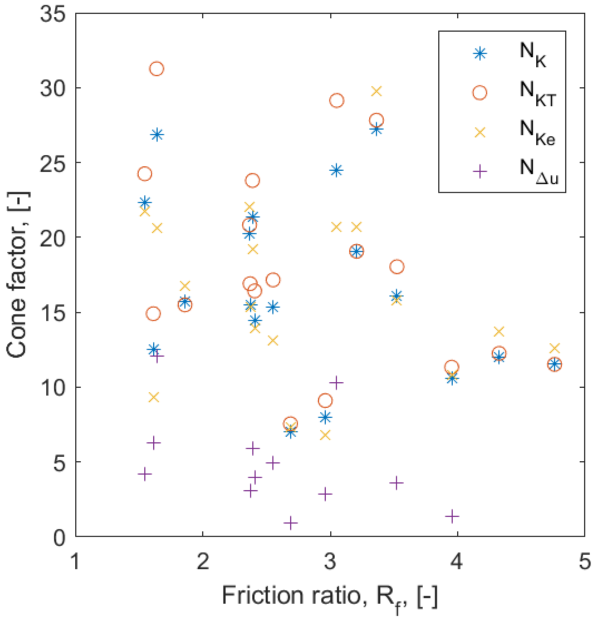

Figure 4.13: Relation between cone factors and friction ratio for Project 2.

In Project 1, only three cone factors are determined. No dependencies are therefore looked for, but it is assumed that the dependencies determined from Project 2 are also valid for Project 1. In Figure 4.14 the derived values of $N_{\Delta u}$ from Project 1 and 2 are plotted against the pore pressure ratio, and by doing a regression analysis, it is seen that the dependency seems to be the applicable for both Project 1 and 2.

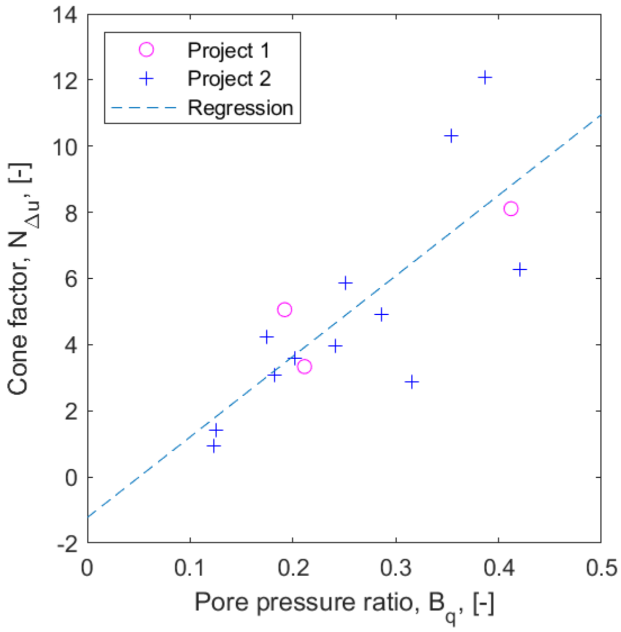

Figure 4.14: Determined linear dependency between pore pressure ratio and $N_{\Delta u}$ with selected measurements from Project 1 and 2.

The equation of the regression line is given in equation (4,1) and the coefficient of determination is $R^2 = 0.69$.

$$N_{\Delta u}(B_q) = 24\,B_q - 1.2 \tag{4,1}$$

Where

B_q	Pore pressure ratio	$[-]$

The equation of the regression is useful, since it can be inserted into equation (1,6), and thereby the undrained shear strength can be estimated from the pore pressure ratio. This is favorable, since the pore pressure ratio changes through the depth and thereby includes the variation in the soil that might affect the changing values of $N_{\Delta u}$. An alternative is to use a constant value of $N_{\Delta u}$ in equation (1,6), but as it is seen in Table 4.3, the value of $N_{\Delta u}$ varies between 0.9-12.1, and depending on the chosen constant value of $N_{\Delta u}$, the estimated undrained shear strength would either be over or underestimated.

No dependencies are determined for the other cone factors, which means that a constant value must be determined for the other cone factors. This constant value can be expected to lay within the intervals shown in Table 4.3, but this is investigated in the next chapter, where the characteristic undrained shear strength is estimated.

5 The characteristic undrained shear strength

The standard procedure in EN1990, Annex D (DS/EN, a, 2007), is used to estimate the characteristic shear strength. To determine a characteristic value, the different uncertainties must be considered. The uncertainties are divided into four types (Sørensen, 2004):

The physical uncertainty: is related to the natural randomness of a quantity, for example the undrained shear strength in clay.

The measurement uncertainty: is caused by imperfections in measurements of for example a geometrical quantity.

The statistical uncertainty: is caused by a limited number of tests for the observed quantity.

The model uncertainty: is related to imperfect knowledge or idealization of a mathematical model used to estimate a quantity, e.g. the bearing capacity.

In this report, the measurement uncertainty is assumed to be neglectable and is not considered, since the gathered data from Project 1 and 2 are measured by other contractors. To estimate the characteristic shear strength, the process is divided into three steps which are shown in Figure 5.1.

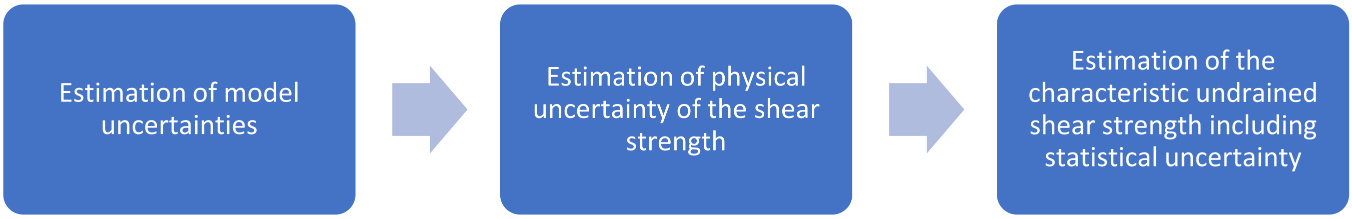

Figure 5.1: The proces of determining the undraind shear strength.

The model uncertainties are considered from the models given in equation (1,2), (1,4), (1,5) and (1,6). Here the uncertainty of each model is determined and further a representable value of each cone factor is determined. Hereafter the physical uncertainty of the shear strength is considered. The physical uncertainty is expressing the variation of the shear strength and by considering a specific geotechnical structure, the physical uncertainty can be reduced depending on the size of the geotechnical structure. Lastly, the characteristic shear strength is determined by including three of the mentioned uncertainties above. The statistical uncertainty is shortly explained, and it is therefore presented in the last step along with calculating the characteristic shear strength.

It is stated earlier that equation (1,2), which uses N_K, cannot take the effect of the pore pressure on the cone resistance into account. Søvind Marl is a soft clay and the pore pressure is in the same magnitude as the cone resistance. It is therefore important to account for the pore pressure, which equation (1,4) does. Equation (1,4), which uses N_{KT} is therefore better than equation (1,2), and the model in equation (1,2) is therefore discarded in the rest of this report. Thereby the model uncrtainty is only determined for the three models given in equation (1,4), (1,5) and (1,6) with their respectative cone factor.

5.1 Estimation of model uncertainties

For determining the model uncertainties, the experimental and theoretical results are compared. The experimental results are the undrained shear strengths determined by the triaxial test. It is assumed that the triaxial test determines the true undrained shear strength, and no errors influences these results. The theoretical results are the undrained shear strengths determined by the models in equation (1,4), (1,5) and (1,6). The relation between the experimental and theoretical results is shown in equation (5,1).

$$f_e = b\ \Delta\ h_t \tag{5,1}$$

Where

f_e	Experiment results from triaxial test	[kPa]
b	Bias	[−]
Δ	A Lognormal distributed stochastic variable with mean 1 and coefficient of variation, V_Δ	[−]
h_t	Theoretical results from equation (1,4), (1,5) and (1,6)	[kPa]

The coefficient of variation, V_Δ, for the stochastic variable Δ, is a measure if the model uncertainty is high or low. Coefficient of variations at the value of around 0.2 or lower is seen as good, while values of 0.5 and above are high model uncertainties.

The coefficient of variation and bias is determined in Appendix D.1 for all three models. Further the representative value of N_{KT} and N_{ke} is determined by a trial and error method, until the associated bias is one. If the bias is greater than one, it means that the models are underestimating the shear strength, and further, when calculating the characteristic shear strength, the bias will compensate for the underestimation. Therefore, if the bias is equal to one, the determined values of N_{KT} and N_{ke} are representable for the Søvind Marl, and these values can therefore be used for further studies.

A representable value of $N_{\Delta u}$ is not determined in Appendix D.1, since a dependency has been determined with the pore pressure ratio which is shown in equation (4,1). This dependency is therefore inserted into equation (1,6) instead of a value of $N_{\Delta u}$. In Table 5.1 the calculated bias, V_Δ and values of N_{KT} and N_{ke} are shown.

Table 5.1: Estimated bias and model uncertainties for equation (1,4), (1,5) and (1,6) along with representable values of N_{KT} and N_{ke}.

	Equation (1,4)	**Equation (1,5)**	**Equation (1,6)**
Cone factor	$N_{KT} = 17.1$	$N_{ke} = 13.1$	$N_{\Delta u} = 24\ B_q - 1.2$
b	1.00	1.00	1.15
V_Δ	0.40	0.40	0.37

From the table it is seen that the bias of equation (1,6) is greater than one, because the trial and error method has not been used for determining the value of $N_{\Delta u}$, but the dependency from equation (4,1) has been used instead.

It is seen that the coefficient of variation is almost the same for all the models, and a difference of 0.03 is therefore neglectable. The value of 0.4 is a relatively high coefficient of variation, and since all the values are in the same magnitude, none of the models seems to be preferable than the others with regards to the model uncertainty. If the coefficient of variation deviated with more than 0.1 between the different models, then the difference could not have been neglected and the model with the lowest coefficient of variation would have been preferred.

The values of N_{KT} and N_{ke} which are calibrated so the bias is one, are determined to be 17.1 and 13.1 respectively. By calculating the mean values of the determined values in Table 4.2, it is seen that these are 18.4 and 14.8 respectively, and therefore 17.1 and 13.1 seems as reasonable values to represent the for N_{KT} and N_{ke}.

The experimental results and the theoretical results are plotted together in Figure 5.2 to Figure 5.4, where the y-coordinate and x-coordinate is respectively the experimental and theoretical results of the points. The theoretical results are obtained by equation (1,4), (1,5) and (1,6) with the used cone factors shown in Table 5.1. The slope of the dashed line is equal to the bias, which ideally should be equal to 1, which means that the mean values of the theoretical and experimental results are equal. Further, if the experimental and theoretical results are equal, the points would have been on the dashed line, but due to the model uncertainties this is not the case. It should be noted that Figure 5.3 and Figure 5.4 have six points less than Figure 5.2 because some of the calculated cone factors have been discarded in Table 4.2 due to the poorly measured pore pressure.

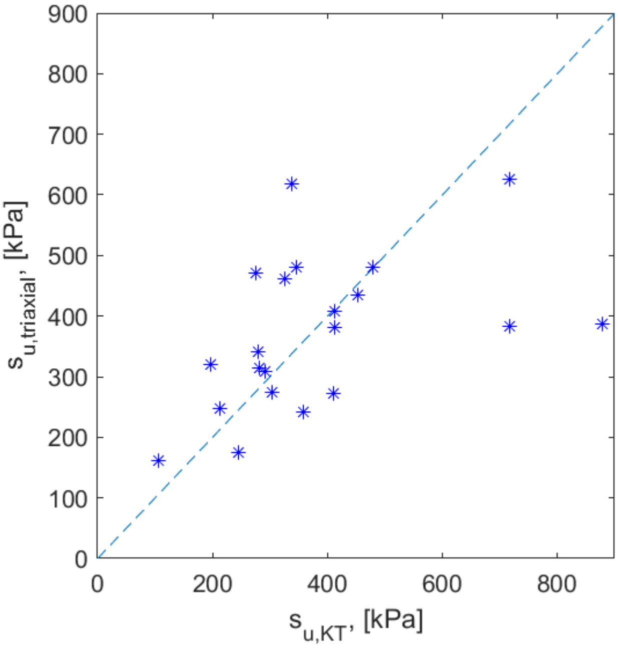

Figure 5.2: Comparison of the experimental and theoretical results determined from equation (1,4) and Table 5.1.

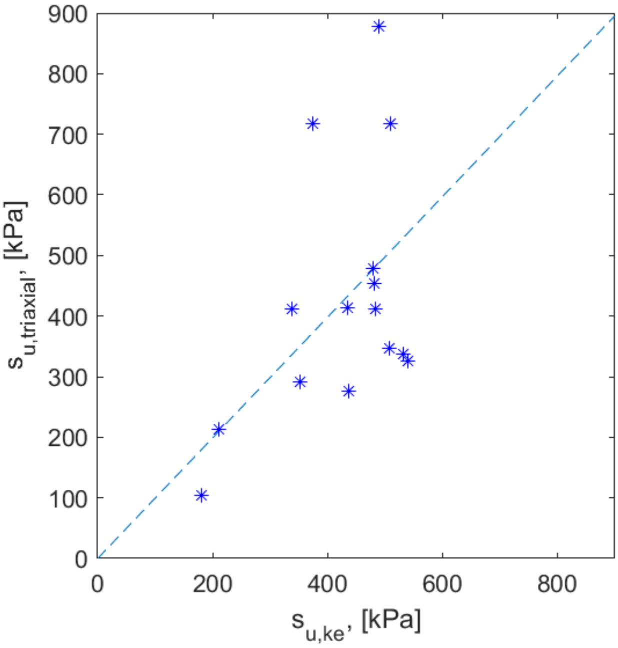

Figure 5.3: Comparison of the experimental and theoretical results determined from equation (1,5) and Table 5.1.

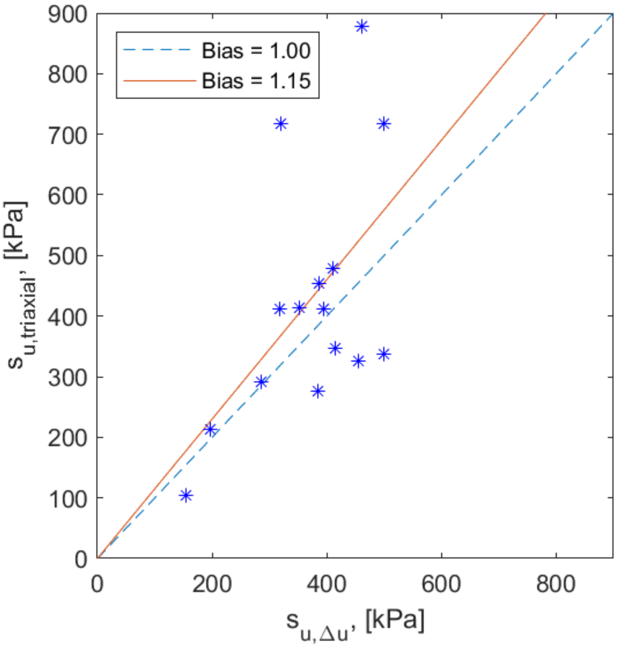

Figure 5.4: Comparison of the experimental and theoretical results determined from equation (1,6) and Table 5.1.

Since the three models are equally good with regards to the coefficient of variation, only one model is chosen for estimating the characteristic shear strength. It has been stated above, that equation (1,4) is not strongly affected by the poorly measured pore pressure, since the pore pressure is only included through the corrected cone resistance. Further, the models in equation (1,5) and (1,6) are more likely to be affected by the poor measurements, which is seen on the derived values of $N_{\Delta u}$ determined before the depth of 40 m in Table 4.2. This does not mean that the models are poor, compared to equation (1,4), but due to the gathered data, the models are not applicable in this report at depths before 40 m. For this reason, the model in equation (1,4), using $N_{KT} = 17.1$, is used for estimating the characteristic undrained shear strength.

5.2 Estimation of physical uncertainty of the shear strength

The physical uncertainty is expressing the natural variability of a quantity in the soil, which for this report is the undrained shear strength that is relevant to investigate. The uncertainty is represented through the coefficient of variation, V_h, of the shear strength, which should not be confused with the coefficient of variation, V_Δ from the model uncertainty, which has been presented in the above section.

The coefficient of variation, V_h, is determined as shown in equation (5,2), from the standard deviation and mean value of the undrained shear strength. It is therefore expressing the variations in the undrained shear strength and if the coefficient of variation, V_h, is high, then the physical uncertainty of the shear strength is high. Further if the coefficient of variation, V_h, is low then the physical uncertainty is also low.

$$V_h = \frac{\sigma_{su}}{\mu_{su}} \qquad (5,2)$$

Where

σ_{su}	Standard deviation of the measured undrained shear strength	$[\text{kPa}]$
μ_{su}	Mean value of the measured undrained shear strength	$[\text{kPa}]$

The mean value and standard deviation of the undrained shear strength can be determined from laboratory tests such as triaxial tests. Since this report has a limited amount of conducted triaxial tests, the coefficient of variation, V_h, is determined from prior studies, where it is assumed that a greater number of tests has been used. According to (JCSS PMC, 2002), the coefficient of variation, V_h, for the undrained shear strength ranges in the interval of 0.1-0.4, where 0.1 is a low uncertainty and 0.4 is a relative high uncertainty. Since Søvind Marl is determined to be homogeneous and isotropic, a low value of the coefficient of variation, V_h, seems reasonable, but if the derived cone factors in Table 4.2 are considered, a lot of variations is observed, so the Søvind Marl does not seem to be as homogeneous as assumed. Therefore, the value of V_h is chosen to be 0.2, which is close to the middle of the interval from (JCSS PMC, 2002).

5.2.1 Reduction of the physical uncertainty due to a size effect

The coefficient of variation, V_h, is often determined by testing devices that has characteristic dimensions in the magnitude of some centimeters to a few decimeters. The soil volume affected by these characteristic dimensions are relatively smaller compared to the soil volume affected by a geotechnical structure, and the coefficient of variation, V_h, is therefore only representing the variation in the undrained shear strength "from point to point" (JCSS PMC, 2002). This is also described in (DS/EN, b, 2007) where the following text is taken from:

"(7) The zone of ground governing the behaviour of a geotechnical structure at a limit state is usually much larger than a test sample or the zone of ground affected in an in situ test. Consequently the value of the governing parameter is often the mean of a range of values covering a large surface or volume of the ground. The characteristic value should be a cautious estimate of this mean value."

For the bearing capacity of a geotechnical structure in clay, it is the mean value of the undrained shear strength along the failure surface, that is essential instead of the soil volume. By increasing the size of the geotechnical structure, the failure surface increases and thereby the characteristic mean value of the undrained shear strength. The coefficient of variation, V_h, from (JCSS PMC, 2002) is overestimated, since the size effect is not accounted for and it should therefore be reduced depending on the size the failure surface.

(JCSS PMC, 2002) presents a method to account for the size effect, due to a lager geotechnical structure, by reducing the coefficient of variation, V_h. The equation of the reduced coefficient of variation is shown in equation (5,3).

$$V_{h,red} = V_h \, \Gamma \tag{5,3}$$

Where

$V_{h,red}$	Reduced coefficient of variation due to the geotechnical structure affecting a large soil volume	$[-]$
V_h	Coefficient of variation for the undrained shear strength for a small reference volume	$[-]$
Γ	Reduction factor depending on the size of the geotechnical structure.	$[-]$

The reduction factor, Γ, is depending on the ratio between the size of the failure surface and the correlation length, D. The correlation length is the distance over which a soil property can be assumed to be the same. In this report it is the distance over, which the undrained shear strength can be assumed the same. The correlation length varies considerably depending on the direction. According to (JCSS PMC, 2002) the correlation length can be in the magnitude of 1 m for the vertical direction and 10 m or more in the horizontal direction for undrained shear strength. The difference can be assumed to be found in the way that the clay has been deposited. The clay has been deposited in horizontal layers over time, and horizontal variation is therefore minimal, while the vertical variation is much greater.

The size of failure surface can be evaluated as one-, two-, or three-dimensional problems. For this report a one-dimensional problem is considered, where the geotechnical structure is chosen to be a pile with the length, L. This is illustrated in Figure 5.5 where the pile is installed at the Port of Aarhus and the sandy fill has been removed.

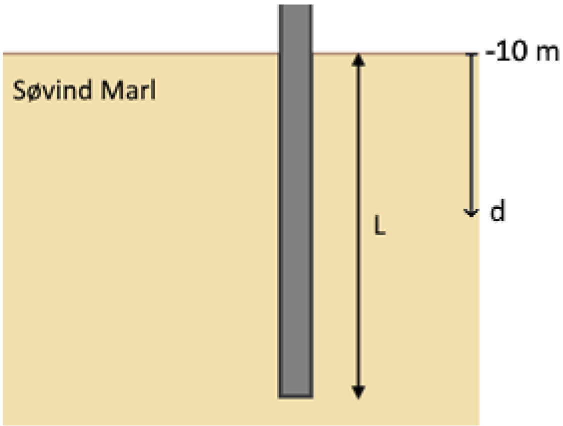

Figure 5.5: A pile with the length, L, into the Søvind Marl at the Port of Aarhus.

By varying the length of the pile, the failure surface is varied, and it is hereby possible to investigate the size effect upon the physical uncertainty. Since it is the length of the pile that is varied, the one-dimensional problem is considered in the vertical direction. The reduction factor, Γ, is therefore calculated from the ratio between the vertical length of the failure surface and the vertical correlation length. For simplicity, the vertical length of the failure surface is assumed to be equal to the pile length, L, and the contribution to the vertical failure surface, from the base of the pile, is neglected.

With the explained example above, the reduction factor can be calculated as a function of the pile length. The method is presented in Appendix D.2, where a correlation length of 0.5 m is determined for the Søvind Marl. Further an example of determining the correlation length and the reduction factor is shown in Appendix E.3. By calculating the reduction factors for various pile lengths, the reduction factor can be seen in Figure 5.6. The figure shows the reduction factor calculated for piles with the length between 1-20 m. It is here seen that the coefficient of variation for the undrained shear strength, can be reduced considerably. When the pile is 5 m the coefficient of variation is reduced to 30 %, which is a noticeable effect.

In Figure 5.7 the reduction factor is shown for piles with the length of 1, 5, 10, 15 and 20 m where the correlation length has been varied. It is seen that, when the correlation length increases, the reduction factor goes towards 1, which thereby is not a reduction any more. Further it is seen that when the correlation length increases, the value of the reduction factor is mostly increased for the shortest piles.

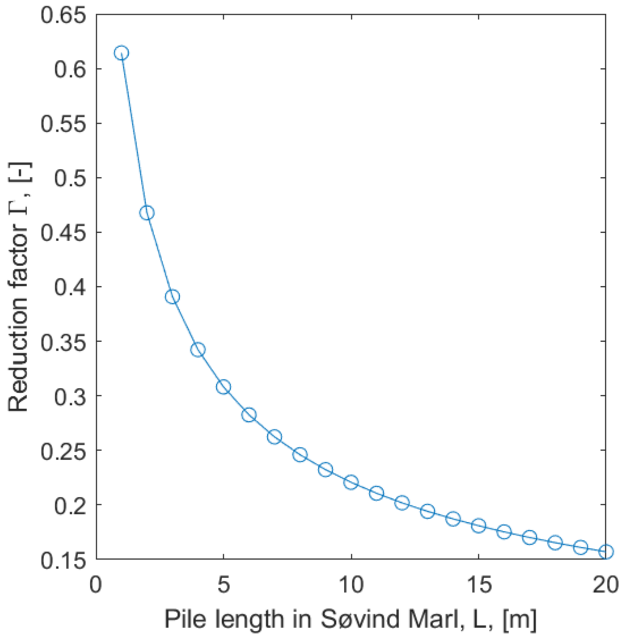

Figure 5.6: The reduction factor as a function of the pile length, L, in Søvind Marl by having a constant correlation length of 0.5 m.

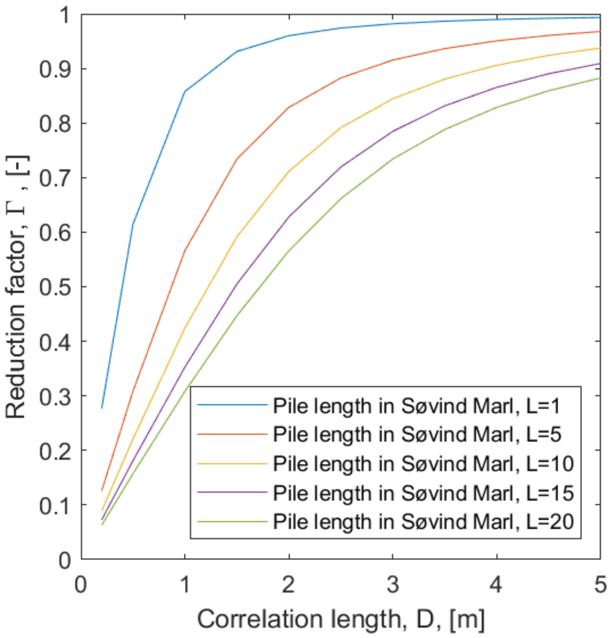

Figure 5.7: The effect on the reduction factor for five pile lengths with different correlation lengths.

It should be noted that the only variable that changes the reduction factor is the length of the failure surface, which is represented as the pile length in this report. The coefficient of variation, V_h, and the reduction factor is constant along the whole pile and only a change in the pile length will change the value of the reduction factor. The correlation length, D, is a constant depending on, which soil property is investigated and the variation of the correlation length in Figure 5.7, is only to show the influence of the correlation length upon the reduction factor. It is hereby seen that the reduction factor has the greatest influence on the coefficient of variation, V_h, when the correlation length, D, is considerably smaller than the pile length.

5.3 Estimation of the undrained shear strength

After the model and physical uncertainties are determined, the characteristic shear strength can be estimated. It is seen that the undrained shear strength increases with the depth, by plotting the triaxial shear strength vs the depth from Table 3.1. This is shown in Figure 5.8. The estimated shear strength is modeled by equation (1,4) and since the shear strength is increasing with depth, then the value of the numerator, $(q_t - \sigma_{v0})$, in equation (1,4) also should. This is seen by plotting the numerator, $(q_t - \sigma_{v0})$, from equation (1,4) in Figure 5.9. The data of the corrected cone resistance and the vertical overburden pressure is taken from Project 2. It is therefore chosen that the characteristic shear strength should increase with the depth, instead of being a constant value, and a linear regression is therefore conducted for the numerator in equation (1,4). This is shown in Appendix D.3, where the equations for calculating the characteristic shear strength is also shown. The characteristic shear strength is calculated as a 5 % quantile, since this is recommended by Annex D in EN1990, (DS/EN, a, 2007) and an example of the calculation for the characteristic shear strength is shown in Appendix E.4.

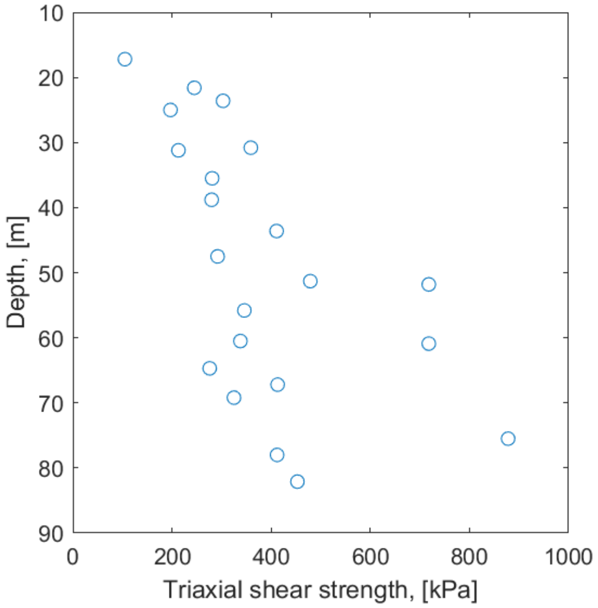

Figure 5.8: Plotted triaxial shear strength vs the depth from Table 3.1. Note that the depth is including the thickness of the sandy fill.

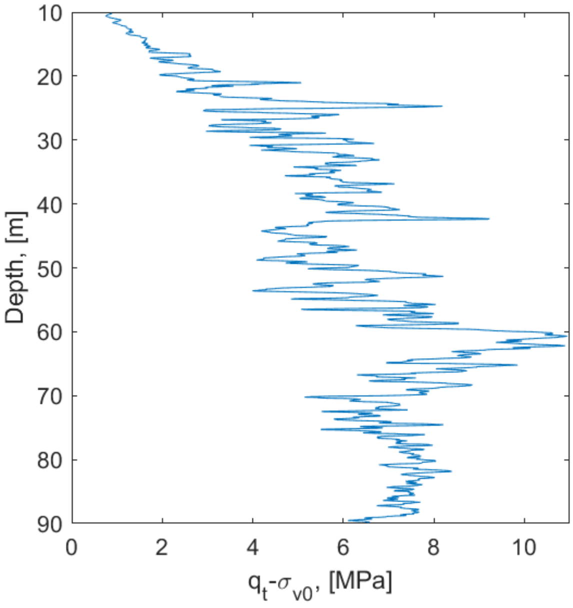

Figure 5.9: The value of numerator in equation (1,4) vs the depth, from Project 2. Note that the depth is including the thickness of the sandy fill.

In Figure 5.10 the estimated characteristic shear strength is shown for five different pile lengths. It is seen that due to the varying pile length, the characteristic shear strength is greater for the longest piles, since the reduction of the physical uncertainty is greatest for the longest piles. Further, it is seen that the influence is minimal, since the increase is shear strength is very small. A better way of visualizing the difference in the characteristic shear strength, is by comparing the characteristic shear strengths from Figure 5.10 at a chosen depth. This is shown in Figure 5.11, where the characteristic shear strength at det depth of 0.5 m is plotted for the different pile lengths. It is seen that the increase in shear strength is less than 1 kPa between a 3 m and 20 m pile and the size effect is thereby neglectable.

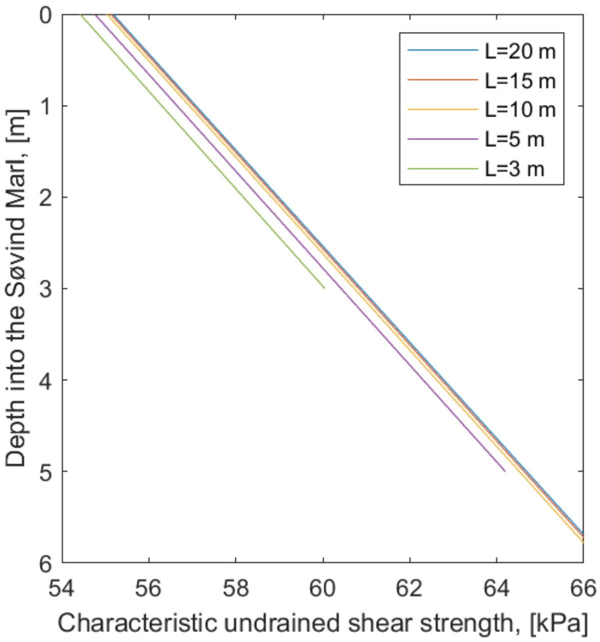

Figure 5.10: Linear increasing characteristic undrained shear strength for various pile lengths at the Port of Aarhus.

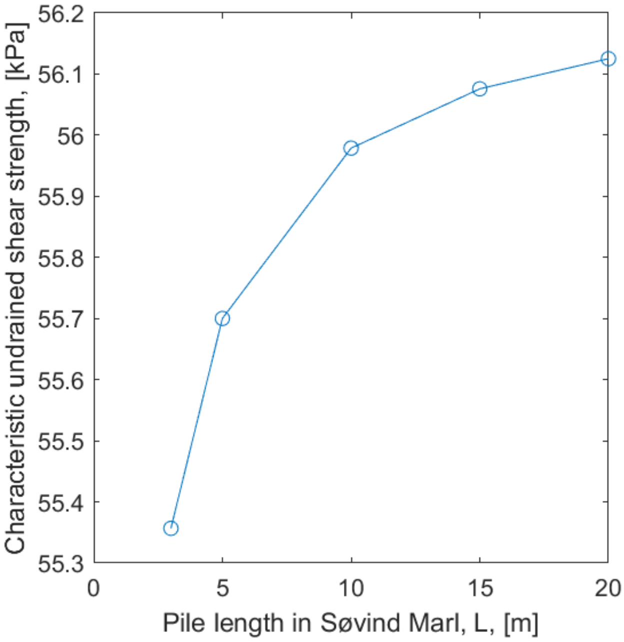

Figure 5.11: The characteristic shear strength at the depth of 0.5 m into the Søvind Marl for different pile lengths from Figure 5.10.

The characteristic shear strength is hereby estimated to be 56 kPa at the depth of 0.5 m into the Søvind Marl and it is linear increasing as shown in Figure 5.10. The reduction of the physical uncertainty has a neglectable effect on the characteristic shear strength in the above given example with a pile installed in Søvind Marl.

It should be noticed that if a noticeable reduction is seen in the characteristic shear strength with the above approach, the characteristic value can only be used for calculating of the bearing capacity of the belonging pile, with the length that has been used to reduce the physical uncertainty.

6 Discussion

This chapter is discussing the sensitivity of the models given from equation (1,4), (1,5) and (1,6) with regards to the measured CPT data that are used in the respective equation. Further the influence of the uncertainties is investigated to understand their influence on the characteristic undrained shear strength. Lastly, each of the models from equation (1,2), (1,4), (1,5) and (1,6) are discussed and the most feasible models are evaluated with regards to their usability.

6.1 Parameter study

It is seen in chapter 3, that the CPT data varies considerable over short distances. A parameter study is therefore conducted to determine the sensitivity of the models in equation (1,4), (1,5) and (1,6), which are the three models that has been carried on with in chapter 5. The sensitivity is determined by keeping the undrained shear strength constant, at the values determined in Table 3.1, and hereafter vary the respective CPT data that is inserted into equation (1,4), (1,5) and (1,6). The deviation in the calculated cone factors can hereby be used to determine the sensitivity of the models with regards to the different CPT data. Since the cone factors are proportional with the undrained shear strength in equation (1,4), (1,5) and (1,6), the percentage deviations measured in the cone factors are the same for the undrained shear strength.

The smoothing which has been carried out as the last step in the data processing, is also investigated. The sphere diameter is variated to see the effect upon the derived cone factors and hereby the effect of the smoothening is determined.

6.1.1 Influence of a variation in the total unit weight

The total unit weight of Søvind Marl is only included in equation (1,4) through the vertical overburden stress. From the introduction it is stated that the total unit weight of Søvind Marl varied between 16-19 kN/m^3 and it has a mean value of 17.7 kN/m^3. The mean value is used in this report, but in case that it is a bad assumption, it is relevant to see how much, the total unit weight influenced the derived value of N_{KT}. In Table 6.1 the difference is shown if the total unit weight has been 16 kN/m^3 or 19 kN/m^3 instead of 17.7 kN/m^2.

It is seen that the effect of the total until weight increases with depth, which is logical since the total unit weight is included through the vertical overburden stress. Further it is seen that the change in total unit weight, results in a maximum change of 1.7 % in the value of N_{KT}. In case the total unit weight is poorly estimated, it is seen that the influence on the derived values of N_{KT}, is not significant.

Table 6.1: The Influence on the values of N_{KT} with regards to a variation in the total unit weight for Project 2.

Total unit weight	**16 kN/m^3**	**19 kN/m^3**
depth	**Difference**	
[m]	**[%]**	**[%]**
21.6	-0.6	0.4
23.6	-0.4	0.3
25	-0.4	0.3
30.8	-0.8	0.6
35.5	-0.8	0.6
38.8	-0.8	0.6
43.6	-1.2	0.9
47.5	-1.2	0.9
51.3	-0.8	0.6
51.8	-1.1	0.8
55.8	-1.0	0.8
60.5	-0.8	0.6
60.9	-0.8	0.6
64.7	-1.3	1.0
69.2	-1.3	1.0
75.5	-1.7	1.3
78.0	-1.7	1.3
82.1	-1.7	1.3

6.1.2 Influence of a variation in the cone resistance

When the cone resistance is varied, equation (1,4) and (1,5) are the only ones influenced through the corrected cone resistance. The cone resistance is varied between 50-150 % of the original measured cone resistance, where 100 % is equivalent to the original measured cone resistance. The influence of the cone resistance is shown in Table 6.2 and Table 6.3. From the tables, it is seen that the influence in the variation of the cone resistance is relatively high. It is seen that the variation of N_{KT} is around 49-57 %, and for N_{ke} the variation is around 50-76 %, when the cone resistance is varied with $\pm$ 50 %. It is therefore important to measure and process the cone resistance correctly, since it is seen that the deviations in the cone resistance is influencing the values of N_{KT} and N_{ke} considerably.

Table 6.2: The Influence on the values of N_{KT} with regards to a variation in the cone resistance for Project 2.

Cone resistance	**50 %**	**150 %**
Depth	**Difference on N_{KT}**	
[m]	**[%]**	**[%]**
21.6	-56.6	56.6
23.6	-54.6	54.6
25	-54.1	54.1
30.8	-56.4	56.4
35.5	-55.7	55.7
38.8	-55.3	55.4
43.6	-55.9	55.9
47.5	-54.7	54.7
51.3	-51.4	51.4
51.8	-52.3	52.4
55.8	-55.2	55.2
60.5	-49.6	49.6
60.9	-49.2	49.1
64.7	-57.1	57.1
69.2	-55.8	55.8
75.5	-57.4	57.4
78.0	-56.6	56.6
82.1	-55.7	55.7

Table 6.3: The Influence on the values of N_{ke} with regards to a variation in the cone resistance for Project 2.

Cone resistance	**50 %**	**150 %**
Depth	**Difference on N_{ke}**	
[m]	**[%]**	**[%]**
21.6	50.5	-50.5
23.6	50.3	-50.3
25	50.5	-50.5
30.8	51.3	-51.3
35.5	51.2	-51.2
38.8	52.1	-52.1
43.6	57.8	-57.8
47.5	61.3	-61.3
51.3	65.5	-65.5
51.8	67.9	-67.9
55.8	63.2	-63.2
60.5	72.9	-72.9
60.9	76.0	-76.0
64.7	70.8	-70.8
69.2	59.9	-59.9
75.5	58.3	-58.3
78.0	61.0	-61.0
82.1	64.1	-64.1

6.1.3 Influence of a variation in the pore pressure

It has been determined that both the gathered projects had problems with the measured pore pressure. For Project 1, the pore pressure transducer reached its maximum capacity and in Project 2 there has been problems with the saturation of the filter. By varying the pore pressure, the consequence of a wrong measured pore pressure is investigated. This is done for N_{KT}, N_{ke} and $N_{\Delta \mathrm{u}}$, where the pore pressure is only influencing N_{KT} through the corrected cone resistance.

Again, only the cone factors derived from Project 2 is used, where the pore pressure is varied between 50-150 % of the original pore pressure, where 100 % is equivalent to the original measured pore pressure. Since there is a poorly measured pore pressure in the depth between 10-40 m, the cone factors estimated in this depth interval is not included in this investigation. The effect of the variation of N_{KT}, N_{ke} and $N_{\Delta \mathrm{u}}$ is shown in Table 6.4 to Table 6.6.

From the tables it is seen that the values of N_{KT} varies around 4-8 %, N_{ke} varies around 8-26%, and $N_{\Delta u}$ varies around 57-96 %. The change in the values of the cone factors is therefore most significant for $N_{\Delta u}$ and hereafter N_{ke}, since the pore pressure is used directly in equation (1,5) and (1,6). Lastly N_{KT} is the least influenced cone factor because the cone factor is only slightly affected by the pore pressure through the corrected cone resistance.

The models in equation (1,5) and (1,6) should therefore not be used when the pore pressure is poorly measured, since the change is so significant in the values of N_{ke} and $N_{\Delta u}$. Meanwhile equation (1,4) is only slightly affected, and therefore seems to be more stable to use in case of poorly measurements of the pore pressure.

Table 6.4: The Influence on the values of N_{KT} with regards to a variation in the pore pressure for Project 2.

Pore pressure	**50 %**	**150 %**
Depth	**Difference on N_{KT}**	
[m]	**[%]**	**[%]**
43.6	-3.5	3.5
47.5	-4.6	4.6
51.3	-5.6	5.6
51.8	-6.3	6.3
55.8	-5.0	5.0
60.5	-7.1	7.1
60.9	-7.6	7.6
64.7	-7.0	7.0
69.2	-4.2	4.2
75.5	-3.8	3.8
78.1	-4.7	4.7
82.1	-5.6	5.6

Table 6.5: The Influence on the values of N_{ke} with regards to a variation in the pore pressure for Project 2.

Pore pressure	**50 %**	**150 %**
Depth	**Difference on N_{ke}**	
[m]	**[%]**	**[%]**
43.6	-7.8	7.8
47.5	-11.3	11.3
51.3	-15.5	15.5
51.8	-17.9	17.9
55.8	-13.2	13.2
60.5	-22.9	22.9
60.9	-26.0	26.0
64.7	-20.8	20.8
69.2	-9.9	9.9
75.5	-8.3	8.3
78.1	-11.0	11.0
82.1	-14.1	14.1

Table 6.6: The Influence on the values of $N_{\Delta u}$ with regards to a variation in the pore pressure for Project 2.

Pore pressure	**50 %**	**150 %**
Depth	**Difference on $N_{\Delta u}$**	
[m]	**[%]**	**[%]**
43.6	-87.7	87.7
47.5	-72.6	72.6
51.3	-60.9	60.9
51.8	-62.6	62.6
55.8	-63.7	63.7
60.5	-57.4	57.4
60.9	-56.8	56.8
64.7	-61.4	61.4
69.2	-75.2	75.2
75.5	-96.4	96.4
78.1	-80.7	80.7
82.1	-72.9	72.9

6.1.4 Influence of smoothing the CPT data

The last parameter that is varied, is the smoothing of all the CPT data, which is done as the last step in the data processing. According to (Lunne, et al., 1997), it is stated that the cone is influenced by the soil within a sphere with the diameter for 2-3 cone diameters. For this reason, 3 cone diameters have been used as the spherical diameter for smoothing all the CPT data.

By varying the diameter of the sphere, the influence on the cone factors is investigated. The effect on the derived values of N_{KT}, N_{ke} and $N_{\Delta u}$ are shown in Figure 6.1 to Figure 6.3. Note that the cone diameter is 35.7 mm.

Each line in Figure 6.1, Figure 6.2 and Figure 6.3 represents a derived value of N_{KT}, N_{ke} and $N_{\Delta u}$ respectively. By varying the sphere diameter between 1-10 cone diameters, the change for each specific derived value of N_{KT}, N_{ke} and $N_{\Delta u}$ is seen. This method is also used in Appendix C.3, where the representative value of Δa has been determined.

For this investigation it is not important, which line belongs to which cone factor, but the variations of the lines are significant. It is seen that by varying the diameter of the sphere, the change in the cone factors are negatable until the diameter of the sphere reaches seven cone diameters. From seven cone diameters and further, some of the cone factors starts to change value due the smoothening, which is the opposite effect that is wanted from the smoothening.

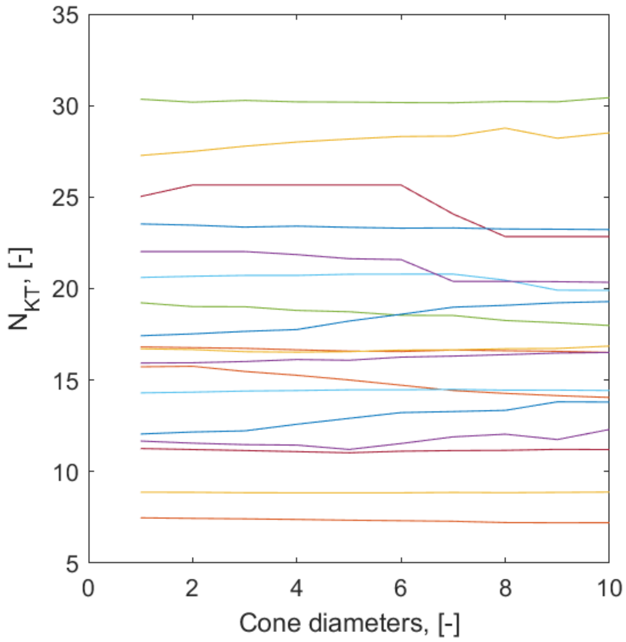

Figure 6.1: The Influence of a variation in the size of the spherical diameter for smoothing, with regards to the values of N_{KT}.

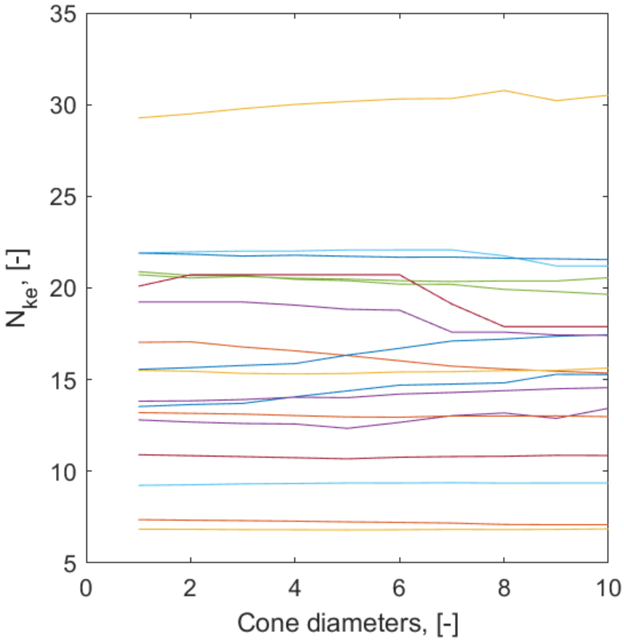

Figure 6.2: The Influence of a variation in the size of the spherical diameter for smoothing, with regards to the values of N_{ke}.

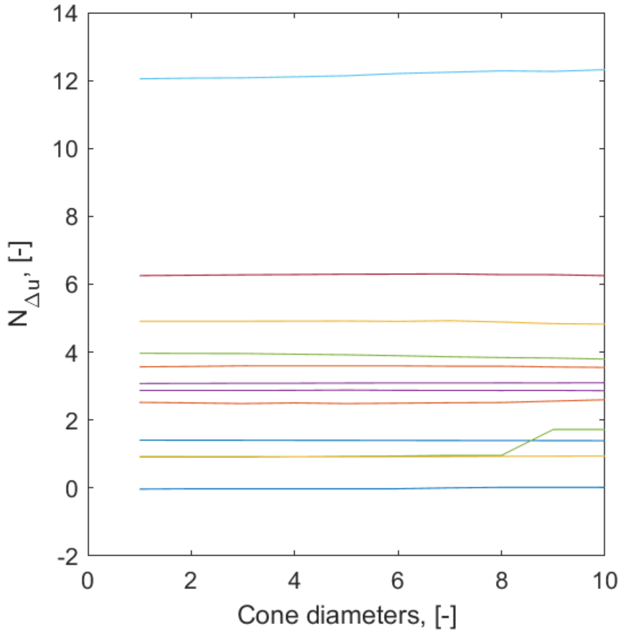

Figure 6.3: The Influence of a variation in the size of the spherical diameter for smoothing, with regards to the values of $N_{\Delta u}$.

From the above observations it is debatable if the smoothening is necessary. The influence from the smoothening is minimal, since the derived cone factors do not vary significantly with changing sphere diameter. Further the used CPT data for deriving the cone factors are averaged by using the interval Δa. Thereby the CPT data is averaged twice before they are inserted into equation (1,4), (1,5) and (1,6), and this can thereby explain why the effect of the smoothening is minimal.

Even though the smoothening is carried out, the CPT data still had significant variations within short distances and therefore the interval Δa is determined to be more efficient to use. From the experience of this report, it seems more reasonable to manually remove peaks with thresholds and hereafter use Δa to average the CPT data before using them to calculate the cone factors.

6.2 Influence of physical and model uncertainties

In this report, it has been shown that the considered example, the size effect did not have any noticeable effect on the characteristic shear strength. The situation which has been investigated, used $V_\Delta = 0.4$ and $V_h = 0.2$, which are the coefficient of variation for the model and physical uncertainty respectively.

By looking into the equation for the characteristic shear strength, which is shown in equation (6,1), it is seen that the weighting factors, α_r and α_δ, influences heavily the contributions from each of the uncertainties. In equation (6,1) the calculated example, which is presented in Appendix E.4, shows that $\alpha_r = 0.081$ and $\alpha_\delta = 0.997$. The physical uncertainty is implemented in the characteristic shear strength through Q_r related to α_r and the model uncertainty is implemented in the characteristic shear strength through Q_δ related to α_δ. It is hereby seen that the model uncertainty is the most dominating uncertainty due to the weighting factors, which can explain why a change in the pile length did not influence the undrained shear strength.

$$s_{u.c}(d,L) = b\left(\frac{(a+b'd)}{N_{KT}}\right) exp(-k_N\ \alpha_r(L)\ Q_r(L) - k_n\ \alpha_\delta(L)\ Q_\delta(L) - 0.5\ Q(L)^2) \tag{6,1}$$

$$\Downarrow$$

$$s_{u.c}(d,L) = 1.00\left(\frac{\left(2011\ \mathrm{kPa} + 69\ \frac{ton}{\mathrm{m^2 s^2}} \cdot 0.5\ \mathrm{m}\right)}{17.1}\right) exp(-1.65 \cdot 0.081 \cdot 0.031 - 1.77 \cdot 0.997 \cdot 0.385 - 0.5 \cdot 0.386^2) = 56\ \mathrm{kPa}$$

By investigating how the values of the α_r, α_δ, Q_r and Q_δ are determined, it is seen that the magnitude of the coefficient of variation for the model and physical uncertainty are essential. If V_Δ is much greater than V_h, then the model uncertainty is weighted more than the physical uncertainty. The equations for determining α_r, α_δ, Q_r and Q_δ are shown in Appendix D.3.

It is therefore decided to vary the coefficient of variation for the model and physical uncertainty, to see if the effect of the pile length changes the characteristic shear strength. By varying both V_Δ and V_h between 0.1 and 0.4 and combining them differently, the estimated characteristic shear strength is shown in Figure 6.4. The figure is the similar to Figure 5.11, where the characteristic shear strength is observed at the depth of 0.5 m for piles with various lengths. The correlation length, D, is set to 0.5 m and a 5 % quantile has been used for calculating the characteristic shear strength again.

The lines in Figure 6.4, which has the same color also have the same value of V_Δ, while the line style illustrates the different values of V_h. The legend for Figure 6.4 is shown in Figure 6.5. It is seen in the teal dotted plot, when the model uncertainty is low ($V_\Delta = 0.1$), and the physical uncertainty is great ($V_h = 0.4$), the characteristic shear strength is mostly affected by the change of the pile length. For the teal lines, which have a small model uncertainty, it is seen that the four lines in general have a much greater steepness in the beginning than the red lines, which means that the reduction factor for the physical uncertainty has a greater effect. The red lines have a great model uncertainty ($V_\Delta = 0.4$) and therefore this uncertainty dominates the most, which result in very small increases in the shear strength due to the pile length, since this only reduces the physical uncertainty.

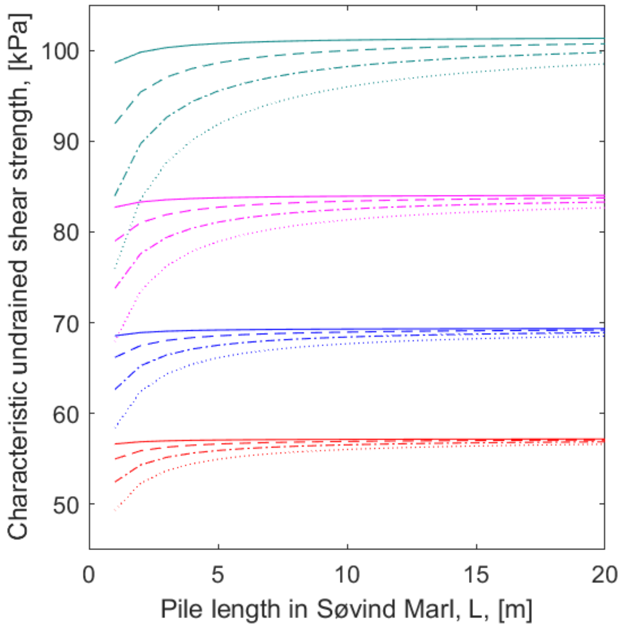

Figure 6.4: The characteristic shear strength with various model and physical uncertainties.

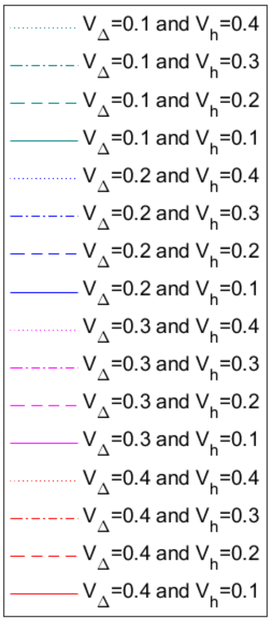

Figure 6.5: Legend for Figure 6.4.

It is hereby seen that if the model uncertainty is small and the physical uncertainty is great, the effect of the pile length could have increased the undrained shear strength considerably more, than what has been seen in chapter 5. It is seen to be realistic that the physical uncertainty could be greater than the chosen value of 0.2 in chapter 5, and thereby the size effect is more noticeable, but it is not deemed realistic to reduce the model uncertainty, since it has been shown in section 5.1 that all the investigated models, showed a model uncertainty of roughly 0.4.

Lastly, it should be noticed that piles with the length of 1-2 m is not deemed feasible. The characteristic shear strength for 1-2 m piles is only shown in Figure 6.4 to better illustrate the size effect, when the model and physical uncertainties changes size.

6.3 The most favorable cone factor in Søvind Marl

Four models with their respective cone factor has been investigated in this report. From the report several observations have been made upon the different models, and these are here presented to explain which model is the most favorable. The observations that are explained here, should be confirmed in further studies, to verify if the observations only are applicable for soft clay, or for clay in general.

Equation (1,2), which is using N_K, is not evaluated to be a favorable model. The metod cannot take the pore pressure into consideration, which is proven to affect the cone resistance. This is especially affecting the cone resistance in soft clay, where the pore pressure can be in the same magnitude as the cone resistance. For this reason, equation (1,4) is developed to take the pore pore pressure into consideration using the corrected cone resistance. Only in a case where no pore pressure is measured, equation (1,2) is useable compared to the other models, since it is the only model, which does not need measurements of the pore pressure.

Equation (1,4), which is using N_{KT}, is evalued to be one of the more favorable models. The model can account for the effect of the pore pressure, and at the same time, if the pore pressure is poorly measured, the model can still be used. As it has been determiend above, the model is primarily sensitive with regards to the cone resistance. By processing the CPT data and thereby removing errors, such as peaks in the cone resistance, the model is deemed to be the most favorable model.

Equation (1,5), which is using N_{ke}, is not evaluated to be a favorable model. From the parameter study, it is seen that N_{ke} is more sesitive with regards to the cone resistance and pore pressure, than N_{KT}. Further the model is not recommended in genereal, which can explain, why not many investigations of the value of N_{ke} has been derived in prior studies. Due to the poorly measured pore pressure between the depth of 10-40 m in Project 2, the model has been discarded, when the characteristic shear strength should have been determined.

Equation (1,6), which is using $N_{\Delta u}$, is evaluated to be a favorable model. The model is good in soft soils, where the the pore pressure ratio is not too small. Further there is determined a dependency between $N_{\Delta u}$ and the pore pressure ratio, which is good, since the values of the cone factor is determined to be in the interval of 0.9-12.1. The model has one weakness with regards to the measured pore pressure. It is seen from the parameter study that the model is sensitive towards the pore pressure, and between the depth of 10-40 m, the pore pressure has been poorly measured, which resulted in very low or negative values of $N_{\Delta u}$. Therefore the model has been discarded when the chaarcteristic shear strength should have been determined. It should be noted that the model is worth investigating more, if good pore pressure measurement are pressents, which has not been the case for this report.

From the above observations, two models are deemed more useful than the others. Equation (1,4) and (1,6) are both favorable in in Søvind Marl. Equation (1,4) is the most stable and useful model, since it is not influenced greatly by the poorly measured pore pressure. Equation (1,6) is also seen as beeing good, since it could vary the value of N_{Δ} with the pore presure ratio, but due to the poorly measured pore pressure, the model could not be used for determining a characteristisc shear strength. Equation (1,4) is therefore evaluated to be the most favorable model, which is using N_{KT}.

7 Conclusion

Is it shown that the penetration rate, inclination of the of the cone penetrometer and the saturation of the filters, influences the measured cone resistance and pore pressure. Further, it is shown that the CPT data contains errors which should be accounted for to prevent the errors to be carried on in the derivation of the cone factors or the undrained shear strength. The CPT data can vary considerably over short distances and therefore a single value of the CPT data is not used for deriving the cone factors. Instead the CPT measurements within 8 cm above or underneath the depth of the triaxial test is averaged and used, since this gave more stable results for the cone factors.

It has been shown that four models exist for determining the undrained shear strength by comparing CPT data and triaxial tests. Each model uses different CPT measurements and the cone factors N_K, N_{KT}, N_{ke} and $N_{\Delta u}$ respectively. The derived values for the different cone factors are in the interval of 7-27.2 for N_K, 7.3-31.4 for N_{KT}, 6.9-22.6 for N_{ke} and 0.9-12.3 for $N_{\Delta u}$.

The models using the respective cone factors N_{KT}, N_{ke} and $N_{\Delta u}$, are further investigated, since these models could take the pore pressure into account. The representable values of N_{KT} and N_{ke} are respectively determined to be 17.1 and 13.1, which caused the modes to have a bias equal to one. Further a dependency is determined between $N_{\Delta u}$ and the pore pressure ration, which gave the ability to have a varying value of $N_{\Delta u}$, if the undrained shear strength is estimated.

The characteristic undrained shear strength in Søvind Marl is estimated by the method given in Annex D from EN1990 (DS/EN, a, 2007). The method includes the model, physical and statistical uncertainties, which have been determined. The model uncertainties are determined to be 0.4 for the models using N_{KT} and N_{ke} while the model uncertainties for the model using $N_{\Delta u}$ is determined to be neglectable smaller at the value of 0.37. The models using N_{ke} and $N_{\Delta u}$ are shown to be affect by the poorly measured pore pressure in the gathered CPT data, and these are therefore not used for calculating the undrained shear strength. The model using N_{KT} has been used to estimate the characteristic undrained shear strength, since the model is only slightly affected by the poorly pore pressure. Further it has been shown that the model using N_{KT} is the least sensitive model, with regards to the CPT data in general.

It has been shown that the size of a geotechnical structure can allow a reduction in the physical uncertainties of the undrained shear strength. The physical uncertainty has been chosen to be 0.2 from prior studies, and hereafter the physical uncertainty has been reduced depending on the size of a pile installed at the Port of Aarhus. It is shown that the reduction of the physical uncertainty, due to the size of a pile, had no noticeable effect on the outcome of the characteristic undrained shear strength. This is caused by the difference in the magnitude of the two uncertainties, and the model uncertainty is therefore weighted more in the calculations of the characteristic undrained shear strength.

Bibliography

Acar, Y.B. 1981. Piezocone penetration testing in soft cohesive soils. *Fugro Postdoctoral Geotechnical Engineering Report No.Ge-81/01.* s.l. : Louisiana State University, 1981.

Alshibli, Khalid A., et al. 2011. Reliability Analysis of CPT measurements for Calculating Undrained Shear Strength. *Geotechnical Testing Journal vol. 34, No. 6.* 2011.

Bjerrum, Lauritz. 1973. Problems of soil mechanics and construction on soft clays and structurally unstable soils (collapsible, expansive and others). 1973. Vol. vol 3, pp. 111-159.

Browning, John Adam. 2005. Cone tip apex angle effects on cone penetration testing. Raleigh : Faculty og North Carolina State University, 2005.

Brozetti, J., et al. 1991. Background Dokumentation: Background information on Fatiguq design rules for hollow sections. 1991. pp. 179-187.

BSI Group. 2013. Geotechnical investigation and testing - Field testing. *Part 1: Electrical cone and piezocone penetration test.* London : BSI Standards Limited, 2013. BE EN ISO 22476-1:2012.

Budhu, Muni. 2011. *Soil Mechanics and Foundations.* 3. s.l. : John Wiley & Sons, INC., 2011.

Campanella, R.G., Gillespie, D. and Robertson, P.K. 1982. Porepressures during cone penetration testing. *Prepared for ESOPT II 2nd European Symposium on Penetration Testing.* Vancouver, Canada : University of British Columbia, 1982.

Danziger, F.A.B, et al. 2018. Rate effect of piezocone testing in two soft clays. *Cone Penetration Testing 2018.* Delft : Delft University of Technology, , 2018.

DGF's Feltkomite, b. 1999. *Referenceblad Nr. 1 - Vingeforsøg.* Revision 3. s.l. : Dansk Geoteknisk Forenings Feltkomité, 1999.

DGF's Laboratoriekomitet. 2001. DGF-Bulletin 15: Laboratoriehåndbogen. s.l. : Dansk Geoteknisk Forening, 2001.

DS/EN, a. 2007. *Eurocode 0: Projekteringsgrundlag for bærende konstruktioner.* 2. udgave. København : Dansk Standard, 2007.

DS/EN, b. 2007. *Eurocode 7: Geoteknik - Del 1: Generelle regler.* 2. udgave. København : Dansk Standard, 2007.

DS/EN, d. 2011. *Eurocode 7: Geoteknik - Del 2: Jordbundsundersøgelser og -prøvning.* København : Dansk Standard, 2011.

Envi. 2019. https://www.envi.se. [Online] 04 26, 2019. https://www.envi.se/downloads/flyers/Memocone_CordlessSet.pdf.

Google. 2019. Maaps.google.com. *Google maps.* [Online] 2019.

Grønbech, Gitte Lyng. 2015. Søvind Marl - Behaviour of a plastic fissured Eocene clay. s.l. : Aalborg: Aalborg Universitetsforlag., 2015. Vols. Ph.d.-serien for Det Teknisk-Naturvidenskabelige Fakultet.

Grønbech, Gitte Lyng, et al. 2014. Geotechnical properties of Søving Marl - a plastic Eocene clay. *Canadian Geotechnical Journal.* 2014, pp. 469-478.

Holmsgaard, Rikke, Nielsen, Benjamin Vagn Nordahl and Ibsen, Lars Bo. 2011. Field Cone Penetration Tests with Various Penetration Rates - Test Results. *DCE Technical reports, No. 123.* Aalborg : Department of Civil Engineering, Aalborg University, 2011.

JCSS PMC. 2002. JCSS Probabilistic Model Code, Section 3.5: SOIL PROPERTIES. s.l. : Rackwitz, R.; Denver, H.; Calle, E., 2002.

Jensen, Bjarne Chr. 2013. Teknisk ståbi. s.l. : Nyt teknisk forlag, 2013. 22. udgave.

Kim, Dae-Kyu. 2009. Interpretation of Emperical Cone Factors for Determining Undrained Strength. *한국산학기술학회논문지.* s.l. : Dept. of Civil Engineering, Sangmyung University, 2009. Vol. 10, 11.

Krak. 2018. Krak.dk. [Online] 2018. [Cited: 10 31, 2018.] https://map.krak.dk/.

Lunne, T., et al. 2018. Effect of cone penetrometer type on CPTU results at a soft clay test site in Norway. *Cone Penetration Testing 2018.* s.l. : Delft University of Technology, The Netherlands, 2018.

Lunne, T., Powell, J. and Robertson, P. K. 1997. *Cone Penetration Testing in Geotechnical Practice.* s.l. : Taylor & Francis Ltd, 1997.

Martinez, M. F. Garcia, et al. 2016. Influence of penetration rate on CPTU measurements in saturated silty soil. *Geotechnical and Geophysical Site Characterisation 5.* Sydney, Australia : Australian Geomechanics Society, 2016.

Mathalino. 2019. Mathalino.com. [Online] 2019. [Cited: 04 12, 2019.] https://www.mathalino.com/reviewer/geotechnical-engineering/consistency-soil-atterberg-limits.

Nadj, Jakob Lund. 2019. Omsætning af målte vingestyrker til udrænede forskydningsstyrker i danske lerarter. Aalborg : Aalborg Universitet, 2019.

Nowatzki, Edward A. and Karafiath, Leslie L. 1972. The Effect of Cone Angle on Penetration Resistance. s.l. : Grumman Aerospace Corporation, 1972.

Okkels, Nik, Hoff, Marianne Bondo and Rasmussen, Morten. 2008. Conefaktor i Søvindmergel, Septarieler og fedt moræneler. *geo.dk.* [Online] 09 01, 2008. [Cited: 03 05, 2019.] https://www.geo.dk/bibliotek/2008/conefaktor-i-soevindmergel-septarialer-og-fedt-moraeneler/#t=article.

Powell, J.J.M and Quarterman, R.S.T. 1988. The interpretation of cone penetration tests in clays, with particular reference to rate effects. *Proceeding of the International Symposium on enetration Testing.* Rotterdam : Balkema Pub., 1988.

problems of soil mechanics and construction on soft clays and structurally unstable soils (collapsible, expansive and others). **Bjerrum, Lauritz. 1973.** 1973, 8th ICSMFE Moscow Proceedings, Vol. vol 3, pp. 111-159.

Rémai, Zsolt. 2012. Correlation of undrained shear strength and CPT resistance. Budapest : periodica polytechnica, 2012.

Silvestri, Vincent and Fahmy, Yasser. 1995. Influence of Apex Angle on Cone Penetration Factores in Clay. *Geotechnical Testing Journal.* 1995. Vol. Vol. 18, No. 3.

Sørensen, John Dalsgaard. 2011, c. Estimation of Characteristic Values for Material Parameters. [compl.] Department of Civil Engineering. s.l. : Aalborg University, 2011, c.

—. 2004. Notes in Structural Reliability Theory and Risk Analysis. Aalborg : s.n., 2004.

Wong, J.T.F., Kassim, Kasliza and Dobie, M.J.D. 1990. Piezocone testing: saturation of filters. s.l. : Tensar International Limited, 1990.

Appendix A General theory

In this Appendix, general theory is explained. This theory includes correction of CPT data, the different pore pressure that can be measured by at cone penetrometer, derived parameters from the CPT data and soil parameters.

Appendix A.1 CPT data

Pore pressure

The pore pressure can be measured at three locations, on the cone itself, u_1, on the cylindrical extension of the cone, u_2, or above the sleeve, u_3, which all are shown in Figure 1.1. The magnitude of the measured pore pressure is depending on the soil type and filter location. As seen in Figure A.1.1, u_1 is greater than u_2 and u_3. This is caused due to the location of u_1, which is exposed to normal and shear stress, while u_2 and u_3 are primarily exposed to shear stress. For a lightly over consolidated clay, the pore pressure can be in the same magnitude as shown in Figure A.1.2.

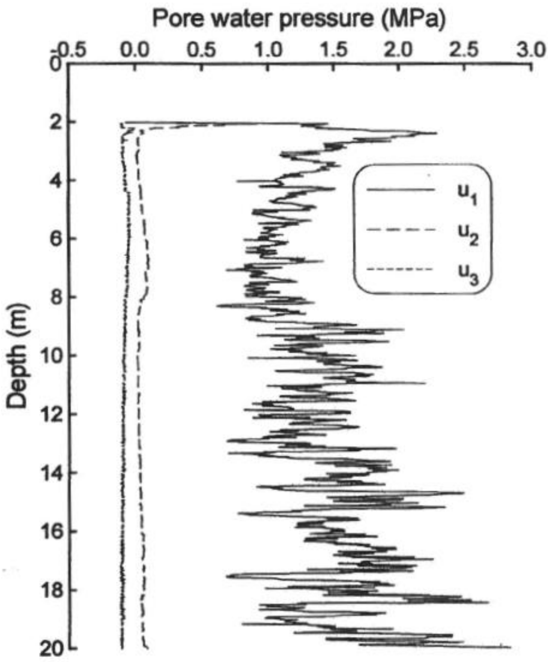

Figure A.1.1: Example of pore pressure for different filter locations in a heavily over consolidated clay from (Lunne, et al., 1997).

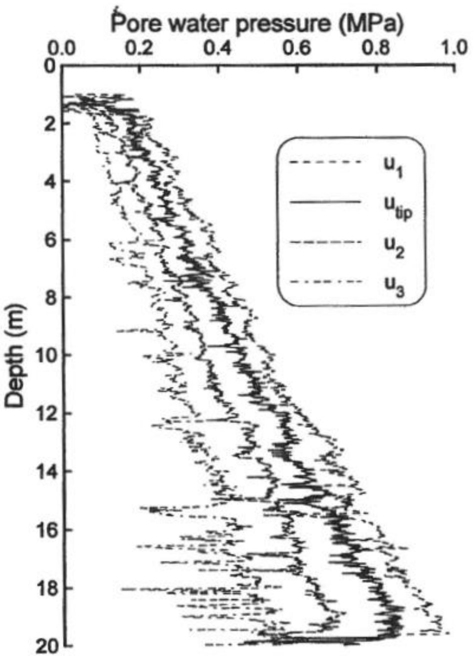

Figure A.1.2: Example of pore pressure for different filter locations in a lightly over consolidated clay from (Lunne, et al., 1997).

The most common used filter location is u_2, which can be used to correct the cone resistance as shown in equation (1,3).

Most cone penetrometers are manufactured with only one filter location, which is often u_2. It is possible to get a cone penetrometer with two or three filter locations, which can be used to correct the sleeve friction (Lunne, et al., 1997). Correction of the sleeve friction is shown in equation (A.1,1). This is not important for this report, since it is not used to estimate the cone factors or the undrained shear strength.

$$f_t = f_s - \frac{u_2\,A_{sb} - u_3\,A_{st}}{A_s} \qquad \text{(A.1,1)}$$

Where

f_t	Corrected sleeve friction	$[\mathrm{kPa}]$
f_s	Sleeve friction	$[\mathrm{kPa}]$
u_2	Pore pressure between the cone and the sleeve	$[\mathrm{kPa}]$
u_3	Pore pressure behind the sleeve	$[\mathrm{kPa}]$
A_{sb}, A_{st}, A_s	Cross-sectional areas shown in Figure A.1.3	$[\mathrm{mm}^2]$

In case of only using one filter location, (Lunne, et al., 1997) and (Campanella, et al., 1982) recommend to use u_2, since the location is giving more stable measurements. At the same time, it is protected by the cone and it is easier to saturate. Also, it gives the opportunity to correct the cone resistance, which can have a great effect in soft clay.

Unequal area effect and the net area ratio

According to (Lunne, et al., 1997) the cone resistance and sleeve friction are affected by the pore pressure. This is caused by the inner geometry of the cone, where the pore pressure acts on the shoulder of the cone and the ends of the friction sleeve. This effect is referred to as the "unequal area effect."

The unequal area effect is represented through the net area ratio, α, which is used in equation (1,3). The ratio is approximated by the ratio between the cross-sectional area of the shaft, A_n, and the cross-sectional area of the base of the cone, A_c, which is shown in equation (A.1,2). The areas are shown in Figure A.1.3. According to (BSI Group, 2013), the net area ratio cannot only be determined by equation (A.1,2) alone, but it should also be confirmed by tests in a pressure chamber or similar. The ratio usually ranges from 0.55 – 0.9, where a high value is preferred.

$$\alpha = \frac{A_n}{A_c} \tag{A.1,2}$$

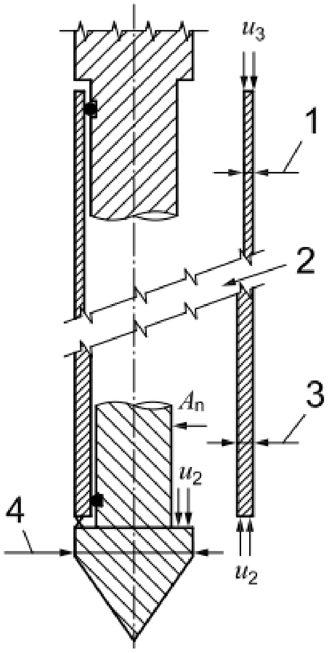

Figure A.1.3: Different areas of the cone penetrometer from (BSI Group, 2013).1: Cross sectional area (top) A_{st}, 2: Friction sleeve surface are A_s, 3: Cross sectional area (bottom) A_{sb}, 4: Cross sectional area A_c.

Appendix A.2 Formulas for interpretation of CPT data

Pore pressure ratio and friction ratio

The pore pressure ratio, B_q, and the friction ratio, R_f, are two often derived parameters from CPT data. They are often plotted with the corrected cone resistance, sleeve friction and the pore pressure, to interpret or classify the soil. The equations for the two parameters are shown in equation (A.2,1) and (A.2,2) respectively.

$$B_q = \frac{\Delta u}{q_t - \sigma_{v0}} = \frac{(u_2 - u_0)}{q_t - \sigma_{v0}} \tag{A.2,1}$$

Where

Δu	Excess pore pressure	[kPa]
q_t	Corrected cone resistance	[kPa]
σ_{v0}	Vertical overburden stress	[kPa]
$N_{\Delta u}$	Empirical cone factor	[−]

$$R_f = \frac{f_s}{q_t} \tag{A.2,2}$$

Where

f_s	Sleeve friction	[kPa]
q_t	Corrected cone resistance	[kPa]

Appendix A.3 Soil parameters

Atterberg limits

The limits are defining the water content for a clay to change from, for example, plastic state to liquid state, which is shown in Figure A.3.1. From the Atterberg limits, the plasticity index, can be determined, which is often used for classifying clay and silt. The limits are determined by laboratory tests, which are described in (DGF's Laboratoriekomitet, 2001) and the plasticity index is calculated from equation (A.3,1).

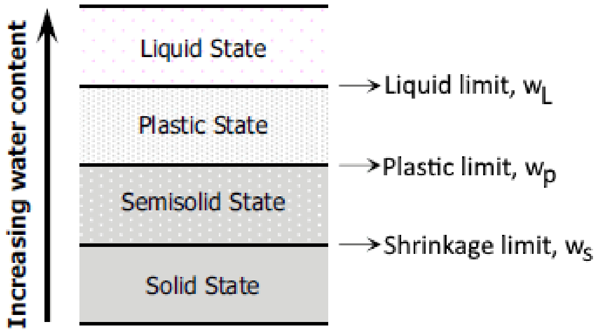

Figure A.3.1: Atterberg limits from (Mathalino, 2019)-edited.

$$I_p = w_L - w_p \tag{A.3,1}$$

Where

w_L	Liquid limit	[%]
w_p	Plastic limit	[%]

Vertical overburden stress and over consolidation ratio

The vertical overburden stress is calculated from equation (A.3,2). The parameter describes the stress that is imposed by the total unit weight of the above soil layers.

$$\sigma_{v0} = \sum_{i=1}^{n} \gamma_i \, d_i \tag{A.3,2}$$

Where

γ_i	Total unit weight of the current soil layer	$\left[\frac{\mathrm{kN}}{\mathrm{m}^3}\right]$
d_i	Height of the current soil layer	[m]
n	Number of soil layers above the selected depth	[−]

The over consolidation ratio can hereafter be determined from equation (A.3,3), which is the relation between the maximum stress, that the soil have been expose to and the stress that the soil is currently exposed to. The preconsolidation stress can be determined by an oedometer test.

$$OCR = \frac{\sigma_{pc}}{\sigma_{v0}} \tag{A.3,3}$$

Where

σ_{pc}	Preconsolidation stress	[kPa]
σ_{v0}	Vertical overburden stress	[kPa]

Appendix B Interpretation of triaxial shear strength

The undrained shear strength is interpreted by the Tresca's failure criteria (Budhu, 2011). The shear stress at failure is the radius of the Mohr total stress circle. This is calculated in equation (B,1) and shown in Figure B.2.

$$s_u = \frac{(\sigma_1)_f - (\sigma_3)_f}{2} = \frac{q}{2} \tag{B,1}$$

Where

$(\sigma_1)_f$	Axial stress on the triaxial specimen at failure	[kPa]
$(\sigma_3)_f$	Radial stress on the triaxial specimen at failure	[kPa]
q	Deviator stress	[kPa]

The axial stress and radial stresses on a triaxial test specimen are shown in Figure B.2.

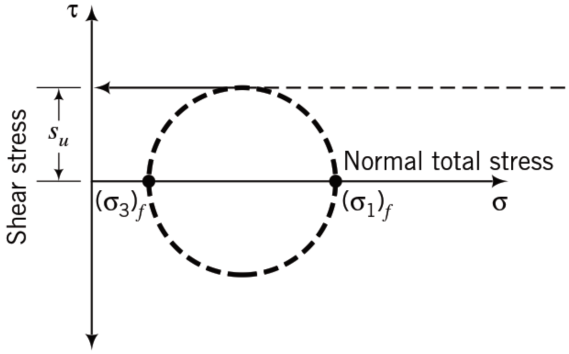

Figure B.1: Tresca's criteria shown with Mohr's circle from (Budhu, 2011)-edited.

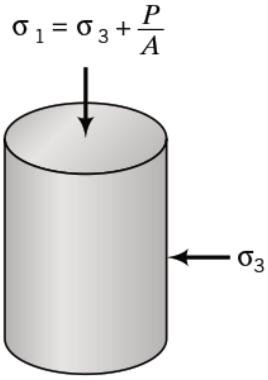

Figure B.2: Direction of axial and radial stress on the triaxial specimen, from (Budhu, 2011)-edited. P: Force from piston, A: cross sectional area of the specimen.

The deviator stress used to calculate the undrained shear strength, is chosen from a stress-strain plot. The stress-strain curves for the six triaxial test from Project 1, are shown in Figure B.3.

The deviator stress is taken, when failure of the specimen occurs. Failure is determined as the deviator stress at ε_1=10 %, where ε_1 is the axial strain. If a peak in the deviator stress occurred before ε_1=10 %, this value is determined as failure. Curve "845" shows an example of failure determined with a peak before ε_1=10 % and curve "910" had no peak, so failure is determined as the deviator stress at ε_1=10 %.

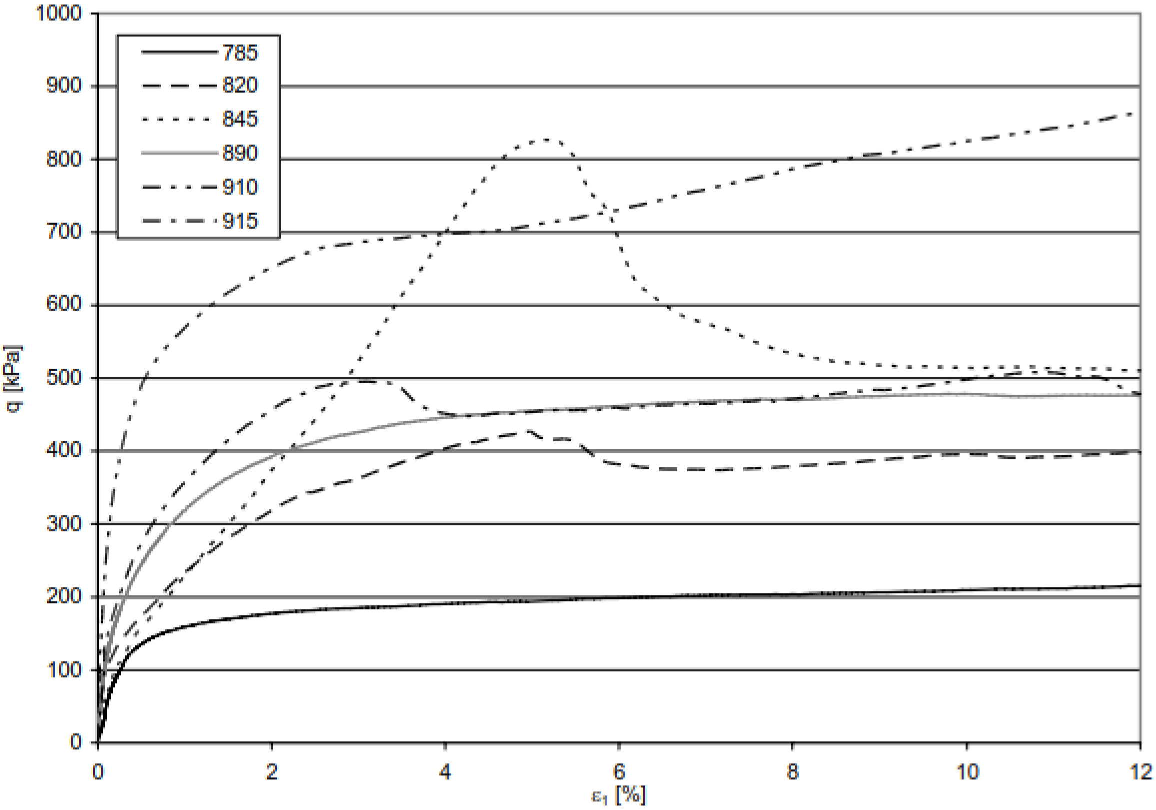

Figure B.3: Stress-strain plot for the triaxial tests carried out for Project 1.

Appendix B.1 Discarded triaxial tests

On Figure B.3, six curves are shown, but in Table 3.1 and Table 3.2 only three triaxial test are used from Project 1. One of these triaxial test are discarded due to the behavior of curve “915” on Figure B.3. The curve first peaks in the deviator stress at the axial strains between 2-4 %. Afterwards another peak is observed at axial strains between 10-12 %.”. It therefore seems that the test specimen, which is plotted as curve “915”, is failing locally at 2-4 %, and after further load shows more strength in the rest of the test specimen. The undrained shear strength derived from the first peak results in a very low shear strength. It is therefore assumed that the first failure in the specimen, is caused by fissures and therefore it is a local failure, that does not represent the true undrained shear strength for Søvind Marl. The second peak shows that the specimen has more strength than the first peak, but due to the unknown effect of the first locally assumed failure, the triaxial test is discarded.

Also, Project 2 had two similar triaxial tests that showed two peaks in the deviator stress. These two tests are also discarded and not used in this report.

Further in Project 1, two triaxial test are discarded due to missing CPT data. The CPT is done as a “down the hole” test and the CPT data and triaxial test specimen is therefore not from the same depth. The vertical distance between the nearest CPT measurement and the triaxial test specimen is more than 40 cm and it is therefore evaluated to be too far apart for a reasonable comparison.

Appendix B.2 Borehole from Project 2

The borehole with belonging laboratory tests for Project 2 is shown in this appendix.

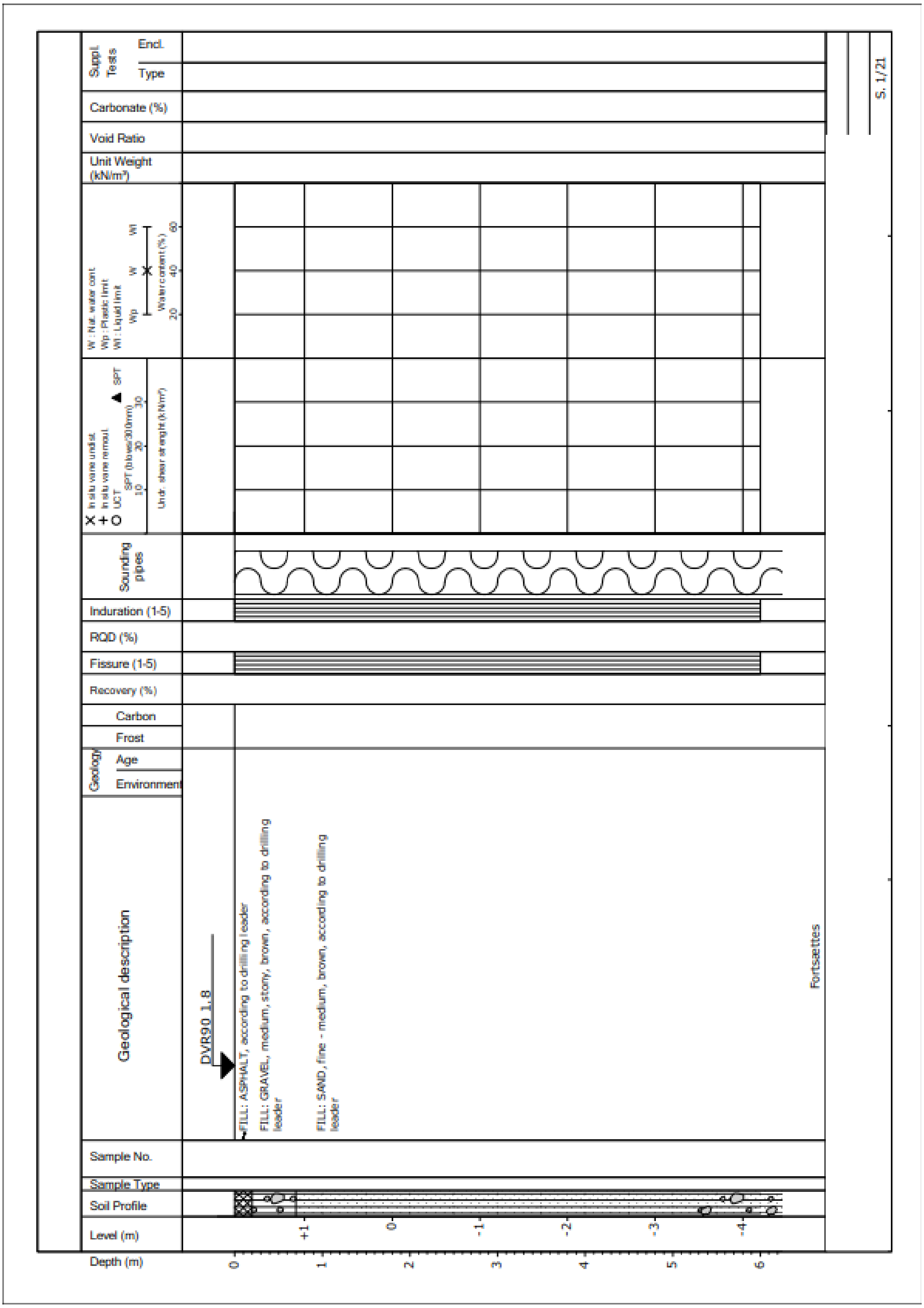

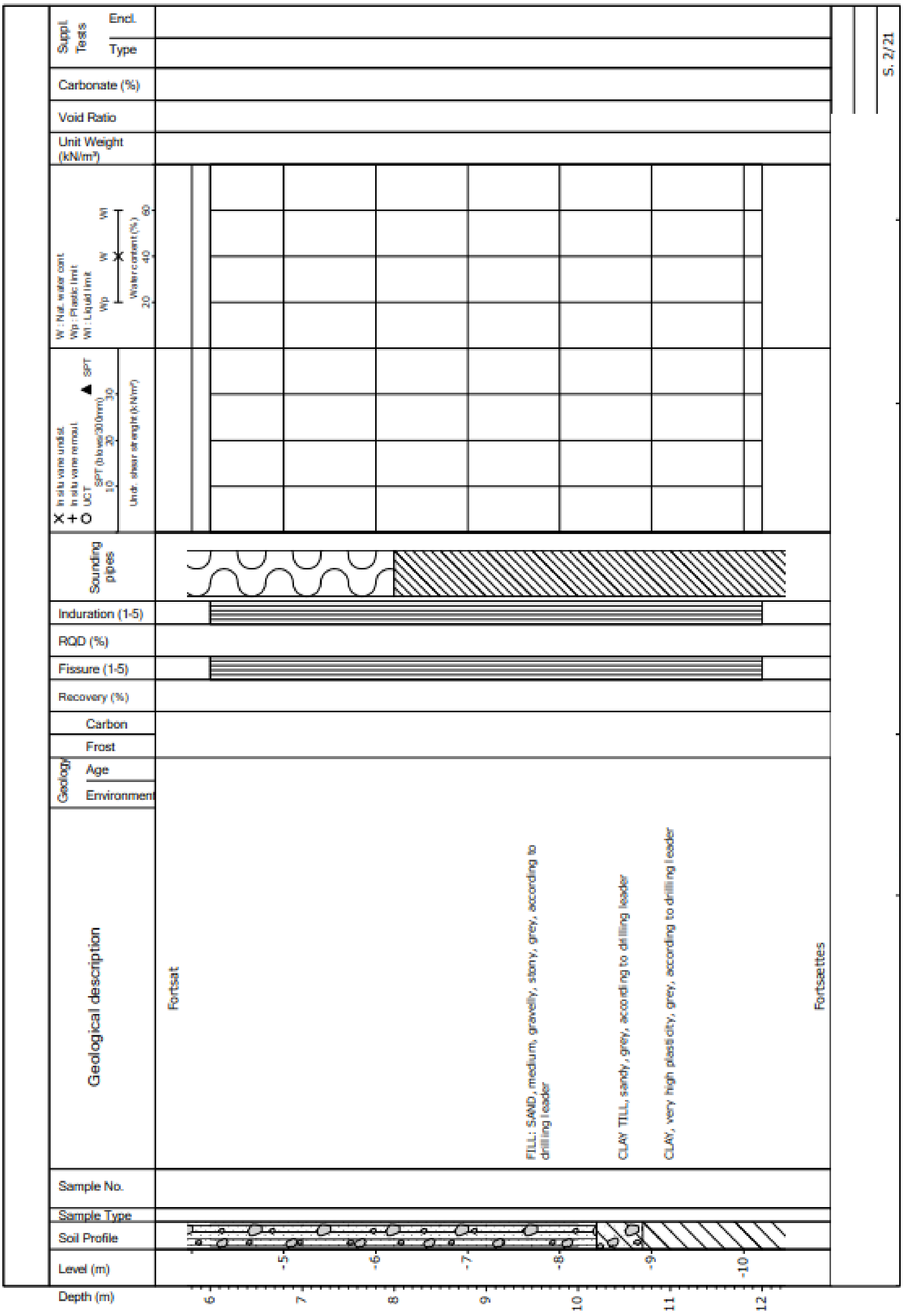
S. 2/21
Suppl. Tests
Encl.
Type
Carbonate (%)
Void Ratio
Unit Weight (kN/m³)
W : Nat. water cont.
Wp : Plastic limit
Wl : Liquid limit
Wp
W
Wl
20
40
60
Water content (%)
In situ vane undist.
In situ vane remoul.
UCT
SPT
10
20
30
SPT (blows/300mm)
Undr. shear strength (kN/m²)
Sounding pipes
Induration (1-5)
RQD (%)
Fissure (1-5)
Recovery (%)
Carbon
Frost
Geology
Age
Environment
Geological description
Fortsat
FILL: SAND, medium, gravelly, stony, grey, according to drilling leader
CLAY TILL, sandy, grey, according to drilling leader
CLAY, very high plasticity, grey, according to drilling leader
Fortsættes
Sample No.
Sample Type
Soil Profile
Level (m)
-5
-6
-7
-8
-9
-10
Depth (m)
6
7
8
9
10
11
12

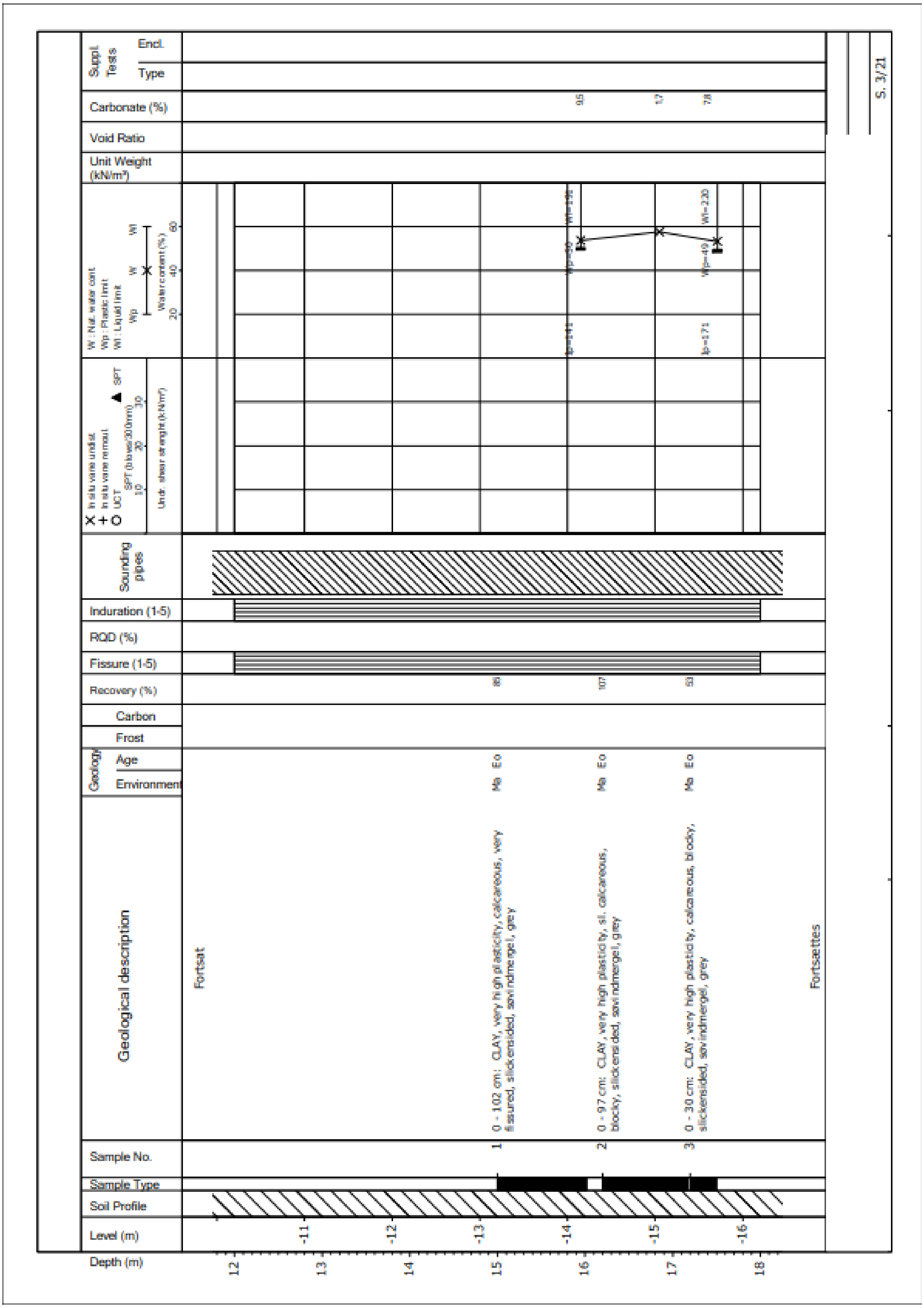
Suppl. Tests
Encl.
Type
Carbonate (%)
9.5
1.7
7.8
Void Ratio
Unit Weight (kN/m³)
W : Nat. water cont.
Wp : Plastic limit
Wl : Liquid limit
Wp
W
Wl
Water content (%)
20
40
60
Wl=132
Wp=50
Ip=141
Wl=220
Wp=49
Ip=171
In situ vane undist.
In situ vane remoul.
UCT
SPT
SPT (blows/300mm)
10
20
30
Undr. shear strength (kN/m²)
Sounding pipes
Induration (1-5)
RQD (%)
Fissure (1-5)
Recovery (%)
85
107
53
Carbon
Frost
Geology
Age
Environment
Ma Eo
Ma Eo
Ma Eo
Geological description
Fortsat
0 - 102 cm: CLAY, very high plasticity, calcareous, very fissured, slickensided, søvindmergel, grey
0 - 97 cm: CLAY, very high plasticity, sl. calcareous, blocky, slickensided, søvindmergel, grey
0 - 30 cm: CLAY, very high plasticity, calcareous, blocky, slickensided, søvindmergel, grey
Fortsættes
Sample No.
1
2
3
Sample Type
Soil Profile
Level (m)
-11
-12
-13
-14
-15
-16
Depth (m)
12
13
14
15
16
17
18
S. 3/21

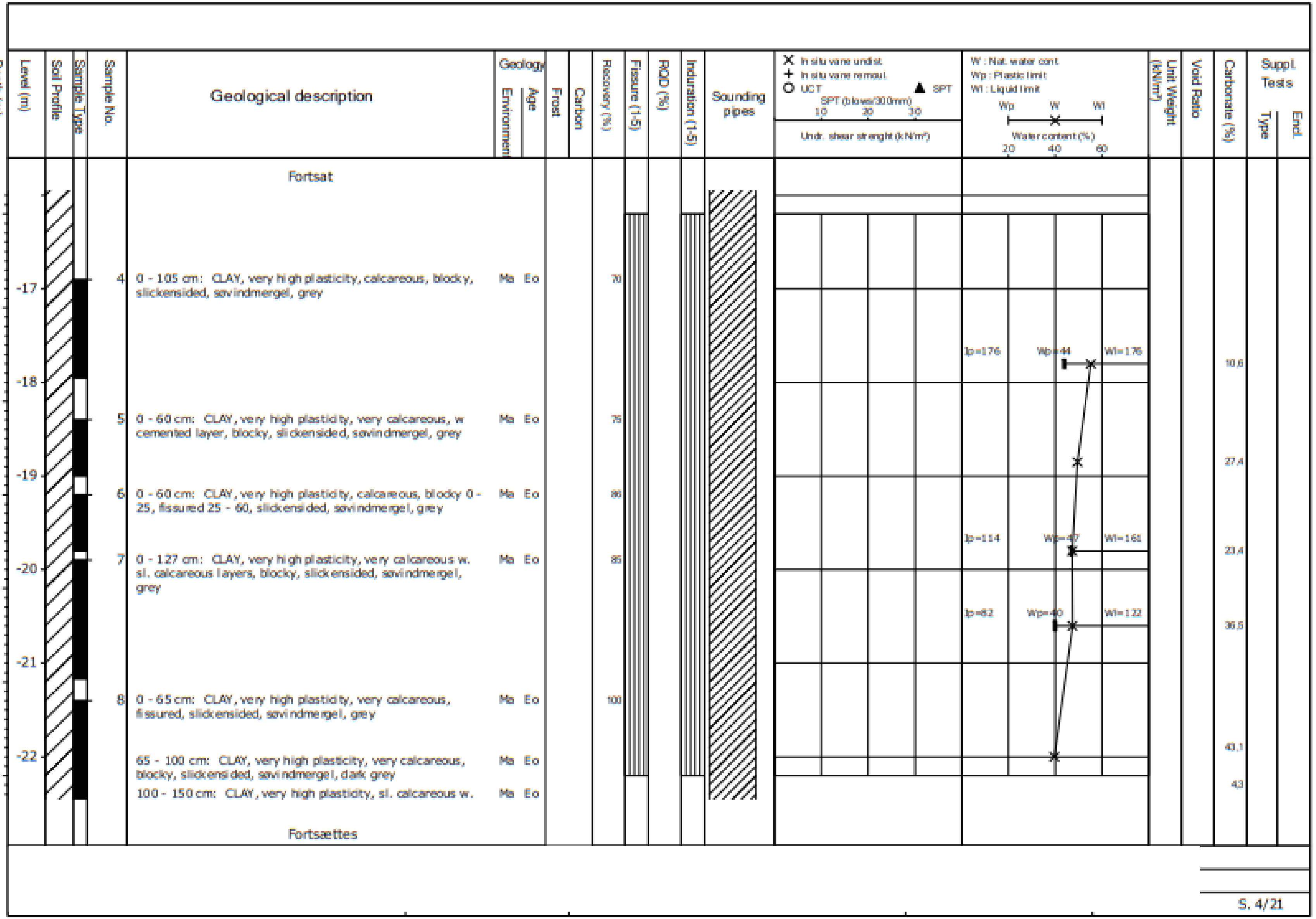

Fortsat

Sample No.	Geological description	Environment	Age	Recovery (%)
4	0 - 105 cm: CLAY, very high plasticity, calcareous, blocky, slickensided, søvindmergel, grey	Ma	Eo	70
5	0 - 60 cm: CLAY, very high plasticity, very calcareous, w cemented layer, blocky, slickensided, søvindmergel, grey	Ma	Eo	75
6	0 - 60 cm: CLAY, very high plasticity, calcareous, blocky 0 - 25, fissured 25 - 60, slickensided, søvindmergel, grey	Ma	Eo	88
7	0 - 127 cm: CLAY, very high plasticity, very calcareous w. sl. calcareous layers, blocky, slickensided, søvindmergel, grey	Ma	Eo	85
8	0 - 65 cm: CLAY, very high plasticity, very calcareous, fissured, slickensided, søvindmergel, grey	Ma	Eo	100
	65 - 100 cm: CLAY, very high plasticity, very calcareous, blocky, slickensided, søvindmergel, dark grey	Ma	Eo	
	100 - 150 cm: CLAY, very high plasticity, sl. calcareous w.	Ma	Eo	

Fortsættes

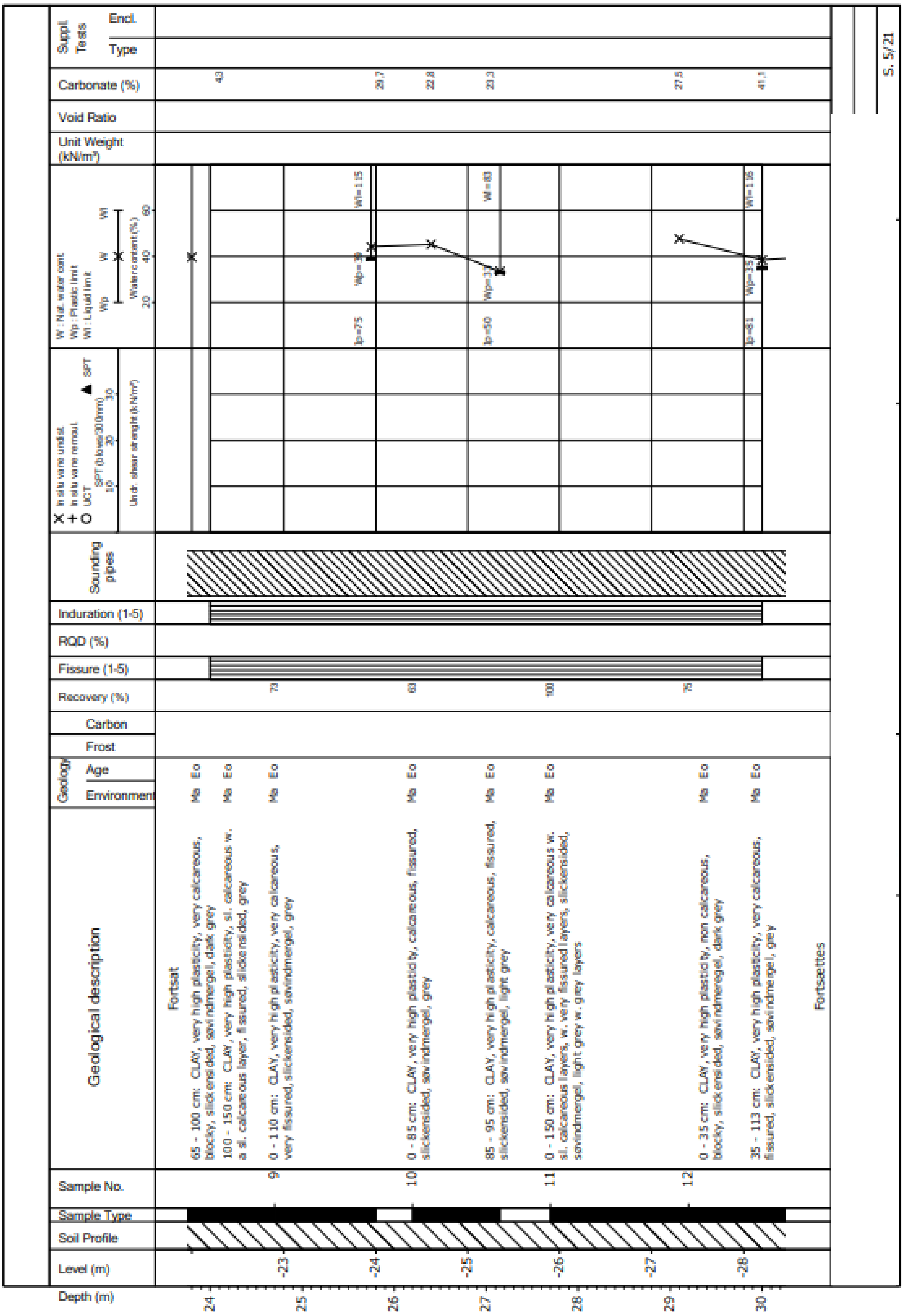
Suppl. Tests
Encl.
Type
Carbonate (%)
43
29,7
22,8
23,3
27,5
41,1
Void Ratio
Unit Weight (kN/m³)
W : Nat. water cont.
Wp : Plastic limit
Wl : Liquid limit
Wp W Wl
Water content (%)
20
40
60
Wl=115
Wp=39
Ip=75
Wl=83
Wp=33
Ip=50
Wl=116
Wp=35
Ip=81
In situ vane undist.
In situ vane remoul.
UCT
SPT
SPT (blows/300mm)
10
20
30
Undr. shear strength (kN/m²)
Sounding pipes
Induration (1-5)
RQD (%)
Fissure (1-5)
Recovery (%)
73
63
100
75
Carbon
Frost
Geology
Age
Environment
Ma Eo
Geological description
Fortsat
65 - 100 cm: CLAY, very high plasticity, very calcareous, blocky, slickensided, søvindmergel, dark grey
100 - 150 cm: CLAY, very high plasticity, sl. calcareous w. a sl. calcareous layer, fissured, slickensided, grey
0 - 110 cm: CLAY, very high plasticity, very calcareous, very fissured, slickensided, søvindmergel, grey
0 - 85 cm: CLAY, very high plasticity, calcareous, fissured, slickensided, søvindmergel, grey
85 - 95 cm: CLAY, very high plasticity, calcareous, fissured, slickensided, søvindmergel, light grey
0 - 150 cm: CLAY, very high plasticity, very calcareous w. sl. calcareous layers, w. very fissured layers, slickensided, søvindmergel, light grey w. grey layers
0 - 35 cm: CLAY, very high plasticity, non calcareous, blocky, slickensided, søvindmergel, dark grey
35 - 113 cm: CLAY, very high plasticity, very calcareous, fissured, slickensided, søvindmergel, grey
Fortsættes
Sample No.
9
10
11
12
Sample Type
Soil Profile
Level (m)
-23
-24
-25
-26
-27
-28
Depth (m)
24
25
26
27
28
29
30
S. 5/21

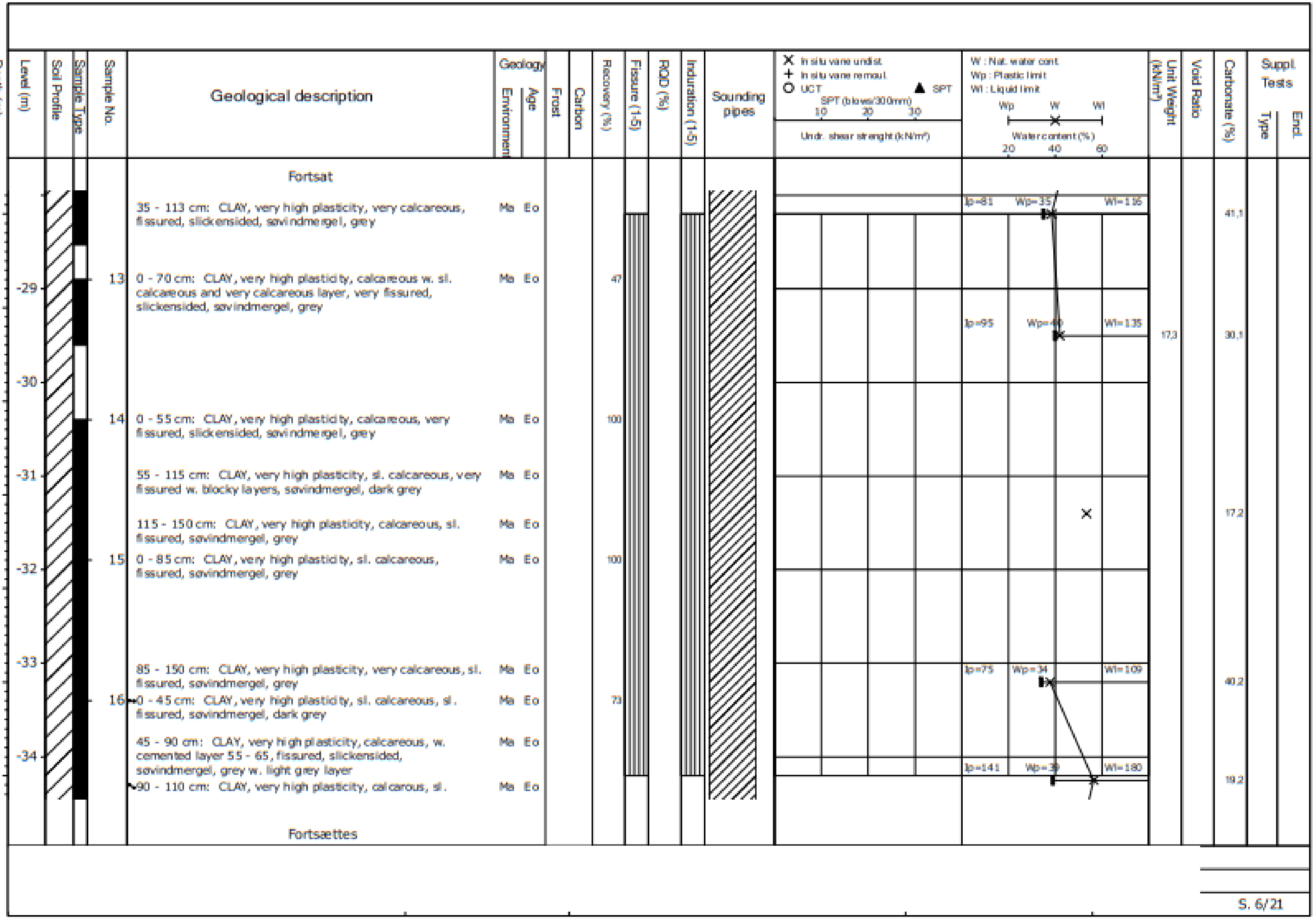

Fortsat

	35 - 113 cm: CLAY, very high plasticity, very calcareous, fissured, slickensided, søvindmergel, grey	Ma	Eo
13	0 - 70 cm: CLAY, very high plasticity, calcareous w. sl. calcareous and very calcareous layer, very fissured, slickensided, søvindmergel, grey	Ma	Eo
14	0 - 55 cm: CLAY, very high plasticity, calcareous, very fissured, slickensided, søvindmergel, grey	Ma	Eo
	55 - 115 cm: CLAY, very high plasticity, sl. calcareous, very fissured w. blocky layers, søvindmergel, dark grey	Ma	Eo
	115 - 150 cm: CLAY, very high plasticity, calcareous, sl. fissured, søvindmergel, grey	Ma	Eo
15	0 - 85 cm: CLAY, very high plasticity, sl. calcareous, fissured, søvindmergel, grey	Ma	Eo
	85 - 150 cm: CLAY, very high plasticity, very calcareous, sl. fissured, søvindmergel, grey	Ma	Eo
16	0 - 45 cm: CLAY, very high plasticity, sl. calcareous, sl. fissured, søvindmergel, dark grey	Ma	Eo
	45 - 90 cm: CLAY, very high plasticity, calcareous, w. cemented layer 55 - 65, fissured, slickensided, søvindmergel, grey w. light grey layer	Ma	Eo
	90 - 110 cm: CLAY, very high plasticity, calcarous, sl.	Ma	Eo

Fortsættes

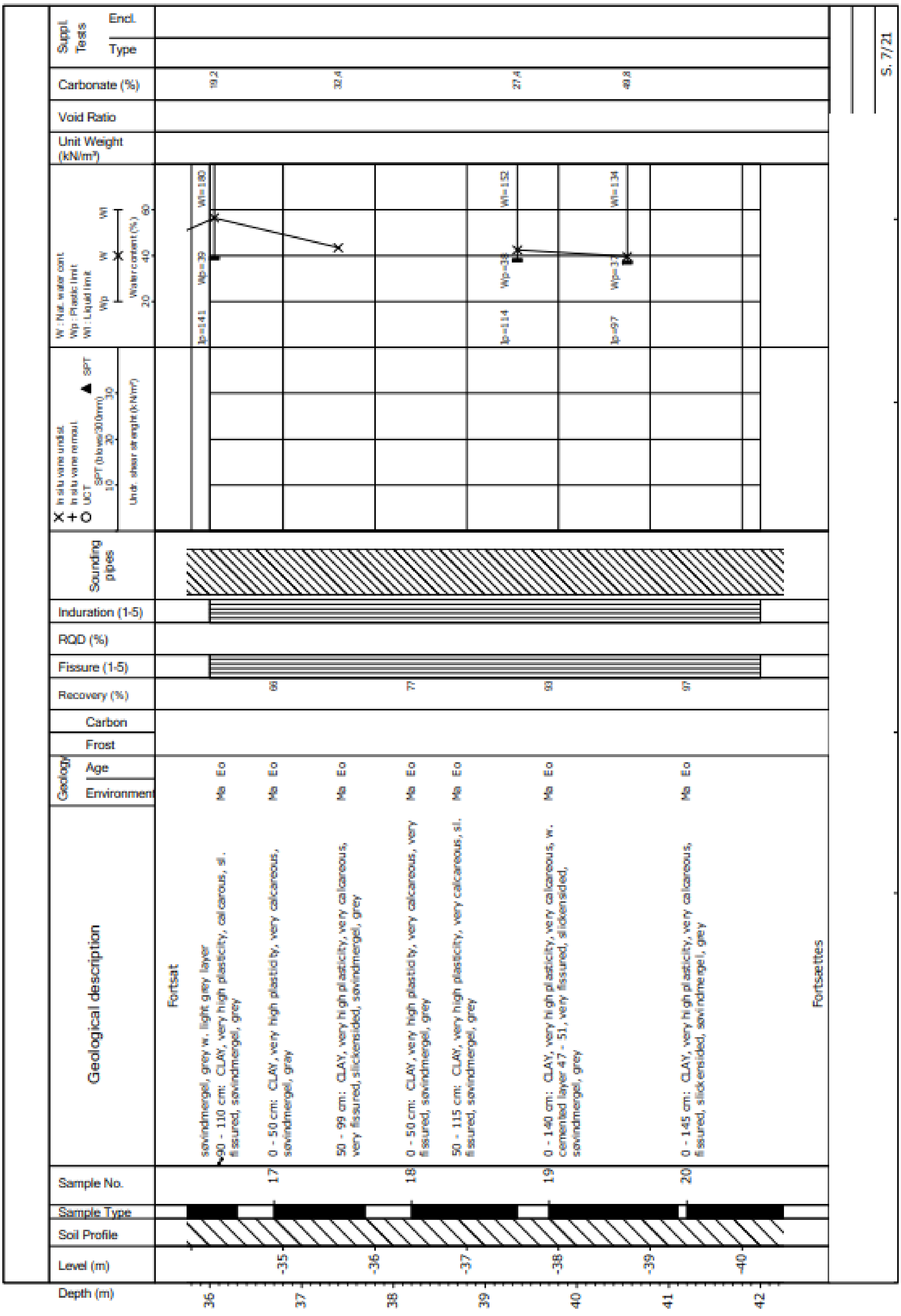

Fortsat

søvindmergel, grey w. light grey layer

90 - 110 cm: CLAY, very high plasticity, calcarous, sl. fissured, søvindmergel, grey — Ma Eo

17 — 0 - 50 cm: CLAY, very high plasticity, very calcareous, søvindmergel, gray — Ma Eo

50 - 99 cm: CLAY, very high plasticity, very calcareous, very fissured, slickensided, søvindmergel, grey — Ma Eo

18 — 0 - 50 cm: CLAY, very high plasticity, very calcareous, very fissured, søvindmergel, grey — Ma Eo

50 - 115 cm: CLAY, very high plasticity, very calcareous, sl. fissured, søvindmergel, grey — Ma Eo

19 — 0 - 140 cm: CLAY, very high plasticity, very calcareous, w. cemented layer 47 - 51, very fissured, slickensided, søvindmergel, grey — Ma Eo

20 — 0 - 145 cm: CLAY, very high plasticity, very calcareous, fissured, slickensided, søvindmergel, grey — Ma Eo

Fortsættes

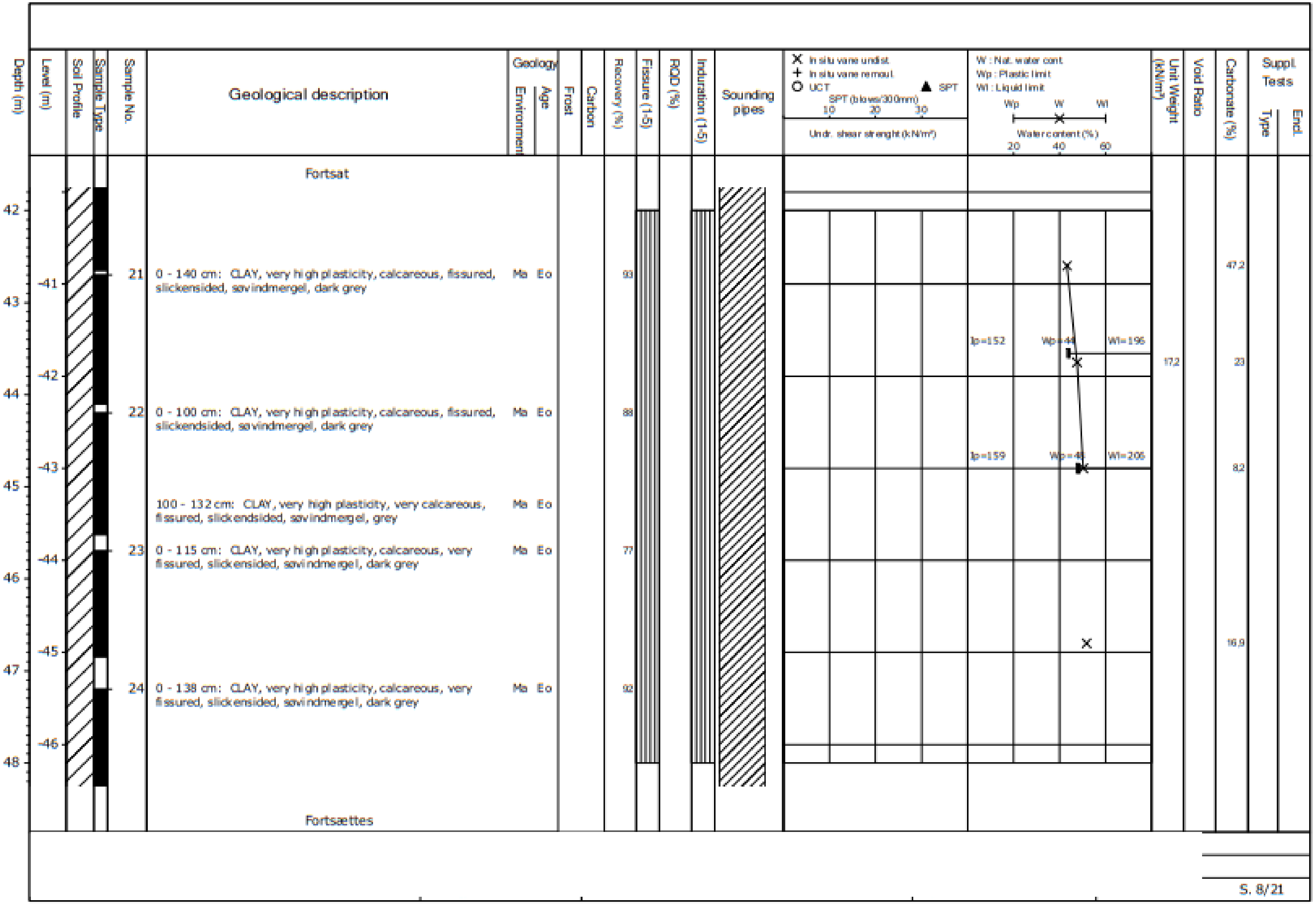

Fortsat

21 0 - 140 cm: CLAY, very high plasticity, calcareous, fissured, slickensided, søvindmergel, dark grey — Ma Eo — Recovery 93

22 0 - 100 cm: CLAY, very high plasticity, calcareous, fissured, slickendsided, søvindmergel, dark grey — Ma Eo — Recovery 88

100 - 132 cm: CLAY, very high plastidity, very calcareous, fissured, slickendsided, søvindmergel, grey — Ma Eo

23 0 - 115 cm: CLAY, very high plasticity, calcareous, very fissured, slickensided, søvindmergel, dark grey — Ma Eo — Recovery 77

24 0 - 138 cm: CLAY, very high plasticity, calcareous, very fissured, slickensided, søvindmergel, dark grey — Ma Eo — Recovery 92

Fortsættes

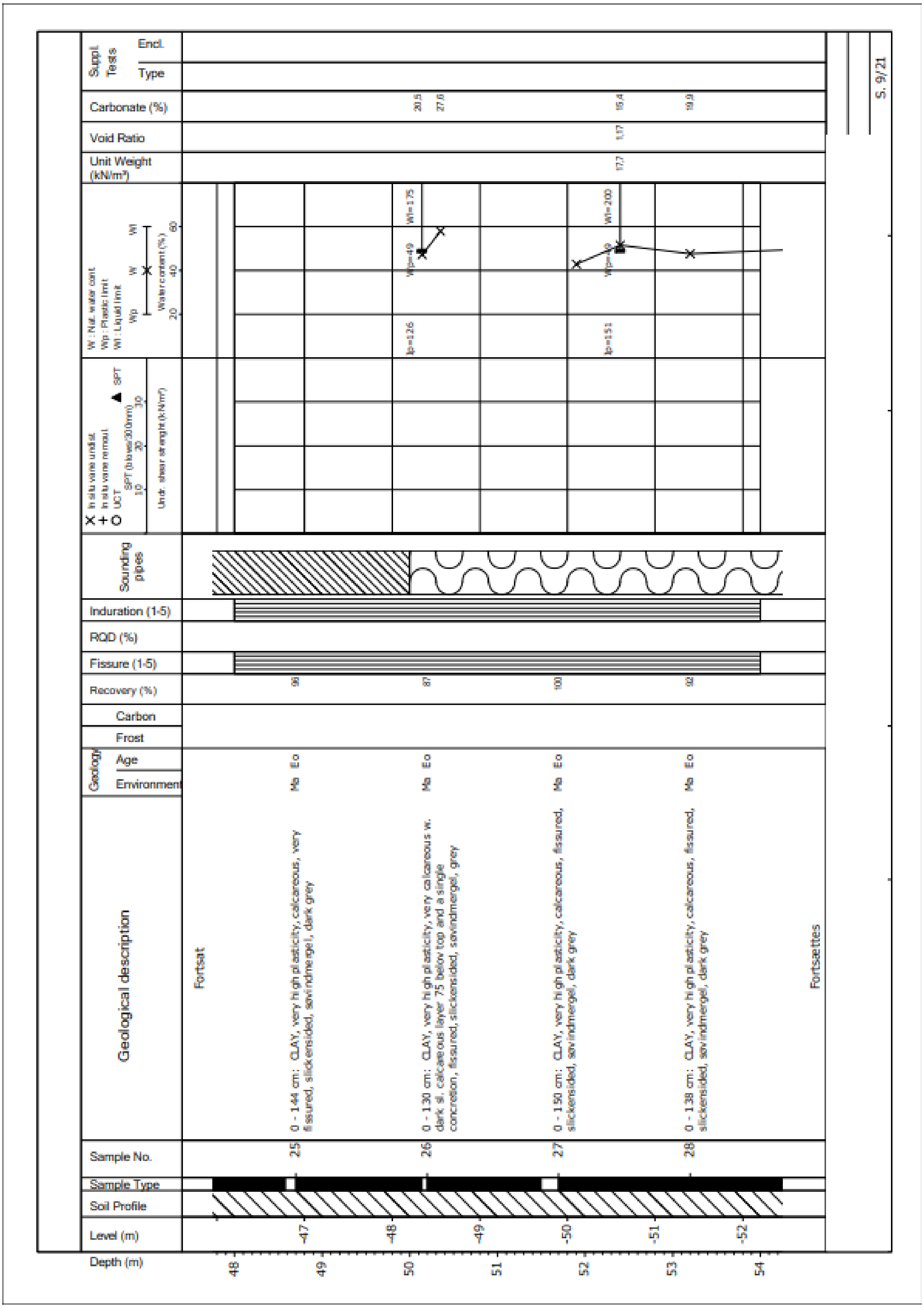
Suppl. Tests
Encl.
Type
Carbonate (%)
20.5
27.6
15.4
19.9
Void Ratio
1.17
Unit Weight (kN/m³)
17.7
W : Nat. water cont.
Wp : Plastic limit
Wl : Liquid limit
Wp
W
Wl
Water content (%)
20
40
60
Wl=175
Wp=49
Ip=126
Wl=200
Wp=49
Ip=151
In situ vane undist.
In situ vane remoul.
UCT
SPT
SPT (blows/300mm)
10
20
30
Undr. shear strength (kN/m²)
Sounding pipes
Induration (1-5)
RQD (%)
Fissure (1-5)
Recovery (%)
98
87
100
92
Carbon
Frost
Geology
Age
Environment
Ma Eo
Ma Eo
Ma Eo
Ma Eo
Geological description
Fortsat
0 - 144 cm: CLAY, very high plasticity, calcareous, very fissured, slickensided, søvindmergel, dark grey
0 - 130 cm: CLAY, very high plasticity, very calcareous w. dark sl. calcareous layer 75 below top and a single concretion, fissured, slickensided, søvindmergel, grey
0 - 150 cm: CLAY, very high plasticity, calcareous, fissured, slickensided, søvindmergel, dark grey
0 - 138 cm: CLAY, very high plasticity, calcareous, fissured, slickensided, søvindmergel, dark grey
Fortsættes
Sample No.
25
26
27
28
Sample Type
Soil Profile
Level (m)
-47
-48
-49
-50
-51
-52
Depth (m)
48
49
50
51
52
53
54
S. 9/21

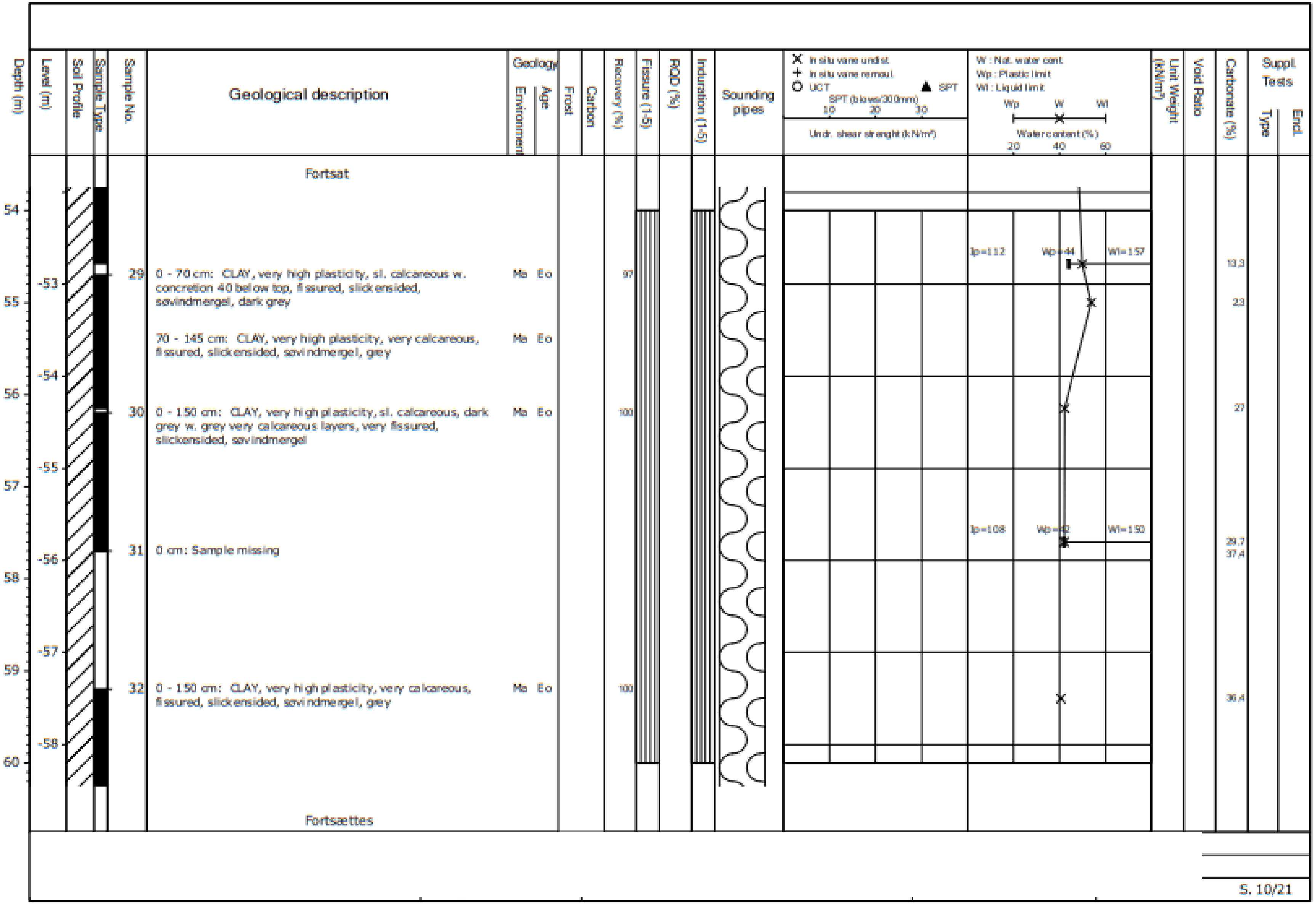

Fortsat

29 0 - 70 cm: CLAY, very high plasticity, sl. calcareous w. concretion 40 below top, fissured, slickensided, søvindmergel, dark grey

70 - 145 cm: CLAY, very high plasticity, very calcareous, fissured, slickensided, søvindmergel, grey

30 0 - 150 cm: CLAY, very high plasticity, sl. calcareous, dark grey w. grey very calcareous layers, very fissured, slickensided, søvindmergel

31 0 cm: Sample missing

32 0 - 150 cm: CLAY, very high plasticity, very calcareous, fissured, slickensided, søvindmergel, grey

Fortsættes

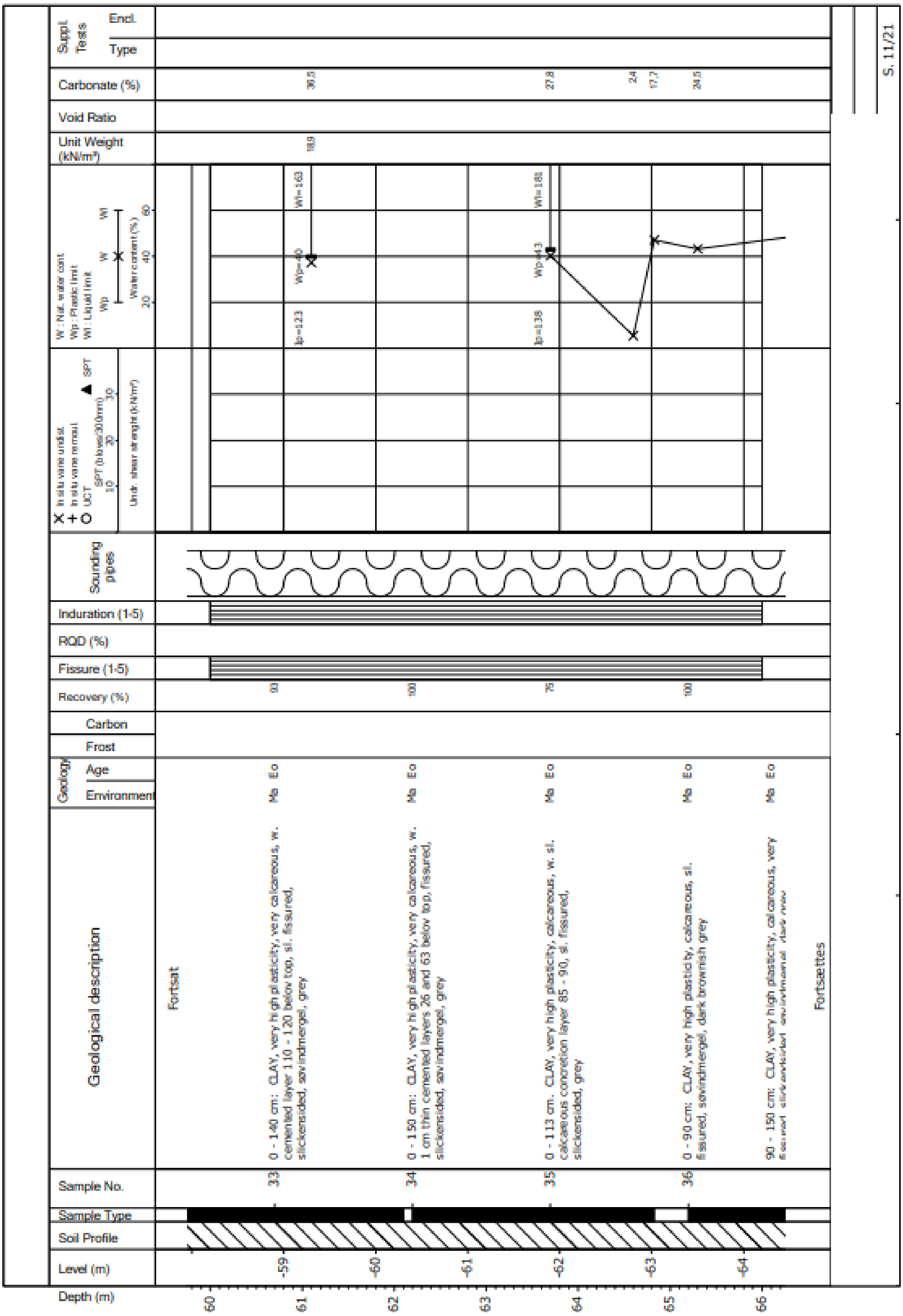
S. 11/21
Suppl. Tests
Encl.
Type
Carbonate (%)
36.5
27.8
24
17.7
24.8
Void Ratio
Unit Weight (kN/m³)
18.9
W : Nat. water cont.
Wp : Plastic limit
Wl : Liquid limit
Wp
W
Wl
Water content (%)
20
40
60
Wl=163
Wp=40
Ip=123
Wl=181
Wp=43
Ip=138
In situ vane undist.
In situ vane remoul.
UCT
SPT
SPT (blows/300mm)
10
20
30
Undr. shear strength (kN/m²)
Sounding pipes
Induration (1-5)
RQD (%)
Fissure (1-5)
Recovery (%)
93
100
75
100
Carbon
Frost
Geology
Age
Environment
Ma Eo
Ma Eo
Ma Eo
Ma Eo
Ma Eo
Geological description
Fortsat
0 - 140 cm: CLAY, very high plasticity, very calcareous, w. cemented layer 110 - 120 below top, sl. fissured, slickensided, søvindmergel, grey
0 - 150 cm: CLAY, very high plasticity, very calcareous, w. 1 cm thin cemented layers 26 and 63 below top, fissured, slickensided, søvindmergel, grey
0 - 113 cm. CLAY, very high plasticity, calcareous, w. sl. calcareous concretion layer 85 - 90, sl. fissured, slickensided, grey
0 - 90 cm: CLAY, very high plasticity, calcareous, sl. fissured, søvindmergel, dark brownish grey
90 - 150 cm: CLAY, very high plasticity, calcareous, very fissured, slickensided, søvindmergel, dark grey
Fortsættes
Sample No.
33
34
35
36
Sample Type
Soil Profile
Level (m)
-59
-60
-61
-62
-63
-64
Depth (m)
60
61
62
63
64
65
66

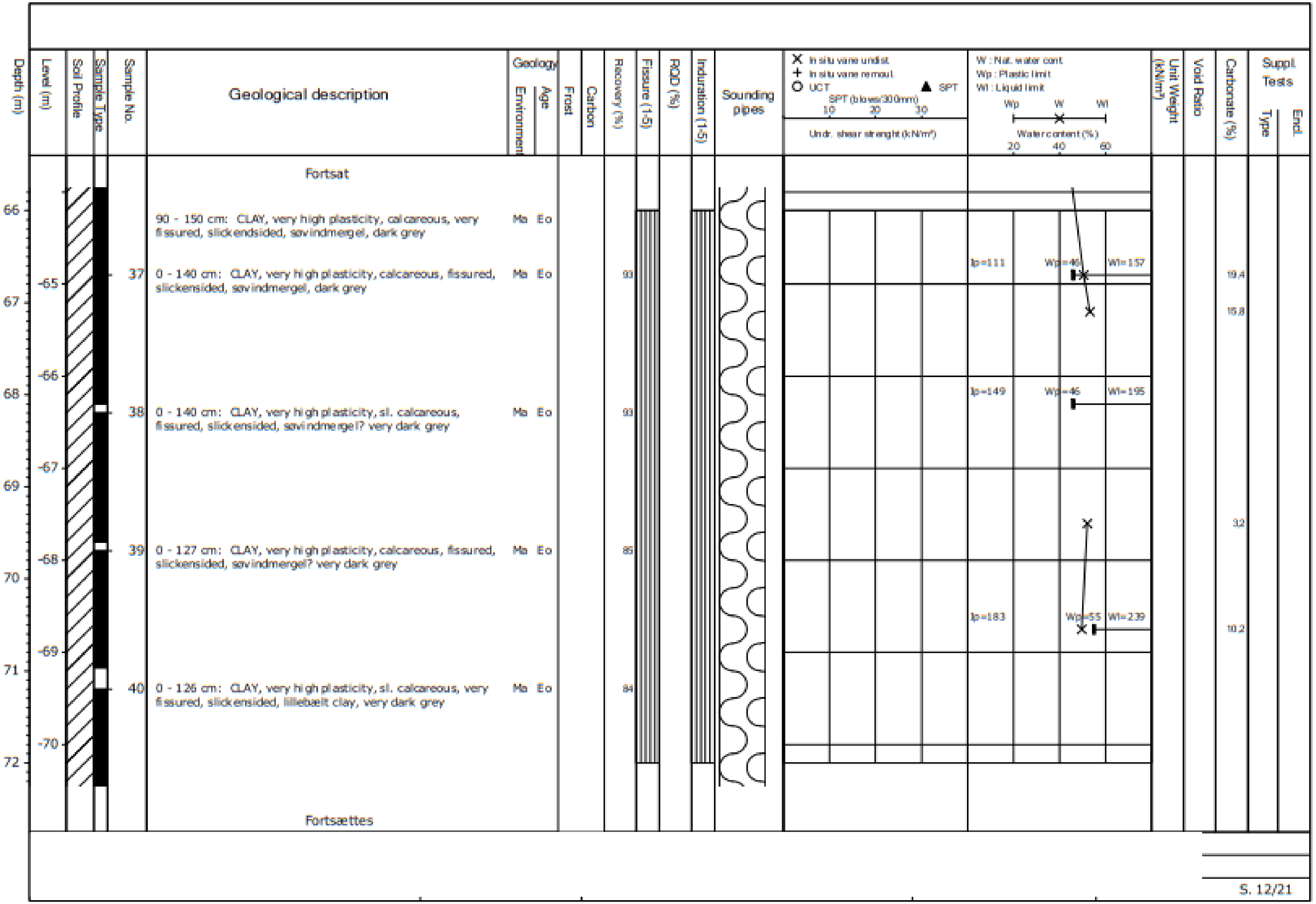

Fortsat

Sample No.	Geological description	Environment	Age
	90 - 150 cm: CLAY, very high plasticity, calcareous, very fissured, slickendsided, søvindmergel, dark grey	Ma	Eo
37	0 - 140 cm: CLAY, very high plasticity, calcareous, fissured, slickensided, søvindmergel, dark grey	Ma	Eo
38	0 - 140 cm: CLAY, very high plasticity, sl. calcareous, fissured, slickensided, søvindmergel? very dark grey	Ma	Eo
39	0 - 127 cm: CLAY, very high plasticity, calcareous, fissured, slickensided, søvindmergel? very dark grey	Ma	Eo
40	0 - 126 cm: CLAY, very high plasticity, sl. calcareous, very fissured, slickensided, lillebælt clay, very dark grey	Ma	Eo

Fortsættes

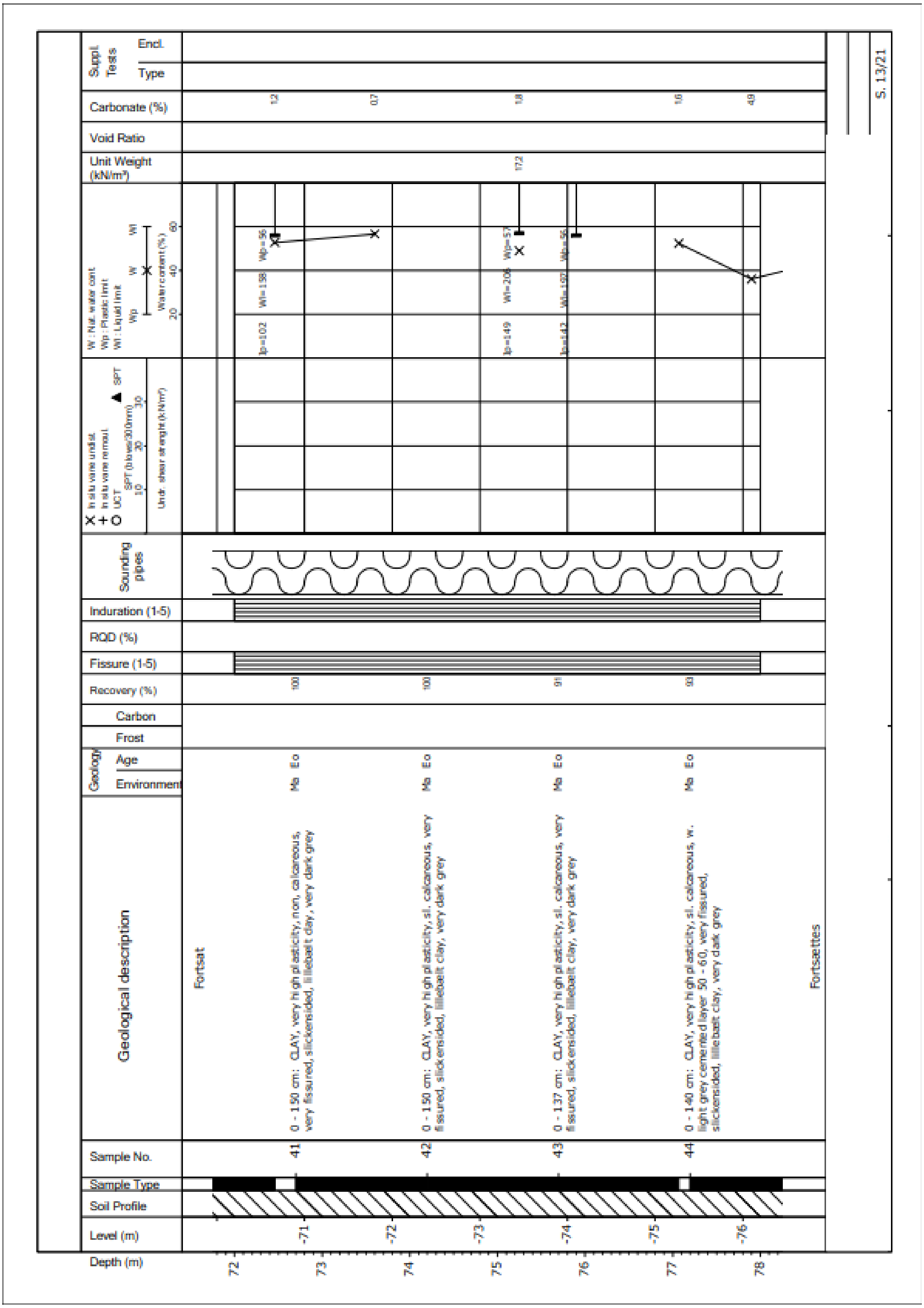
S. 13/21
Suppl. Tests
Encl.
Type
Carbonate (%)
1.2
0.7
1.8
1.6
4.9
Void Ratio
Unit Weight (kN/m³)
17.2
W : Nat. water cont.
Wp : Plastic limit
Wl : Liquid limit
Wp
W
Wl
Water content (%)
20
40
60
Wp=56
Wl=158
Ip=102
Wp=57
Wl=206
Ip=149
Wp=55
Wl=197
Ip=142
In situ vane undist.
In situ vane remoul.
UCT
SPT
SPT (blows/300mm)
10
20
30
Undr. shear strength (kN/m²)
Sounding pipes
Induration (1-5)
RQD (%)
Fissure (1-5)
Recovery (%)
100
100
91
93
Carbon
Frost
Geology
Age
Environment
Ma Eo
Ma Eo
Ma Eo
Ma Eo
Geological description
Fortsat
0 - 150 cm: CLAY, very high plasticity, non. calcareous, very fissured, slickensided, lillebælt clay, very dark grey
0 - 150 cm: CLAY, very high plasticity, sl. calcareous, very fissured, slickensided, lillebælt clay, very dark grey
0 - 137 cm: CLAY, very high plasticity, sl. calcareous, very fissured, slickensided, lillebælt clay, very dark grey
0 - 140 cm: CLAY, very high plasticity, sl. calcareous, w. light grey cemented layer 50 - 60, very fissured, slickensided, lillebælt clay, very dark grey
Fortsættes
Sample No.
41
42
43
44
Sample Type
Soil Profile
Level (m)
-71
-72
-73
-74
-75
-76
Depth (m)
72
73
74
75
76
77
78

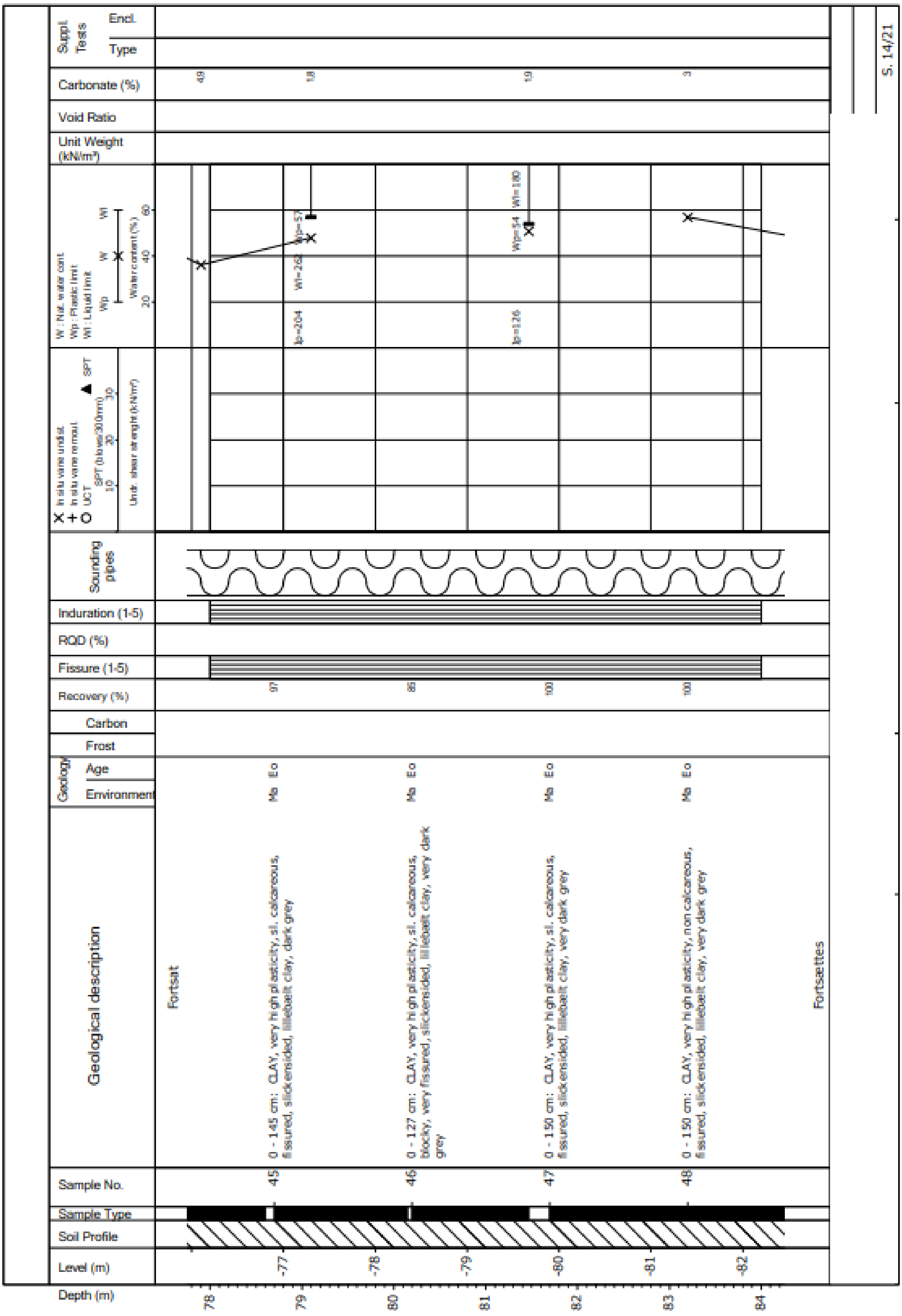
Suppl. Tests
Encl.
Type
Carbonate (%)
49
18
19
3
Void Ratio
Unit Weight (kN/m³)
W : Nat. water cont.
Wp : Plastic limit
Wl : Liquid limit
Wp
W
Wl
20
40
60
Water content (%)
Wl=262
Wp=57
Ip=204
Wl=180
Wp=54
Ip=126
In situ vane undist.
In situ vane remoul.
UCT
SPT
SPT (blows/300mm)
10
20
30
Undr. shear strength (kN/m²)
Sounding pipes
Induration (1-5)
RQD (%)
Fissure (1-5)
Recovery (%)
97
85
100
100
Carbon
Frost
Geology
Age
Environment
Ma Eo
Ma Eo
Ma Eo
Ma Eo
Geological description
Fortsat
0 - 145 cm: CLAY, very high plasticity, sl. calcareous, fissured, slickensided, lillebælt clay, dark grey
0 - 127 cm: CLAY, very high plasticity, sl. calcareous, blocky, very fissured, slickensided, lillebælt clay, very dark grey
0 - 150 cm: CLAY, very high plasticity, sl. calcareous, fissured, slickensided, lillebælt clay, very dark grey
0 - 150 cm: CLAY, very high plasticity, non calcareous, fissured, slickensided, lillebælt clay, very dark grey
Fortsættes
Sample No.
45
46
47
48
Sample Type
Soil Profile
Level (m)
-77
-78
-79
-80
-81
-82
Depth (m)
78
79
80
81
82
83
84
S. 14/21

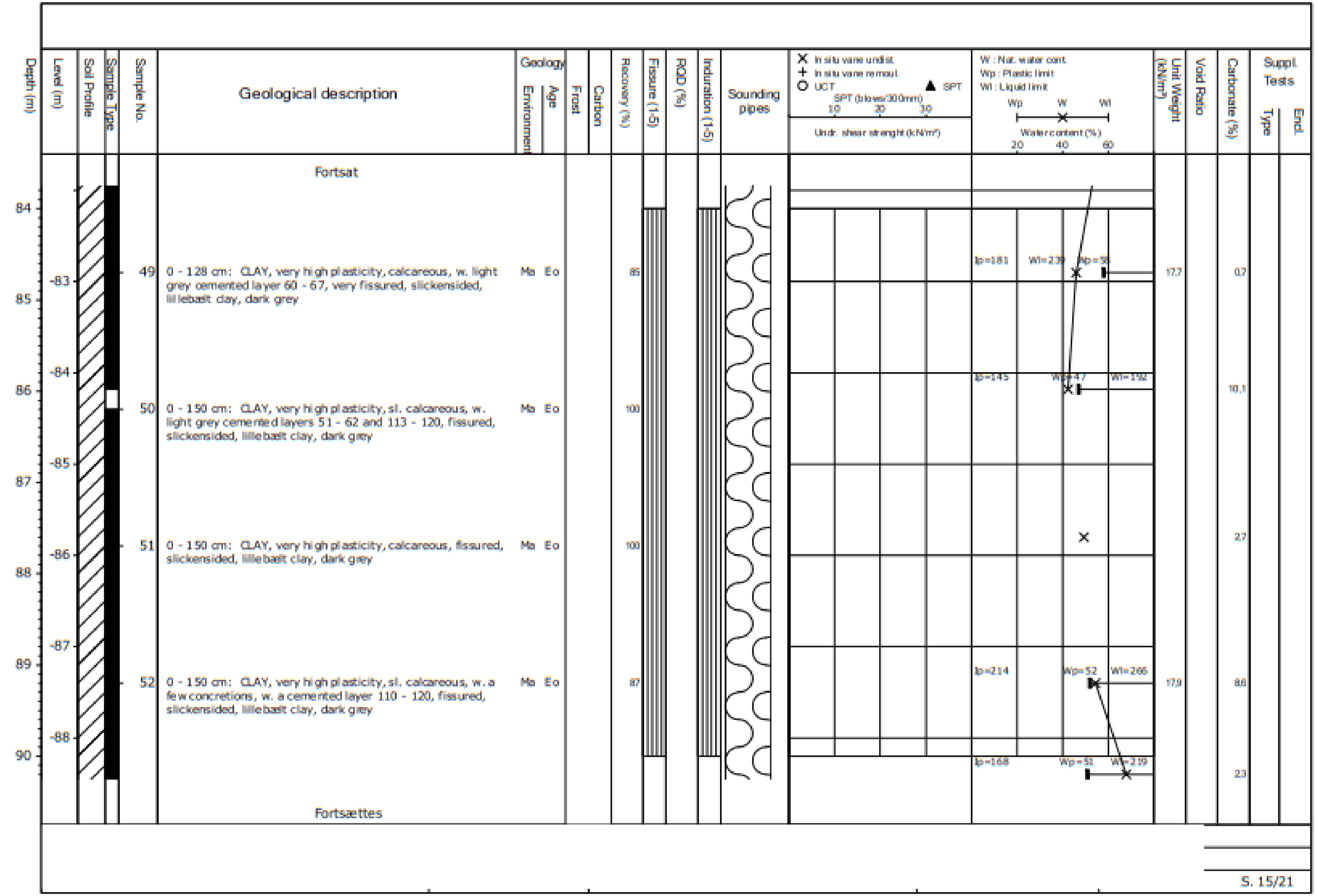

49 0 - 128 cm: CLAY, very high plasticity, calcareous, w. light grey cemented layer 60 - 67, very fissured, slickensided, lillebælt clay, dark grey

50 0 - 150 cm: CLAY, very high plasticity, sl. calcareous, w. light grey cemented layers 51 - 62 and 113 - 120, fissured, slickensided, lillebælt clay, dark grey

51 0 - 150 cm: CLAY, very high plasticity, calcareous, fissured, slickensided, lillebælt clay, dark grey

52 0 - 150 cm: CLAY, very high plasticity, sl. calcareous, w. a few concretions, w. a cemented layer 110 - 120, fissured, slickensided, lillebælt clay, dark grey

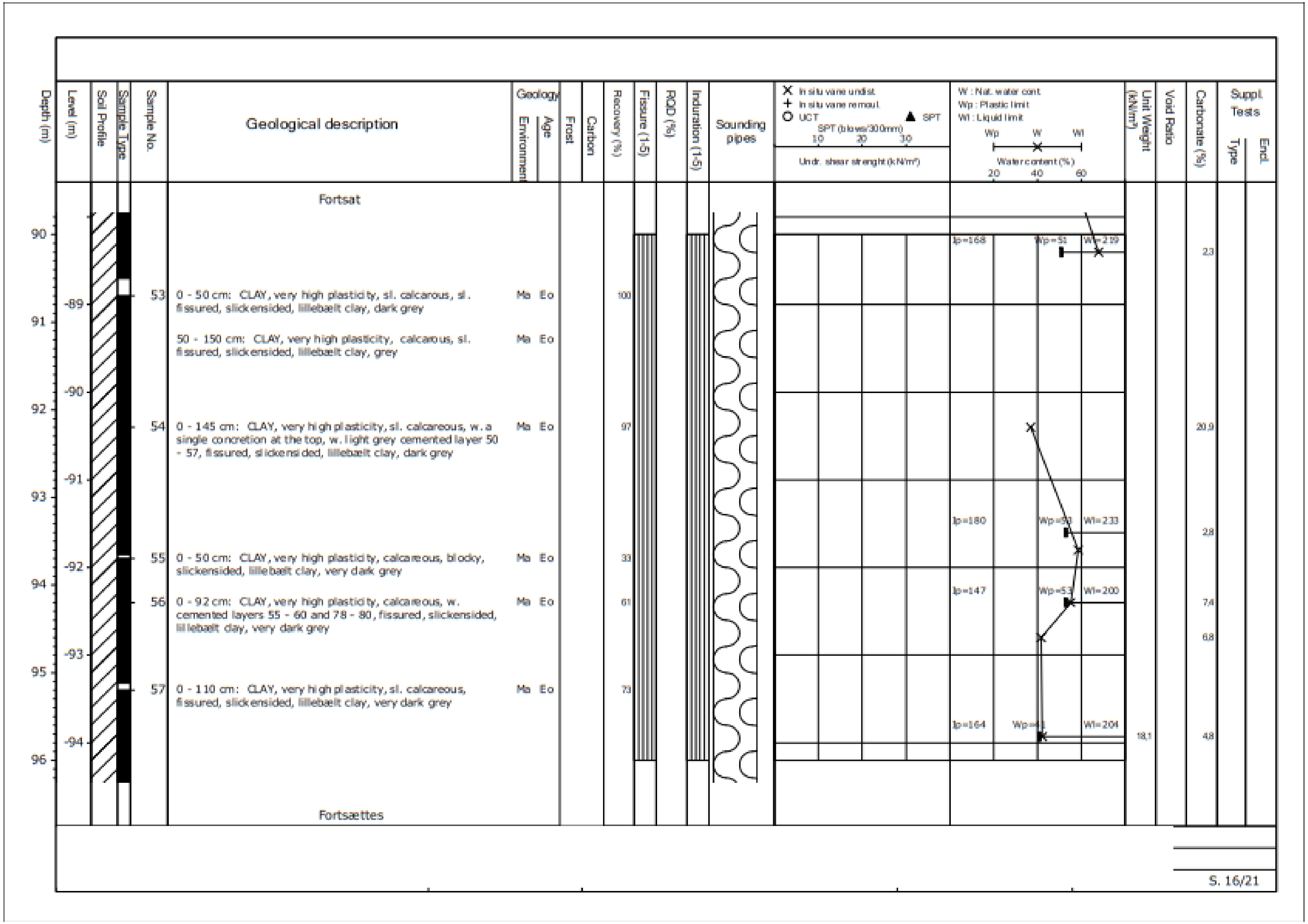

53 0 - 50 cm: CLAY, very high plasticity, sl. calcarous, sl. fissured, slickensided, lillebælt clay, dark grey — Ma Eo

50 - 150 cm: CLAY, very high plasticity, calcarous, sl. fissured, slickensided, lillebælt clay, grey — Ma Eo

54 0 - 145 cm: CLAY, very high plasticity, sl. calcareous, w. a single concretion at the top, w. light grey cemented layer 50 - 57, fissured, slickensided, lillebælt clay, dark grey — Ma Eo

55 0 - 50 cm: CLAY, very high plasticity, calcareous, blocky, slickensided, lillebælt clay, very dark grey — Ma Eo

56 0 - 92 cm: CLAY, very high plasticity, calcareous, w. cemented layers 55 - 60 and 78 - 80, fissured, slickensided, lillebælt clay, very dark grey — Ma Eo

57 0 - 110 cm: CLAY, very high plasticity, sl. calcareous, fissured, slickensided, lillebælt clay, very dark grey — Ma Eo

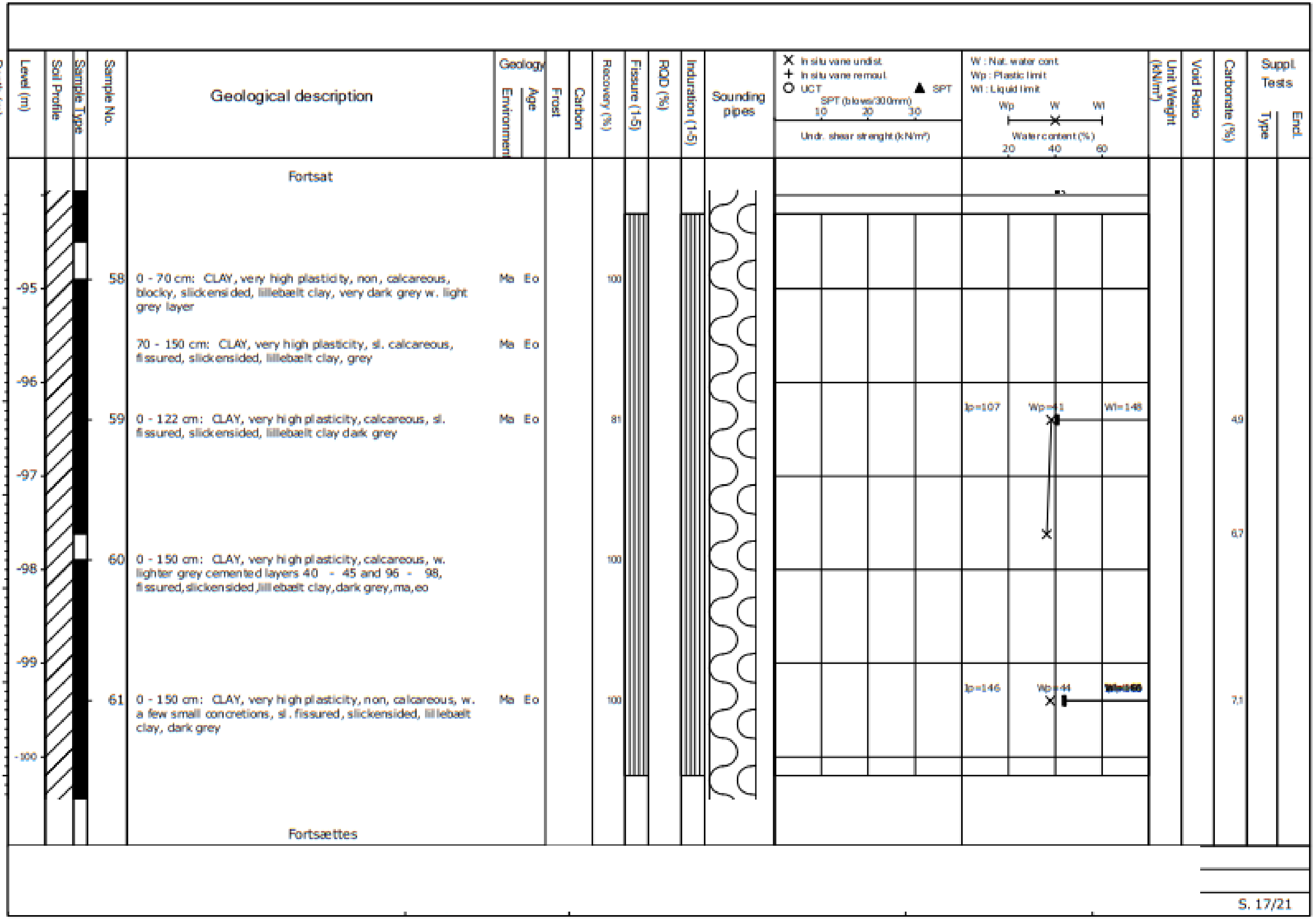

Fortsat

58 0 - 70 cm: CLAY, very high plasticity, non, calcareous, blocky, slickensided, lillebælt clay, very dark grey w. light grey layer — Ma Eo — 100

70 - 150 cm: CLAY, very high plasticity, sl. calcareous, fissured, slickensided, lillebælt clay, grey — Ma Eo

59 0 - 122 cm: CLAY, very high plasticity, calcareous, sl. fissured, slickensided, lillebælt clay dark grey — Ma Eo — 81

60 0 - 150 cm: CLAY, very high plasticity, calcareous, w. lighter grey cemented layers 40 - 45 and 96 - 98, fissured, slickensided, lillebælt clay, dark grey, ma, eo — 100

61 0 - 150 cm: CLAY, very high plasticity, non, calcareous, w. a few small concretions, sl. fissured, slickensided, lillebælt clay, dark grey — Ma Eo — 100

Fortsættes

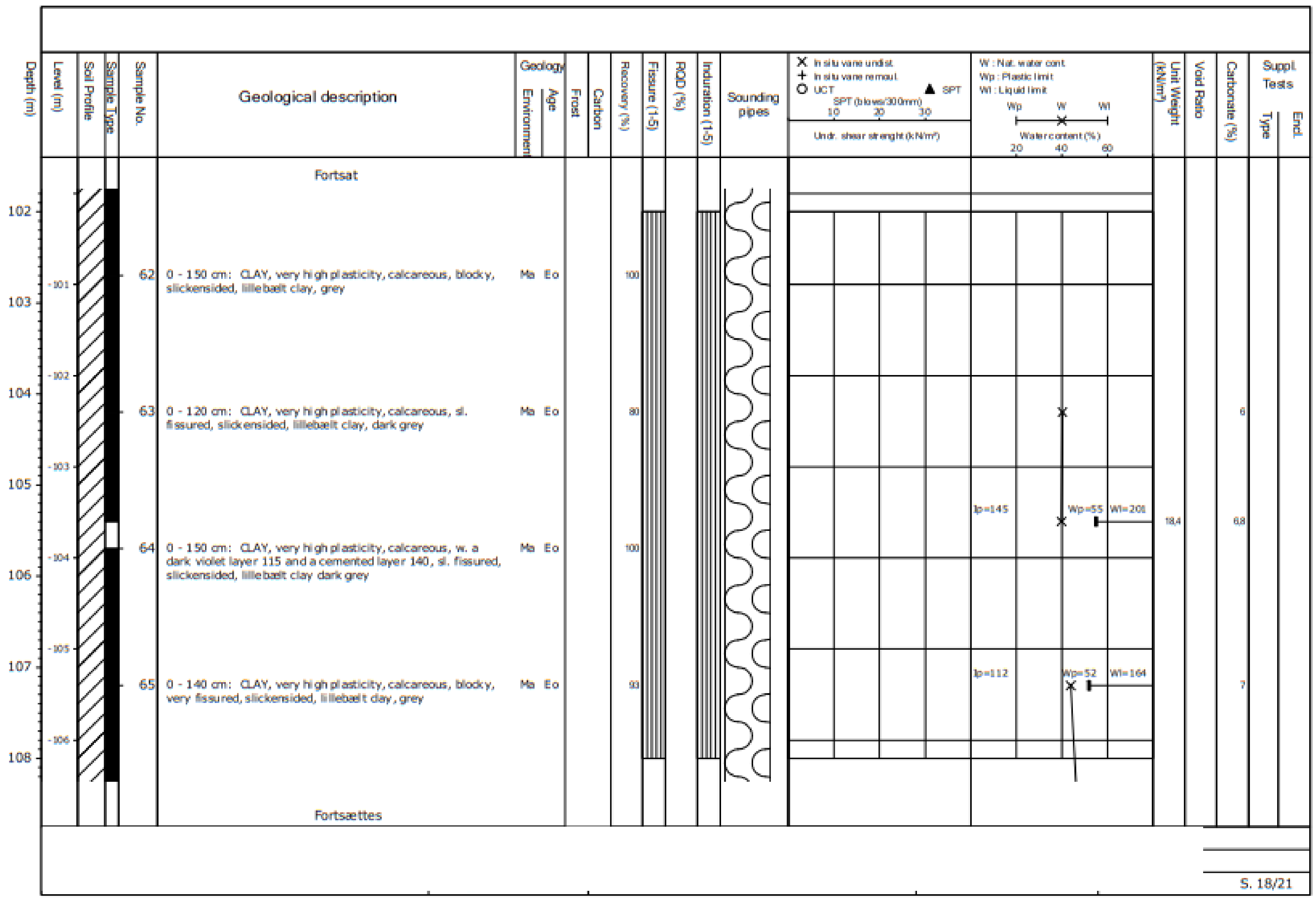

Sample No.	Geological description	Environment	Age	Recovery (%)
62	0 - 150 cm: CLAY, very high plasticity, calcareous, blocky, slickensided, lillebælt clay, grey	Ma	Eo	100
63	0 - 120 cm: CLAY, very high plasticity, calcareous, sl. fissured, slickensided, lillebælt clay, dark grey	Ma	Eo	80
64	0 - 150 cm: CLAY, very high plasticity, calcareous, w. a dark violet layer 115 and a cemented layer 140, sl. fissured, slickensided, lillebælt clay dark grey	Ma	Eo	100
65	0 - 140 cm: CLAY, very high plasticity, calcareous, blocky, very fissured, slickensided, lillebælt clay, grey	Ma	Eo	93

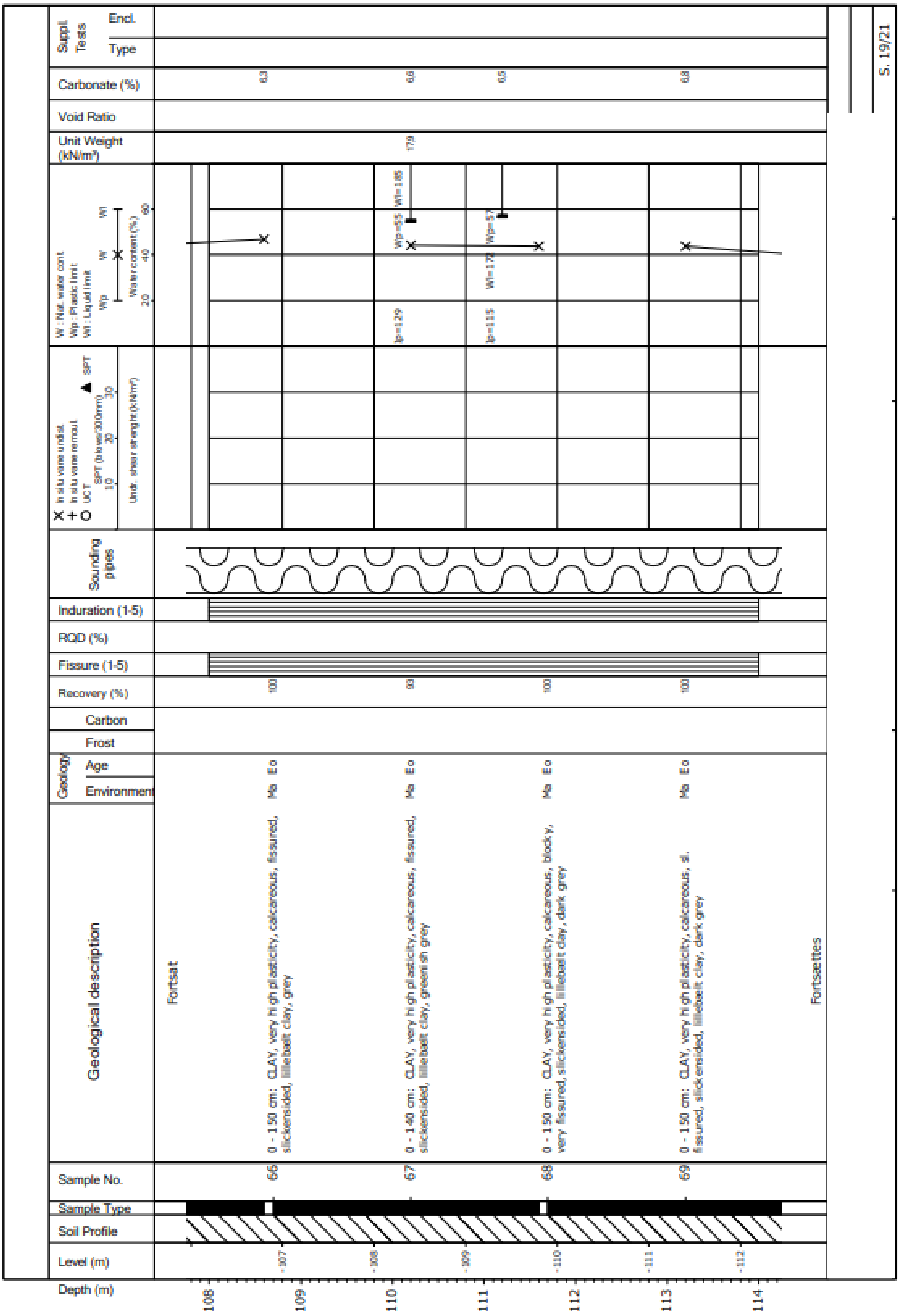
S. 19/21
Suppl. Tests
Encl.
Type
Carbonate (%)
63
66
65
68
Void Ratio
Unit Weight (kN/m³)
17.0
W : Nat. water cont.
Wp : Plastic limit
Wl : Liquid limit
Wp
W
Wl
20
40
60
Water content (%)
Wp=55
Wl=185
Ip=129
Wp=57
Wl=172
Ip=115
✕ In situ vane undist.
+ In situ vane remould.
○ UCT
▲ SPT
10
20
30
SPT (blows/300mm)
Undr. shear strength (kN/m²)
Sounding pipes
Induration (1-5)
RQD (%)
Fissure (1-5)
Recovery (%)
100
93
100
100
Carbon
Frost
Geology
Age
Environment
Ma Eo
Ma Eo
Ma Eo
Ma Eo
Geological description
Fortsat
0 - 150 cm: CLAY, very high plasticity, calcareous, fissured, slickensided, lillebælt clay, grey
0 - 140 cm: CLAY, very high plasticity, calcareous, fissured, slickensided, lillebælt clay, greenish grey
0 - 150 cm: CLAY, very high plasticity, calcareous, blocky, very fissured, slickensided, lillebælt clay, dark grey
0 - 150 cm: CLAY, very high plasticity, calcareous, sl. fissured, slickensided, lillebælt clay, dark grey
Fortsættes
Sample No.
66
67
68
69
Sample Type
Soil Profile
Level (m)
-107
-108
-109
-110
-111
-112
Depth (m)
108
109
110
111
112
113
114

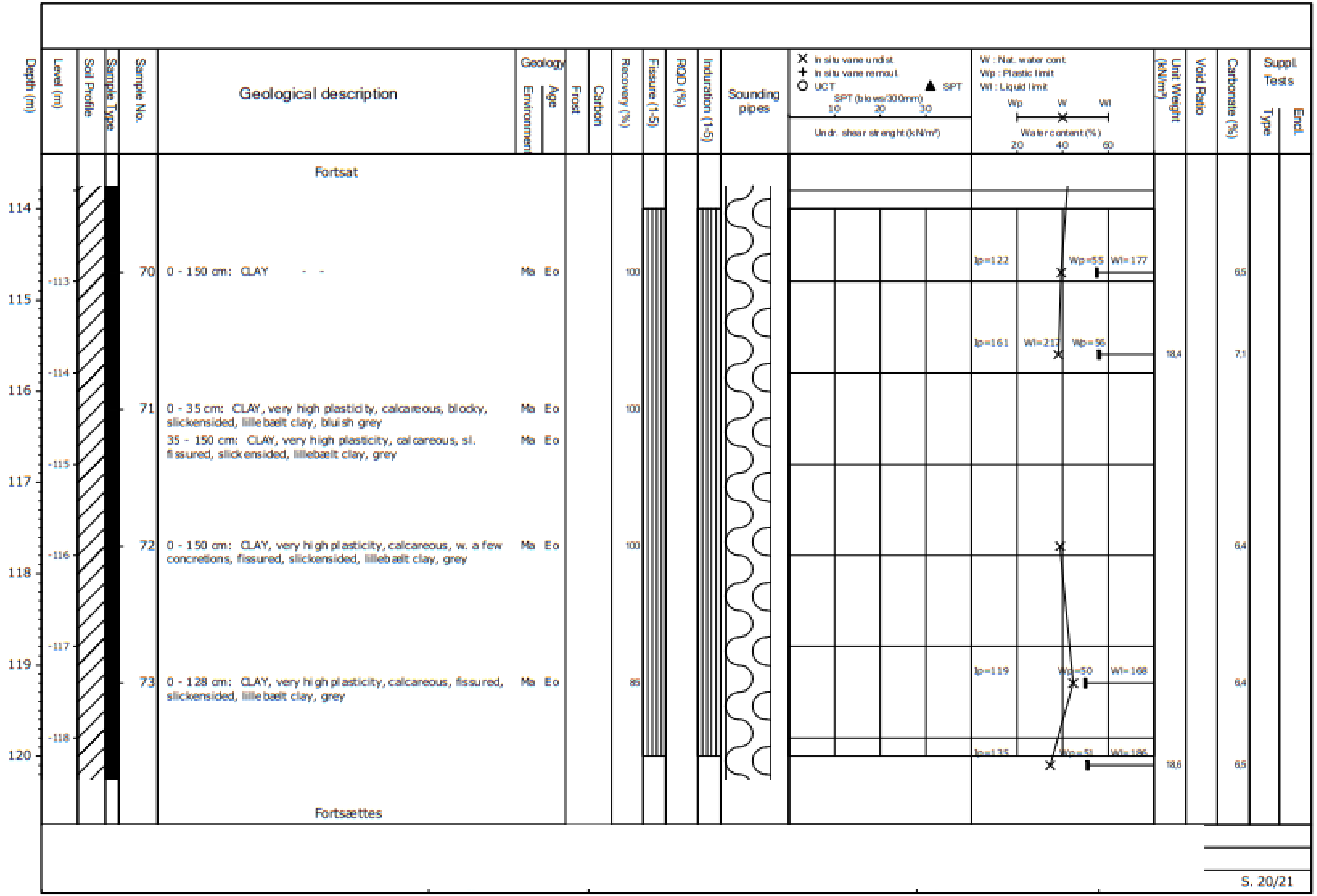

Fortsat

70 0 - 150 cm: CLAY - -

71 0 - 35 cm: CLAY, very high plasticity, calcareous, blocky, slickensided, lillebælt clay, bluish grey

35 - 150 cm: CLAY, very high plasticity, calcareous, sl. fissured, slickensided, lillebælt clay, grey

72 0 - 150 cm: CLAY, very high plasticity, calcareous, w. a few concretions, fissured, slickensided, lillebælt clay, grey

73 0 - 128 cm: CLAY, very high plasticity, calcareous, fissured, slickensided, lillebælt clay, grey

Fortsættes

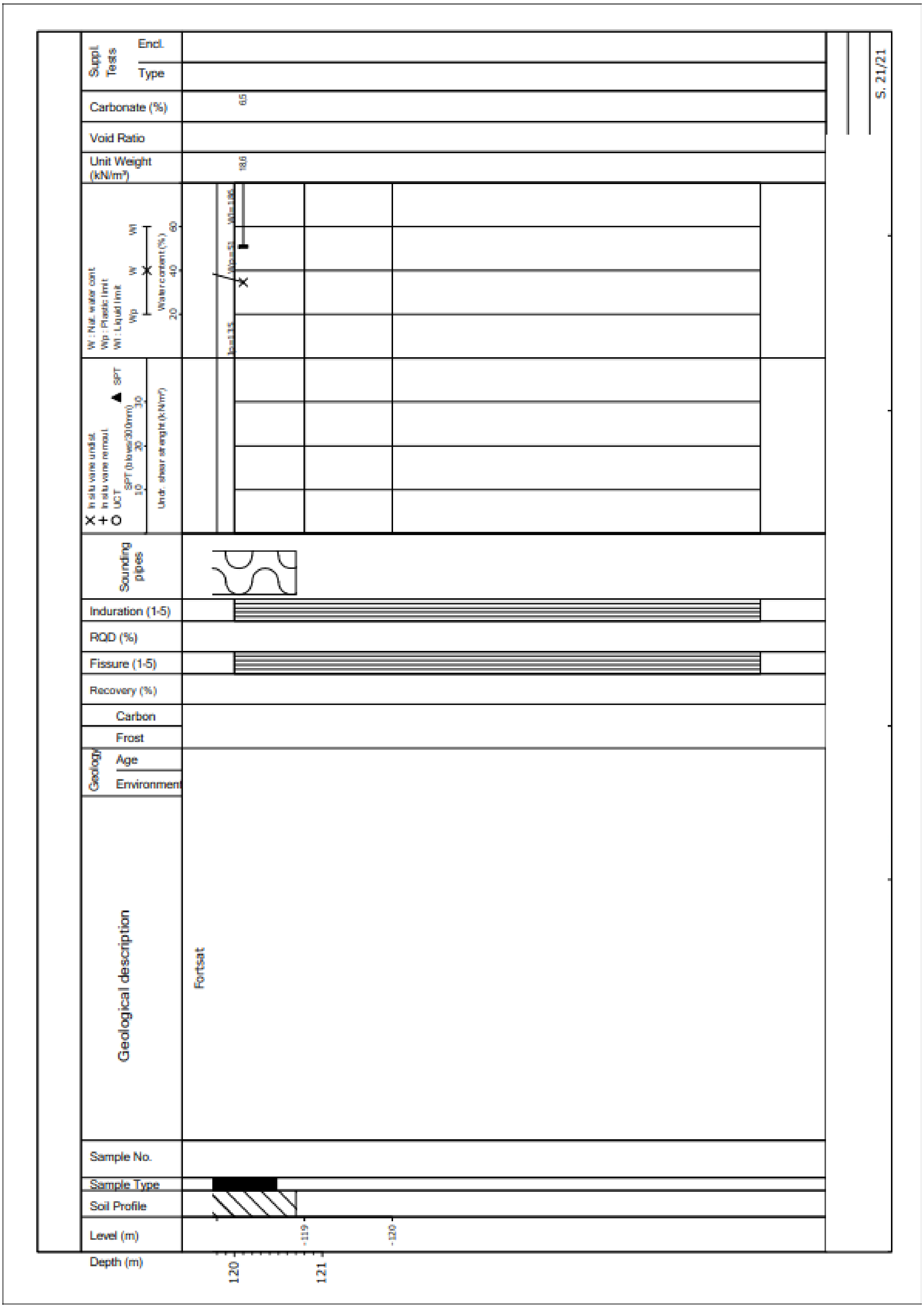
S. 21/21
Suppl. Tests
Encl.
Type
Carbonate (%)
65
Void Ratio
Unit Weight (kN/m³)
18.6
W : Nat. water cont.
Wp : Plastic limit
Wl : Liquid limit
Wp
W
Wl
Water content (%)
20
40
60
Wl=106
Wp=51
Ip=135
X In situ vane undist.
+ In situ vane remoul.
O UCT
SPT (blows/300mm)
SPT
10
20
30
Undr. shear strength (kN/m²)
Sounding pipes
Induration (1-5)
RQD (%)
Fissure (1-5)
Recovery (%)
Carbon
Frost
Geology
Age
Environment
Geological description
Fortsat
Sample No.
Sample Type
Soil Profile
Level (m)
-119
-120
Depth (m)
120
121

Appendix C Interpretation of CPT data

This appendix belongs to chapter 4 in the main report. This appendix present extra figures for the data processing and the investigation of dependency between cone factors and soil parameters. Further the investigation concerning the interval Δa is also presented here.

Appendix C.1 Data processing for Project 1

The different steps in the data processing is here presented for Project 1.

Isolate soil of interest

In Project 1, the Søvind Marls is determined to start at the depth of 10 m. The CPT data above 10 m is therefore removed, which is shown in Figure C.1.1.

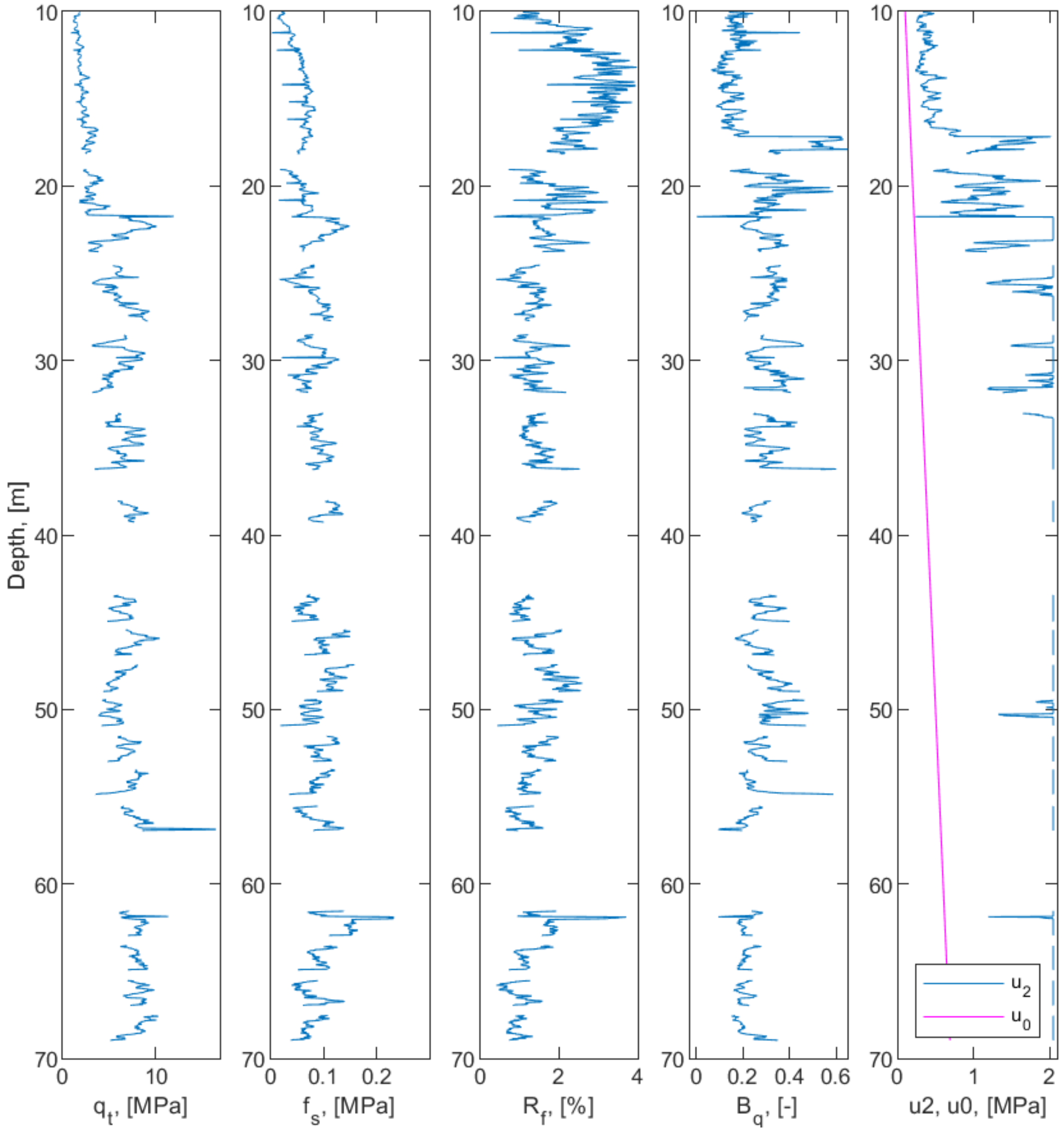

Figure C.1.1: CPT data for Project 1 after isolating the CPT data from the Søvind Marl.

Correction of testing errors

No measurements of the inclination are given for Project 1. It is assumed that this is not measured since the test is conducted as a "down the hole" test. It is therefore assumed that the inclination is not deviating considerably, and no modification is done with regards to the inclination for Project 1.

Project 1 did not have any measurements for the penetration rate. Instead, it is approximated from the gathered CPT data. For Project 1 the CPT data is measured for each 2 cm of penetration. It is assumed that the contractors tried to use a penetration rate given from the standards and by assuming the sampling frequency is once per second, the penetration rate is 2 cm/s. The CPT data from Project 1 is therefore not corrected with regards to the penetration rate, since this is the standard.

Correction of visual errors

For Project 1, there are not many peaks and troughs. The same thresholds are used as for Project 2, which is 11.2 MPa and 0.33 MPa respectively for the cone resistance and sleeve friction. At the depth of 61 m, one peak is hereby removed in the cone resistance, which is shown in Figure C.1.2.

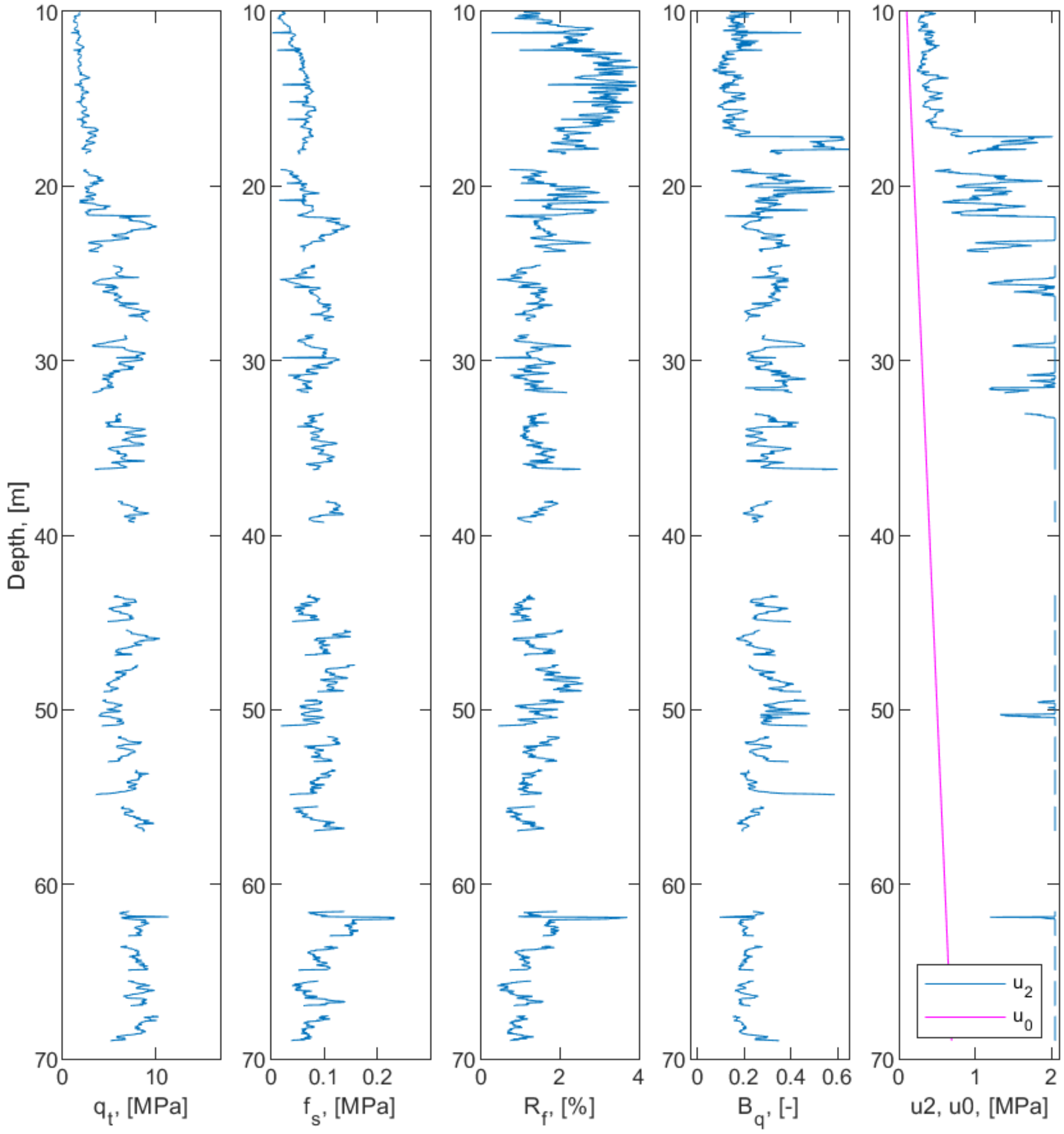

Figure C.1.2: CPT data for Project 1 after removal of peak and trough values in the CPT data.

No major drops are seen in the pore pressure, and therefore no corrections are made with regards to the pore pressure.

Smoothening of the CPT data

The last step in the data processing is smoothening the CPT data. Same procedure is used, as presented in the main report. The smoothened data is shown in Figure C.1.3.

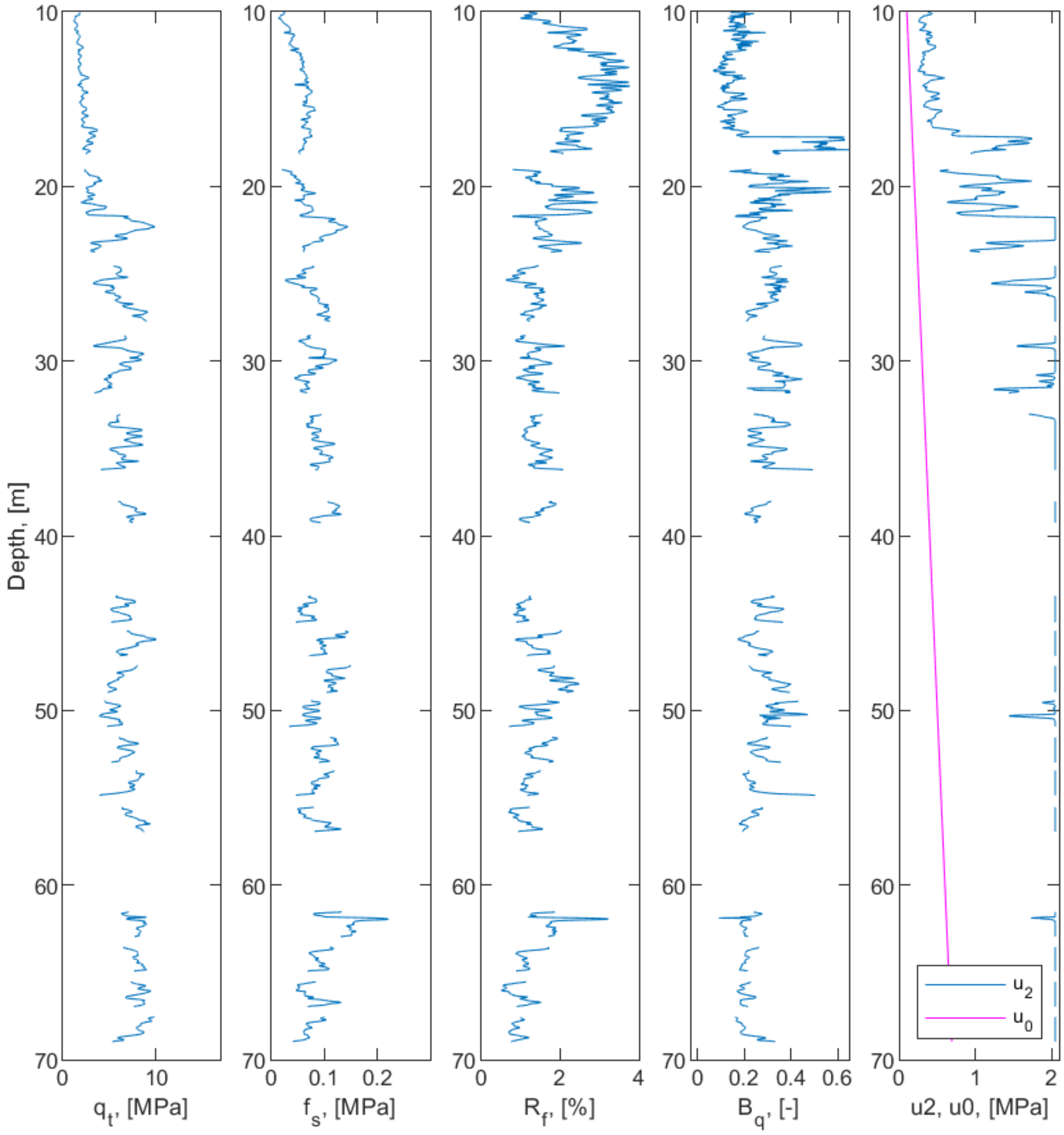

Figure C.1.3: CPT data for Project 1 after smoothening.

The CPT data is hereby processed as the CPT data for Project 2 is, in the main report. It seen that that CPT data has not changed as much as the data from Project 2. This is primarily because no penetration rate or inclination are corrected, and the amount of data is also significantly less, since the cone is pushed 120 m in Project 2 and only 70 m for Project 1.

Appendix C.2 Data processing for Project 2

Here the CPT data is shown again from the data processing of Project 2, but only with the “after” CPT data for each step in the data processing.

Correction of testing errors

In Figure C.2.1 the CPT data from Project 2, can be seen after the removal of the CPT data with greater penetration rate than 2.5 cm/s.

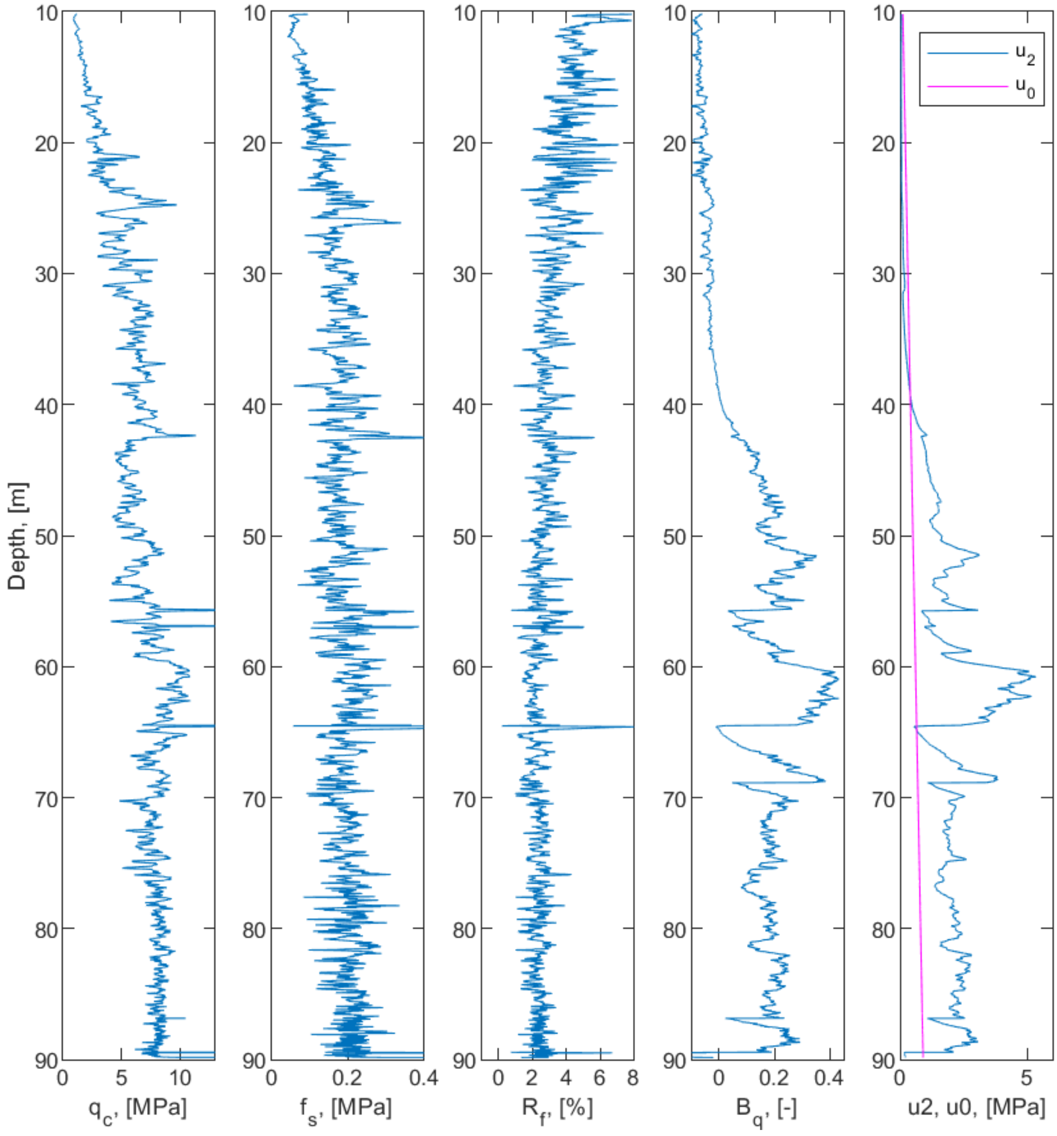

Figure C.2.1: CPT data for Project 2 after removal of CPT data with penetration rates above 2.5 cm/s.

Correction of visual errors

In Figure C.2.2 the CPT data from Project 2, can be seen after the removal peaks and troughs in the cone resistance, sleeve friction and pore pressure.

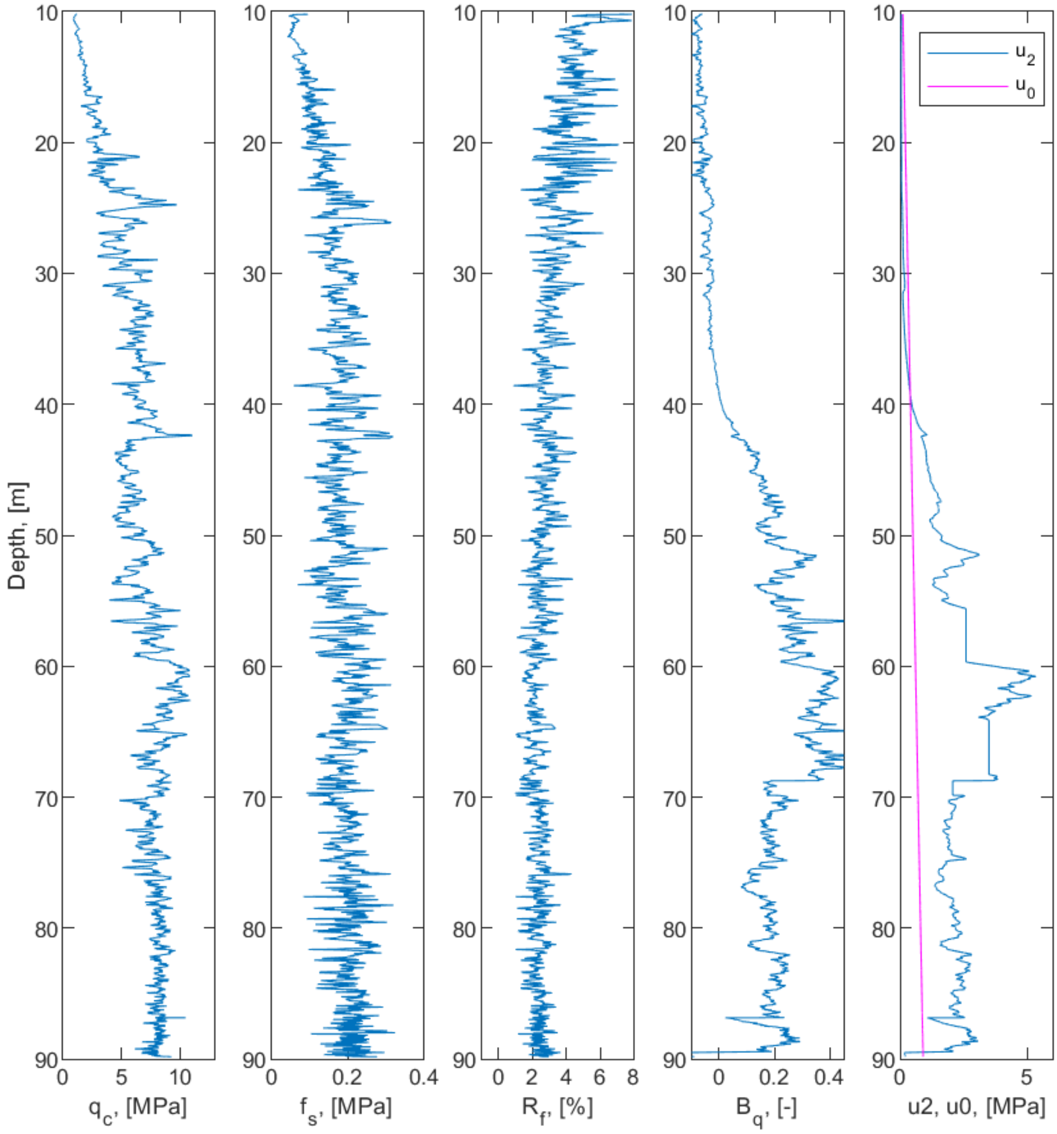

Figure C.2.2: CPT data for Project 2 after removal of peak and trough values in the CPT data.

Smoothing of the CPT data

In Figure C.2.3 the CPT data from Project 2 can be seen after the smoothening.

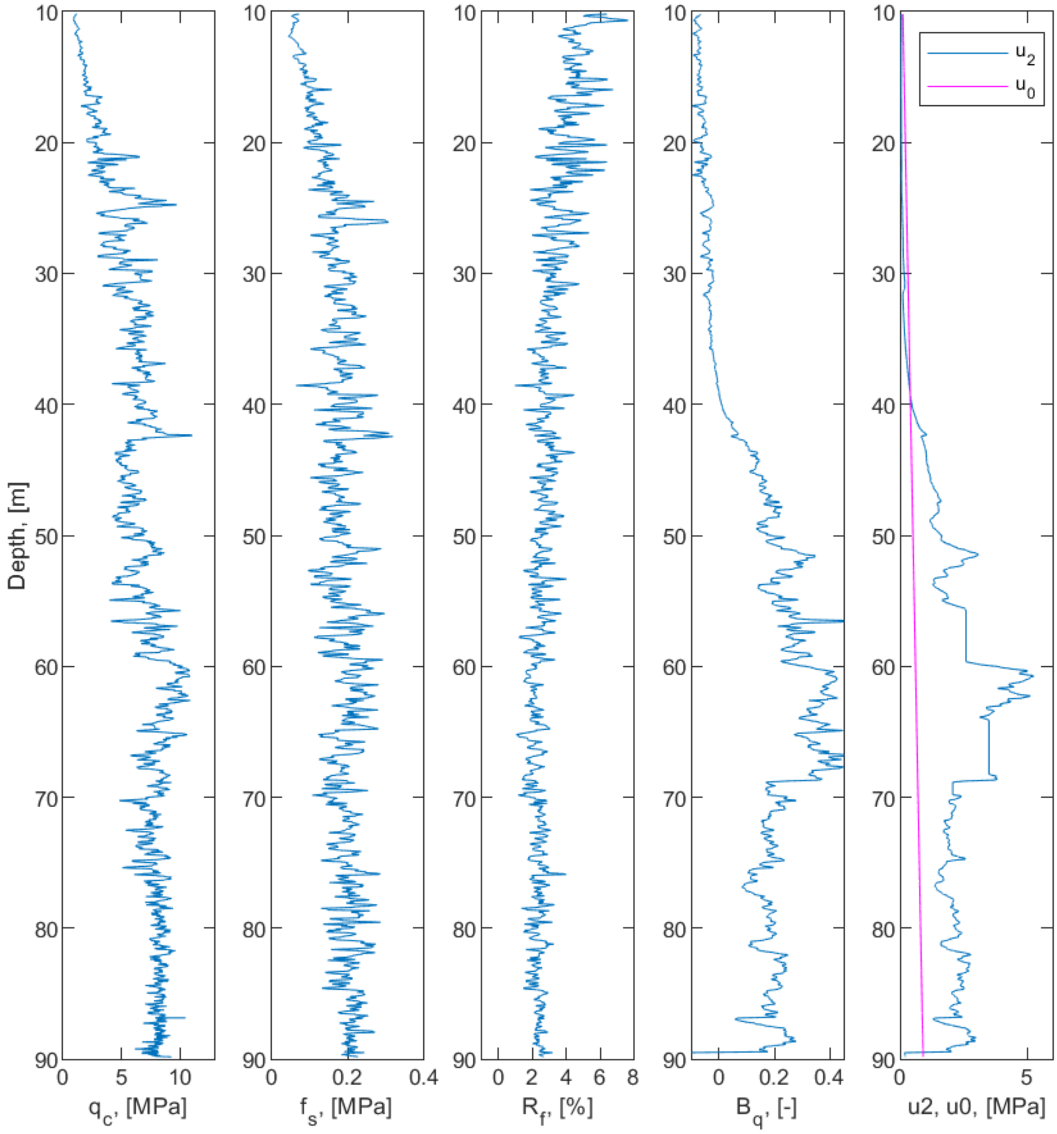

Figure C.2.3: CPT data for Project 2, after smoothening.

Appendix C.3 Influence of the interval Δa

The Interval Δa has been introduced in section 4.1 and the height is here determined, so the cone factors are least influenced by the used number of measurements from the CPT data. The interval Δa, is varied between 2-30 cm, since it is determined that an interval close to 40 cm is unreasonable due to great variations in the triaxial shear strength from Project 2. By increasing Δa with 2 cm each time, it is seen that the estimated value of N_K also changed, which is seen in Figure C.3.1. The used triaxial test is again the one from Project 2, from the depth of 21.6 m, which is also shown in Figure 4.11. An example of how the cone factor is calculated when Δa is 16 cm, is shown in Appendix E.1.

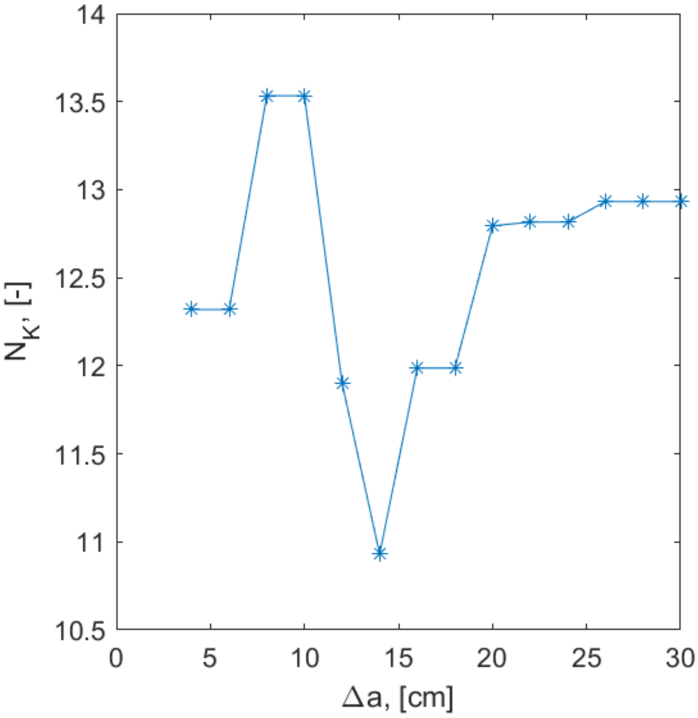

Figure C.3.1: Influence of the size of the interval Δa for the derived value of N_K *at the depth of 21.6 m.*

From Figure C.3.1 it is seen that the first estimated value of N_K is at Δa equal to 4 cm. There is no estimated value of N_K when Δa is equal to 2 cm, since the interval has been too small and therefore no measurements of the cone resistance has been close enough to the triaxial test, to determine a value of N_K.

It is seen that the values of N_K varies a lot when Δa is changing in the interval of 6 cm≤ Δa ≤18 cm. Hereafter it is seen that the value of N_K is much more stable when Δa is increased further. The purpose is to determine a value of Δa, so the value of the cone factor is not sensitive with regards to the number of included cone resistance measurements. When the interval is small, few cone resistance measurements are within the interval and averaged before used to calculate the cone factor. When Δa is increased a bit more, for example from 10 cm to 12 cm, the derived value of N_K changes considerably, and this means that the number of cone resistance measurements is not enough. By increasing Δa until the derived value of N_K does not change considerably anymore, a suitable value of Δa can be determined.

The same procedure is hereafter done for the rest of the triaxial tests in Project 2, where the interval Δa is varied to observe the variation in each of the estimated values of N_K. This is shown in Figure C.3.2, where all the estimated values of N_K is varying with Δa varying between 2-30 cm. Each line that is plotted in Figure

C.3.2 illustrates an estimated value of N_K from a specific triaxial test, and the measured cone resistance inside the changing interval Δa.

The same procedure is hereafter done for the remaining cone factors. The same triaxial tests are used, but instead Δa is used to include the respective CPT measurements in equation (1,4), (1,5) and (1,6), to estimate the values of N_{KT}, N_{ke} and $N_{\Delta u}$. This is shown in Figure C.3.3 to Figure C.3.5, for the different cone factors. The values of the cone factors or which cone factors belongs to which triaxial tests are not important, but instead the height of Δa is looked for, when the lines start to become horizontal. When the interval becomes great enough, the lines tend to become horizontal and thereby enough CPT measurements are included into the interval Δa. This means that the cone factors are not sensitive with regards to the included number of CPT measurements, and the derived value of the cone factor is therefore deemed more representable for the soil at that depth of the used triaxial test.

By observing Figure C.3.2 to Figure C.3.5, it is seen that most of the cone factors started to stabilize, when Δa reached the value 16 cm. This value is therefore determined to be reasonable and is used for determination of the cone factors in Table 4.2. The chosen values of Δa is therefore shown in Figure C.3.2 to Figure C.3.5 as the vertical dashed line, where it is seen that most of the cone factors become stable, and thereby are not heavily influenced of the variations of the measured CPT measurements.

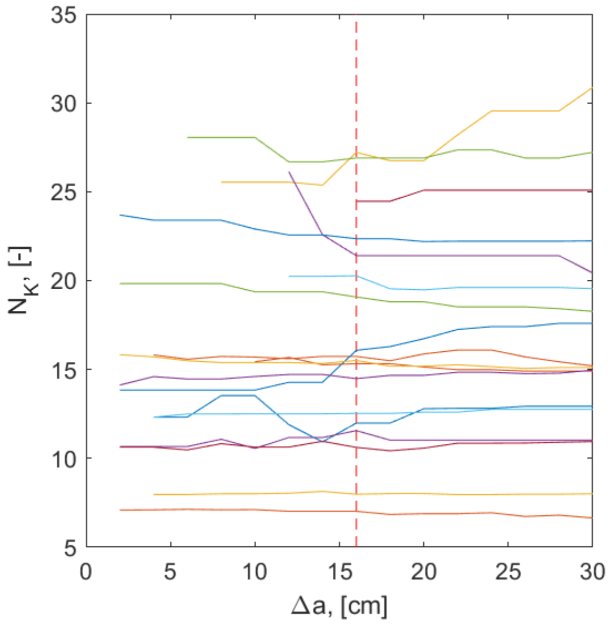

Figure C.3.2: Influence on the values of N_K by varying the size of Δa.

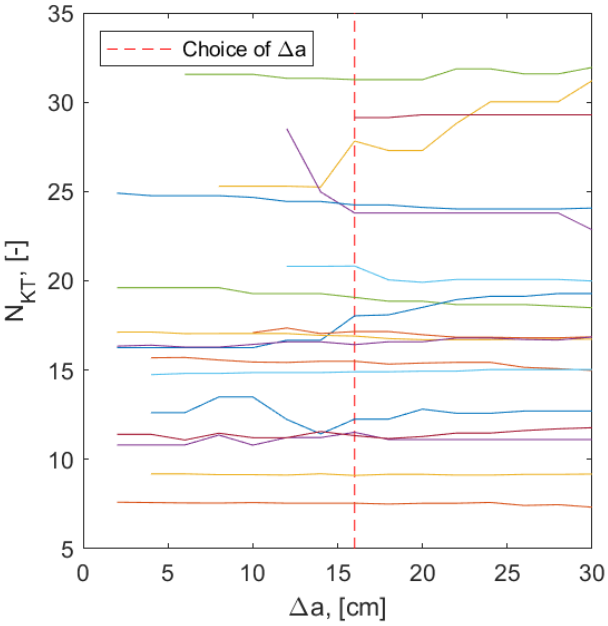

Figure C.3.3: Influence on the values of N_{KT} by varying the size of Δa.

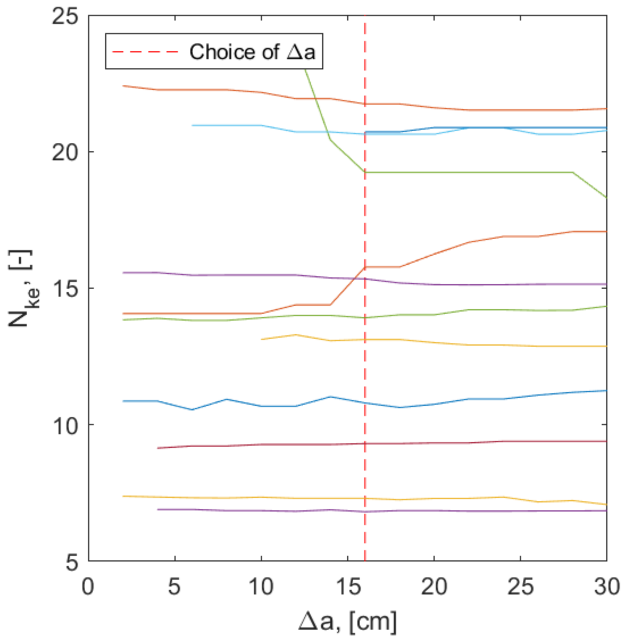

Figure C.3.4: Influence on the values of N_{ke} *by varying the size of* Δa*.*

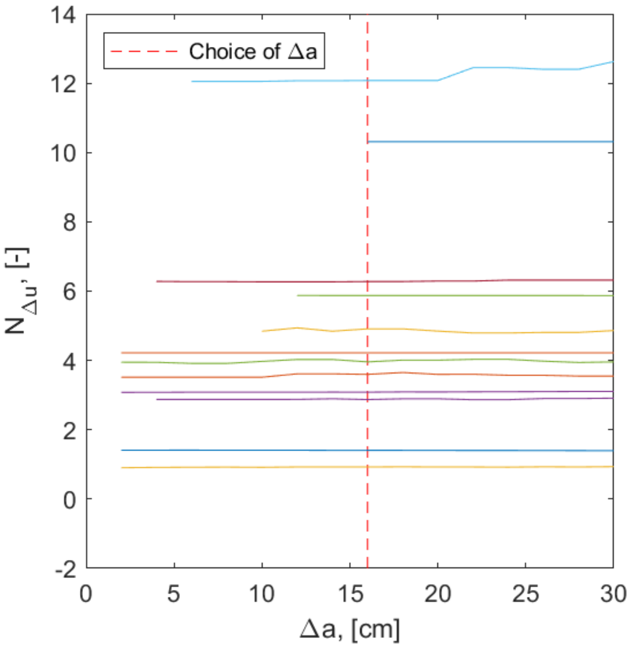

Figure C.3.5: Influence on the values of $N_{\Delta u}$ *by varying the size of* Δa*.*

Figure C.3.5 is different than the other three figures. It is seen that the estimated values of $N_{\Delta u}$ are almost stable no matter the value of Δa. From the CPT data, shown in Figure 4.10, it is seen that the pore pressure varies less locally, than the cone resistance. Since $N_{\Delta u}$ is only depending on the pore pressure, from the CPT measurements, this explains why the values of $N_{\Delta u}$ are far more stable compared to the other cone factors that are estimated from the cone resistance or the corrected cone resistance. The value of Δa being equal to 16 cm is still used for the pore pressure, for consistency.

Appendix C.4 Dependency between cone factors and soil parameters

In Figure C.4.1 to Figure C.4.6 the additional parameters are plotted against the cone factors to determine any dependencies.

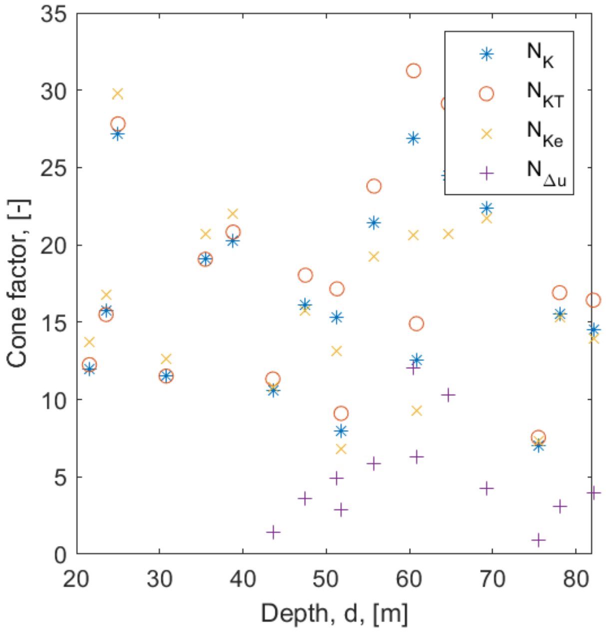

Figure C.4.1: Relation between cone factors and depth for Project 2.

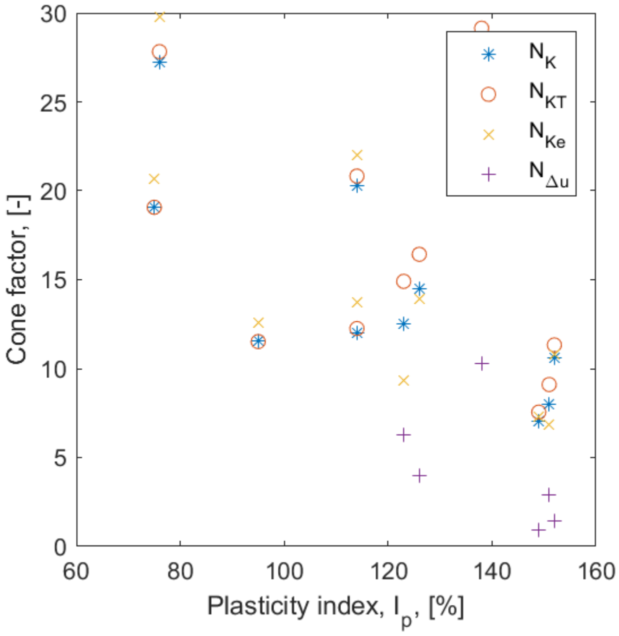

Figure C.4.2: Relation between cone factors and plasticity index for Project 2.

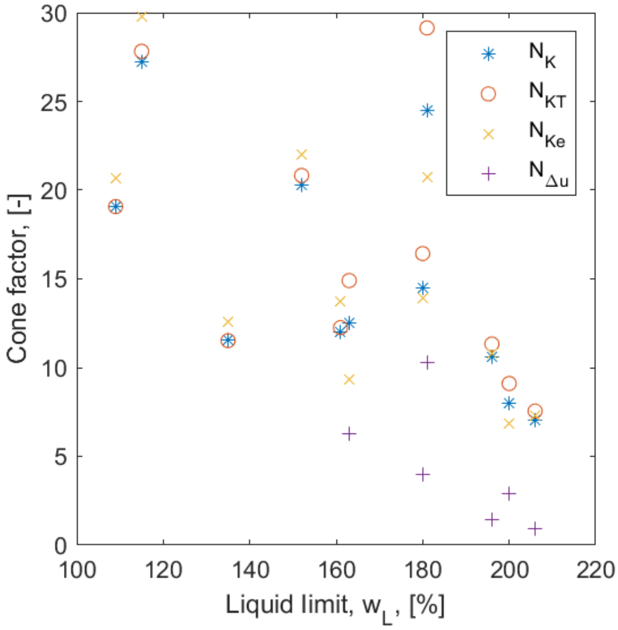

Figure C.4.3: Relation between cone factors and Liquid limit for Project 2.

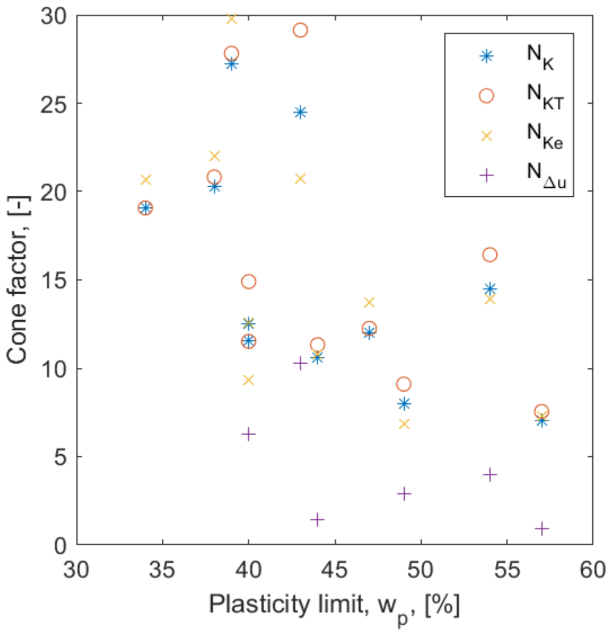

Figure C.4.4: Relation between cone factors and plasticity limit for Project 2.

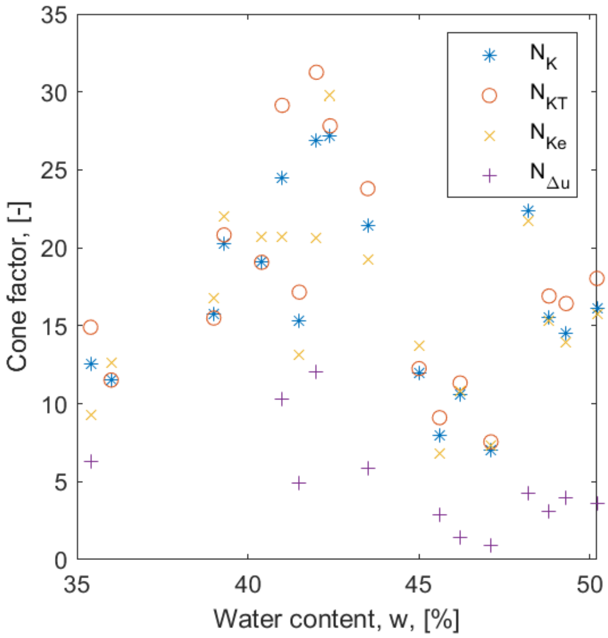

Figure C.4.5: Relation between cone factors and water content for Project 2.

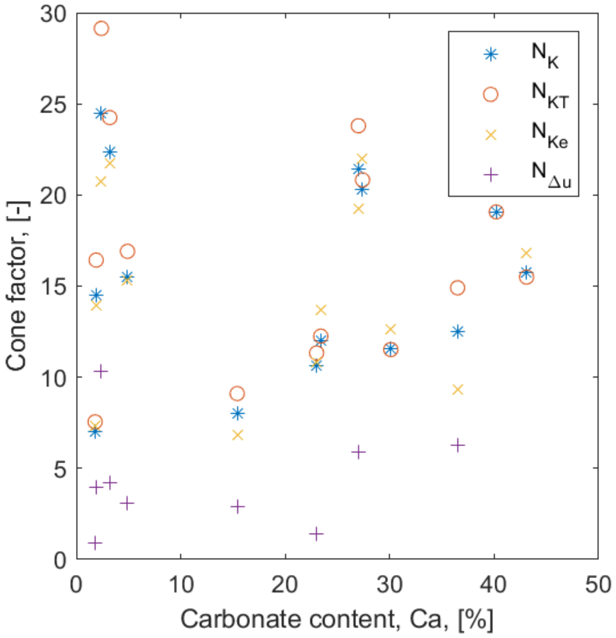

Figure C.4.6: Relation between cone factors and depth for Project 2.

Appendix D Characteristic undrained shear strength

This appendix shows the calculations behind chapter 5. Appendix D.1 shows the calculations of the model uncertainty, bias and representative values of N_{KT} and N_{ke}, while Appendix D.2 shows the calculations of the reduction factor for the physical uncertainties of the undrained shear strength. Lastly, the characteristic shear strength is estimated in Appendix D.3.

Appendix D.1 Calculation of the model uncertainties

When referring to the model uncertainty, it is the coefficient of variation, V_Δ, which is referred to. This is calculated within this section along with the bias, b, which tells about the mean values between the theoretical and experimental results (Sørensen, 2011, c) (DS/EN, a, 2007).

By assuming that the data is statistically independent, the bias can be determined from equation (D.1,1).

$$b = \frac{\sum_{i=1}^{N} y_i \cdot h(\boldsymbol{x}_i)}{\sum_{i=1}^{N} h(\boldsymbol{x}_i)^2} \tag{D.1,1}$$

Where

N	Number of experimental results	$[-]$
y_i	Experiment results from the triaxial tests	$[\mathrm{kPa}]$
$h(\boldsymbol{x}_i)$	Theoretical results calculated from equation (D.1,8) or (D.1,6)	$[\mathrm{kPa}]$

A realization of the lognormal distributed variable model uncertainty is determined from equation (D.1,2).

$$\Delta_i = ln\left(\frac{y_i}{b \cdot h(\boldsymbol{x}_i)}\right) \tag{D.1,2}$$

The estimated mean value and standard deviation is determined in equation (D.1,3) and (D.1,4) respectively.

$$\bar{\Delta} = \frac{1}{N}\sum_{i=1}^{N} \Delta_i \tag{D.1,3}$$

$$s_\Delta = \sqrt{\frac{1}{N-1}\sum_{i=1}^{N}(\Delta_i - \bar{\Delta})^2} \tag{D.1,4}$$

The corresponding coefficient of variation for the model uncertainty is determined in equation (D.1,5).

$$V_\Delta = \sqrt{exp(s_\Delta^2) - 1} \tag{D.1,5}$$

The investigated models are shown in equation (D.1,6), (D.1,7) and (D.1,8). The chosen cone factors for equation (D.1,6) and (D.1,7) are determined by a trial and error method, where the value of the cone factor has been variated until the bias became equal to one. By varying the value of the cone factor, only bias is influenced and not V_{Δ}. The value of the cone factor in equation (D.1,8) is from the dependency, presented in equation (4,1).

$$s_{u,KT} = \frac{q_t - \sigma_{v0}}{N_{KT}} = \frac{q_t - \sigma_{v0}}{17.1} \qquad \text{(D.1,6)}$$

$$s_{u,ke} = \frac{q_t - u_2}{N_{ke}} = \frac{q_t - u_2}{13.1} \qquad \text{(D.1,7)}$$

$$s_{u,\Delta u} = \frac{u_2 - u_0}{N_{\Delta u}} = \frac{u_2 - u_0}{24\,B_q - 1.2} \qquad \text{(D.1,8)}$$

Where

q_t	Corrected cone resistance	[kPa]
σ_{v0}	Vertical overburden stress	[kPa]
u_2	Pore pressure	[kPa]
u_0	Hydrostatic pressure	[kPa]
B_q	Pore pressure ratio	[−]

The calculations of the bias and coefficient of variation for the different models are shown in Table D.1.1 to Table D.1.3.

Table D.1.1: Calculation for estimating the model uncertainties of equation (D.1,6).

					$\mathrm{h}(\mathbf{x_i})$	$\mathrm{y_i}$				
	d	q_t	σ_{v0}	N_{KT}	$s_{\mathrm{u.KT}}$	s_{u}	$\mathrm{y_i} \cdot \mathrm{h}(\mathbf{x_i})$	$\mathrm{h}(\mathbf{x_i})^2$	Δ_i	$(\Delta_\mathrm{i} - \bar{\Delta}_\mathrm{i}\ )^2$
	[m]	[MPa]	[MPa]	[-]	[kPa]	[kPa]	[kPa^2]	[kPa^2]	[-]	[-]
Project 1	17.2	3.07	0.33	17.1	161	105	16860	25785	-0.42	0.169
	31.2	4.79	0.58	17.1	247	213	52519	60797	-0.15	0.018
	67.2	7.74	1.21	17.1	382	413	157585	145590	0.08	0.009
Project 2	21.6	3.41	0.41	17.1	176	245	43014	30824	0.33	0.120
	23.6	5.14	0.44	17.1	275	303	83190	75381	0.10	0.013
	25.0	5.95	0.47	17.1	321	197	63147	102749	-0.49	0.224
	30.8	4.70	0.57	17.1	242	359	86814	58477	0.40	0.167
	35.5	6.01	0.65	17.1	313	281	88063	98214	-0.11	0.009
	38.8	6.54	0.71	17.1	341	280	95484	116290	-0.20	0.034
	43.6	5.45	0.80	17.1	272	411	111937	74176	0.41	0.181
	47.5	6.13	0.86	17.1	308	292	89947	94886	-0.05	0.002
	51.3	9.15	0.93	17.1	481	479	230229	231021	0.00	0.000
	51.8	7.48	0.94	17.1	382	718	274452	146112	0.63	0.415
	55.8	9.25	1.01	17.1	482	346	166604	231856	-0.33	0.101
	60.5	11.66	1.10	17.1	618	338	208851	381804	-0.60	0.348
	60.9	11.80	1.10	17.1	626	718	449363	391692	0.14	0.023
	64.7	9.21	1.17	17.1	470	276	129809	221204	-0.53	0.270
	69.2	9.13	1.25	17.1	461	325	149776	212381	-0.35	0.113
	75.5	7.99	1.36	17.1	388	878	340440	150346	0.82	0.690
	78.0	8.37	1.41	17.1	407	412	167843	165963	0.01	0.001
	82.1	8.92	1.48	17.1	435	453	197128	189364	0.04	0.003
$N = 21$						SUM	3203056	3204912	-0.27	2.906

where

y_i	Experiment results from triaxial test	[kPa]
$h(\boldsymbol{x_i})$	Theoretical results from equation (D.1,6)	[kPa]

The bias and coefficient of variation for the model uncertainty calculated from Table D.1.1 is shown here:

$$b = \frac{3203056}{3204912} = 1.00$$

$$\mathrm{s}_\Delta = \sqrt{\frac{1}{21-1} 2.906} = 0.38$$

$$\mathrm{V}_\Delta = \sqrt{\exp(0{,}38^2) - 1} = 0.40$$

Table D.1.2: Calculation for estimating the model uncertainties of equation (D.1,7).

	d	q_t	u_2	N_{ke}	$\mathrm{h}(\mathbf{x_i})$ $s_{\mathrm{u.KT}}$	$\mathrm{y_i}$ s_{u}	$\mathrm{y_i} \cdot \mathrm{h}(\mathbf{x_i})$	$\mathrm{h}(\mathbf{x_i})^2$	Δ_i	$(\Delta_\mathrm{i} - \overline{\Delta_\mathrm{i}})^2$
	[m]	[-]	[MPa]	[-]	[kPa]	[kPa]	[kPa^2]	[kPa^2]	[-]	[-]
Project 1	17.2	0.19	0.70	13.1	181	105	19014	32791	-0.54	0.2274
	31.2	0.41	2.04	13.1	210	213	44782	44203	0.02	0.0066
	67.2	0.21	2.05	13.1	434	413	179340	188561	-0.05	0.0003
Project 2	43.6	0.13	1.01	13.1	339	411	139250	114790	0.20	0.0682
	47.5	0.20	1.53	13.1	352	292	102664	123616	-0.18	0.0138
	51.3	0.29	2.87	13.1	480	479	229811	230182	0.00	0.0044
	51.8	0.32	2.58	13.1	374	718	268390	139729	0.66	0.5196
	55.8	0.25	2.59	13.1	508	346	175782	258105	-0.38	0.0999
	60.5	0.39	4.69	13.1	532	338	179933	283392	-0.45	0.1491
	60.9	0.42	5.12	13.1	510	718	366528	260595	0.35	0.1674
	64.7	0.35	3.49	13.1	437	276	120486	190570	-0.45	0.1524
	69.2	0.17	2.06	13.1	539	325	175288	290897	-0.50	0.1922
	75.5	0.12	1.57	13.1	490	878	430433	240338	0.59	0.4236
	78.0	0.18	2.05	13.1	482	412	198769	232756	-0.15	0.0081
	82.1	0.24	2.61	13.1	481	453	217965	231513	-0.06	0.0001
$N = 15$						SUM	2848435	2862038	-0.95	2.0332

where

y_i	Experiment results from triaxial test	[kPa]
$h(\boldsymbol{x_i})$	Theoretical results from equation (D.1,7)	[kPa]

The bias and coefficient of variation for the model uncertainty calculated from Table D.1.2 is shown here:

$$b = \frac{2848435}{2862038} = 1.00$$

$$s_\Delta = \sqrt{\frac{1}{15-1} 2.0332} = 0.38$$

$$V_\Delta = \sqrt{exp(0.38^2) - 1} = 0.40$$

Table D.1.3: Calculation for estimating the model uncertainties of equation (D.1,8).

	d [m]	B_q [-]	u_2 [MPa]	u_0 [MPa]	$N_{\Delta u}$ [-]	$\mathrm{h}(\mathbf{x_i})$ $s_{\mathrm{u.KT}}$ [kPa]	$\mathrm{y_i}$ s_{u} [kPa]	$\mathrm{y_i} \cdot \mathrm{h}(\mathbf{x_i})$ [kPa^2]	$\mathrm{h}(\mathbf{x_i})^2$ [kPa^2]	Δ_i [-]	$(\Delta_\mathrm{i} - \overline{\Delta}_\mathrm{i})^2$ [-]
Project 1	17.2	0.19	0.70	0.17	3.45	154	105	16168,09	23710	-0.52	0.207
	31.2	0.41	2.04	0.31	8.81	196	213	41757,07	38433	-0.06	0.000
	67.2	0.21	2.05	0.67	3.92	352	413	145233,3	123661	0.02	0.008
Project 2	43.6	0.13	1.01	0.44	1.82	318	411	130595	100965	0.12	0.034
	47.5	0.20	1.53	0.47	3.68	285	292	83331,47	81443	-0.12	0.002
	51.3	0.29	2.87	0.51	5.74	410	479	196243,4	167849	0.02	0.007
	51.8	0.32	2.58	0.52	6.46	319	718	229159,4	101865	0.67	0.546
	55.8	0.25	2.59	0.56	4.89	415	346	143669,2	172415	-0.32	0.065
	60.5	0.39	4.69	0.61	8.18	499	338	168581,2	248762	-0.53	0.212
	60.9	0.42	5.12	0.61	9.03	499	718	358281,9	249001	0.22	0.085
	64.7	0.35	3.49	0.65	7.39	385	276	106248,3	148192	-0.47	0.164
	69.2	0.17	2.06	0.69	3.02	455	325	147800,5	206816	-0.48	0.166
	75.5	0.12	1.57	0.75	1.76	461	878	405005,2	212781	0.50	0.327
	78.0	0.18	2.05	0.78	3.22	395	412	162665,1	155881	-0.10	0.001
	82.1	0.24	2.61	0.82	4.64	387	453	175119	149441	0.02	0.008
$N = 15$							SUM	2509858	2181216	-1.03	1.832

where

y_i	Experiment results from triaxial test	[kPa]
$h(\boldsymbol{x_i})$	Theoretical results from equation (D.1,8)	[kPa]

The bias and coefficient of variation for the model uncertainty calculated from Table D.1.2 is shown here:

$$b = \frac{2509858}{2181216} = 1.15$$

$$s_\Delta = \sqrt{\frac{1}{15-1} 1.832} = 0.36$$

$$V_\Delta = \sqrt{exp(0.36^2) - 1} = 0.37$$

The calculated bias, coefficient of variation and cone factors are summarized in Table 5.1 in the main report. Here the results are also compared and commented.

Appendix D.2 Calculation of the reduction factor for the physical uncertainty and determination of the correlation length

The correlation length, D, is determined from a normalized autocovariance functions. (JCSS PMC, 2002) presents several one-dimensional admissible types of normalized autocovariance functions, and for this report, an exponential type is chosen, which is shown in equation (D.2.1).

$$\rho_{f_p}(\tau) = \exp\left(-\frac{|\tau|}{D}\right) \tag{D.2.1}$$

$\rho_{f_p}(\tau)$	Normalized autocovariance function	$[-]$
τ	Normalized separation distance	$[-]$
D	Correlation length	$[\mathrm{m}]$

Hereby the correlation radius (also called the scale of fluctuation) can be determined, which is shown in equation (D.2.2).

$$\delta = 2\int_{0}^{\infty} \rho_{f_p}(\tau)\, d\tau \tag{D.2.2}$$

By looking up in tables, the correlation radius can be determined from prior studies, for different soil properties and thereby the correlation length, can be calculated. Table D.2.1, which is taken from (JCSS PMC, 2002), shows prior studies on derived correlation radii. Since it is the length of the pile that is varied, it is the vertical correlation radius, δ_v, which is relevant. In Table D.2.1, a value of δ_v=2 m is chosen for the undrained shear strength, and the correlation length can hereby be calculated in equation (D.2.3).

$$\delta = 2\int_{0}^{\infty} \exp\left(-\frac{|\tau|}{D}\right) d\tau = 2D \quad \Rightarrow \quad 2\,m = 2D \quad \Rightarrow \quad D = 1\text{ m} \tag{D.2.3}$$

The determined correlation length seems large compared to the data gathered from Project 1 and 2. By observing the triaxial test in Table 3.1, it is seen that the triaxial shear strength determined at the depths of 51.3 m and 51.8 m varies with 240 kPa. Further the triaxial shear strength at the depths of 60.5 m and 60.9 m varies with 380 kPa. That are some noticeable variations in the shear strength within an interval of 0.4-0.5 m and it therefore seems more reasonable to reduce the correlation length from 1 m to 0.5 m to account for the mentioned local variations. Hereby the shear strength is assumed to be the same within intervals of 0.5 m instead of 1 m.

Table D.2.1: Prior determined correlation radii presented by (JCSS PMC, 2002)-edited. The chosen value for δ_v is marked with red.

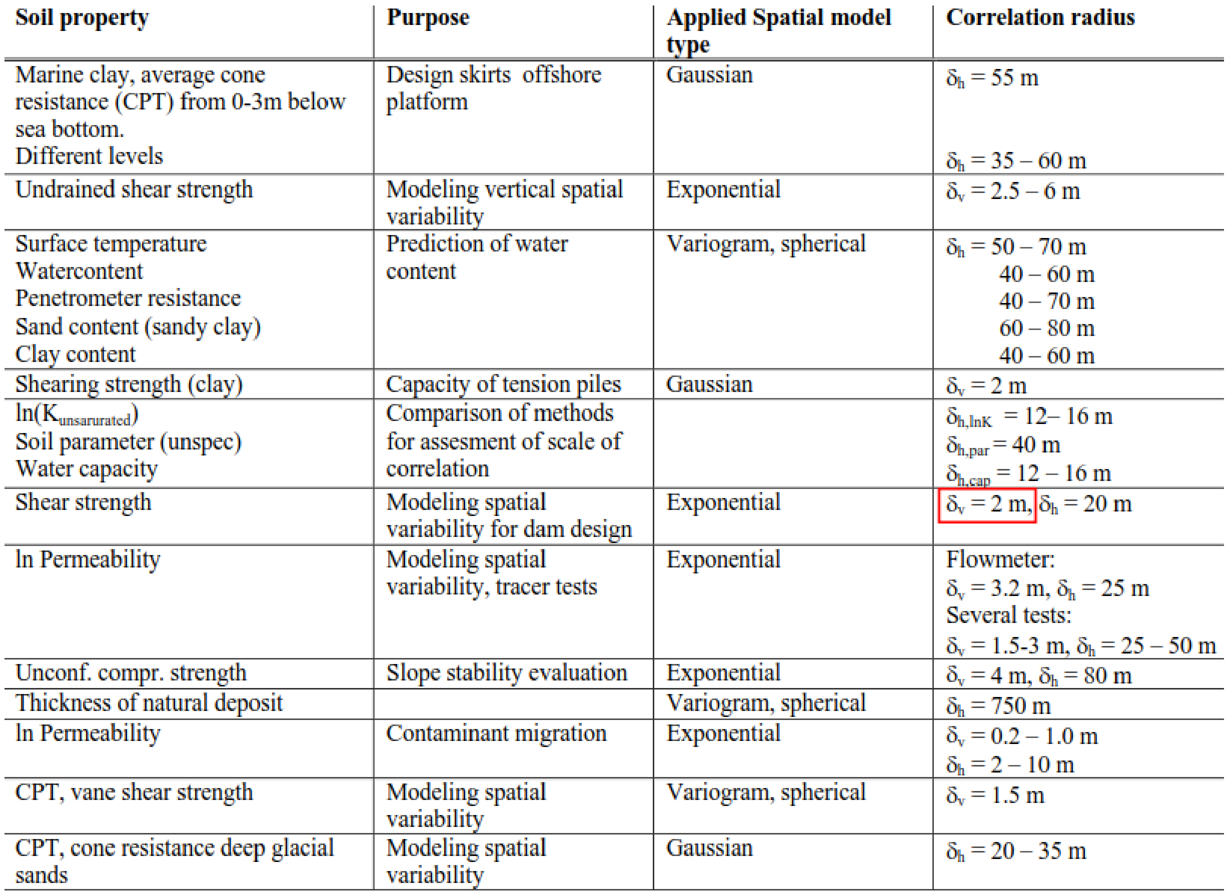

Soil property	**Purpose**	**Applied Spatial model type**	**Correlation radius**
Marine clay, average cone resistance (CPT) from 0-3m below sea bottom. Different levels	Design skirts offshore platform	Gaussian	$\delta_h = 55$ m $\delta_h = 35 - 60$ m
Undrained shear strength	Modeling vertical spatial variability	Exponential	$\delta_v = 2.5 - 6$ m
Surface temperature Watercontent Penetrometer resistance Sand content (sandy clay) Clay content	Prediction of water content	Variogram, spherical	$\delta_h = 50 - 70$ m 40 – 60 m 40 – 70 m 60 – 80 m 40 – 60 m
Shearing strength (clay)	Capacity of tension piles	Gaussian	$\delta_v = 2$ m
ln($K_{unsarurated}$) Soil parameter (unspec) Water capacity	Comparison of methods for assesment of scale of correlation		$\delta_{h,lnK} = 12 - 16$ m $\delta_{h,par} = 40$ m $\delta_{h,cap} = 12 - 16$ m
Shear strength	Modeling spatial variability for dam design	Exponential	$\delta_v = 2$ m, $\delta_h = 20$ m
ln Permeability	Modeling spatial variability, tracer tests	Exponential	Flowmeter: $\delta_v = 3.2$ m, $\delta_h = 25$ m Several tests: $\delta_v = 1.5$-3 m, $\delta_h = 25 - 50$ m
Unconf. compr. strength	Slope stability evaluation	Exponential	$\delta_v = 4$ m, $\delta_h = 80$ m
Thickness of natural deposit		Variogram, spherical	$\delta_h = 750$ m
ln Permeability	Contaminant migration	Exponential	$\delta_v = 0.2 - 1.0$ m $\delta_h = 2 - 10$ m
CPT, vane shear strength	Modeling spatial variability	Variogram, spherical	$\delta_v = 1.5$ m
CPT, cone resistance deep glacial sands	Modeling spatial variability	Gaussian	$\delta_h = 20 - 35$ m

When the correlation length and the pile length is known, the normalized field correlation parameter, b_c, can be calculated in equation (D.2.4). The normalized field correlation parameter is expressing the relation between the size of the failure surface of the geotechnical structure and the correlation length. Note that it is assumed that the length of the pile is equal to the vertical length of the failure surface.

$$b_c = \frac{L}{D} \tag{D.2.4}$$

Where

L	Length of the pile	[kPa]
D	Correlation length	[m]

The variance reduction factor, Γ^2, can hereafter be determined from the normalized field correlation parameter, which is shown in equation (D.2.5). By squaring the variance reduction factor, the reduction factor for the coefficient of variation, V_h, is obtained.

$$\Gamma^2(b_c) = \frac{2}{b_c} \int_0^{b_c} \left(1 - \frac{\tau}{b_c}\right) \rho_{f_p}(\tau)\, d\tau \tag{D.2.5}$$

Where

Γ^2	Variance reduction factor	$[-]$
b_c	Normalized field correlation parameter	$[-]$
τ	Normalized separation distance	$[-]$
ρ_{f_p}	Normalized auto covariance function	$[-]$

For perspectivation it is interesting to observe the correlation radius in the horizontal direction in Table D.2.1. The horizontal correlation radius is in the magnitude of 20 m, which is a tenfold compared to the vertical correlation radius. This results in a much greater correlation length, which again affects the variance reduction factor. The physical uncertainty is therefore reduced less in the horizontal direction, which can be explained by, how the soil has been deposited. In the horizontal direction the variation can be expected to be much lower, than in the vertical direction, and this is also shown in the magnitudes of the correlation radii.

Appendix D.3 Estimation of the characteristic undrained shear strength

The characteristic shear strength is estimated from equation (D.3.1). This includes all the above determined uncertainties (Sørensen, 2011, c) (DS/EN, a, 2007).

$$s_{u.c}(d,L) = b\left(\frac{q_t(d)-\sigma_{v0}(d)}{N_{KT}}\right) exp(-k_N\ \alpha_r(L)\ Q_r(L) - k_n\ \alpha_\delta(L)\ Q_\delta(L) - 0.5\ Q(L)^2) \tag{D.3.1}$$

The equations for calculating the values of Q_i and $\mathrm{\alpha_i}$ are shown in equation (D.3.2) to (D.3.7)

$$Q_r = \sqrt{ln(V_{h.red}^2 + 1)} \tag{D.3.2}$$

$$Q_\delta = \sqrt{ln(V_\Delta^2 + 1)} \tag{D.3.3}$$

$$Q = \sqrt{ln(V^2 + 1)} \tag{D.3.4}$$

$$V = \sqrt{V_\Delta^2 + V_{h.red}^2} \tag{D.3.5}$$

$$\alpha_r = \frac{Q_r}{Q} \tag{D.3.6}$$

$$\alpha_\delta = \frac{Q_\delta}{Q} \tag{D.3.7}$$

Where

$s_{u.c}$	Characteristic undrained shear strength	$[\text{kPa}]$
b	Bias	$[-]$
q_t	Corrected cone resistance	$[\text{kPa}]$
σ_{v0}	Vertical overburden stress	$[\text{kPa}]$
N_{KT}	Empirical cone factor	$[-]$
d	Depth into the Søvind Marl	$[\text{m}]$
L	Length of the pile	$[\text{m}]$
k_N	The characteristic quantile factor for N number of measurements of the corrected cone resistance	$[-]$
k_n	The characteristic quantile factor for n used data for determining the model uncertainty	$[-]$
α_r	Weighting factor for Q_r	$[-]$
α_δ	Weighting factor for Q_δ	$[-]$
V_Δ	Coefficient of variation of the used model	$[-]$
$V_{h.red}$	The reduced coefficient of variation of the physical uncertainty of the undrained shear strength. See equation (5,3)	$[-]$

The statistical uncertainty is included through the characteristic quantile factors, which are determined for an unknown coefficient of variation with a student-t test. This is shown in equation (D.3.8), where a 5 % quantile is used, since it is recommended according to (DS/EN, a, 2007).

$$k_n = t_{v,p}\sqrt{1+\frac{1}{n}} \tag{D.3.8}$$

where

v	Degrees of freedom $v = n - 1$	$[-]$
p	Quantile	$[\%]$
n	Number of measurements	$[-]$

As it is shown in Figure 5.9, the value of the numerator, $(q_t - \sigma_{v0})$, in equation (1,4) is increasing with depth. In order to account for the increasing strength with depth, a linear regression is conducted according to (Brozetti, et al., 1991), to determine a mean value through the depth, as shown in equation (D.3.9).

$$\left(q_t(L) - \sigma_{v0}(L)\right) \quad \Rightarrow \quad a + b' \cdot d \tag{D.3.9}$$

where

a	Regressionsparameter	$[\text{kPa}]$
b'	Regressionsparameter	$\left[\frac{10^3\text{kg}}{\text{m}^2\text{s}^2}\right]$
d	Depth into the Søvind Marl	$[\text{m}]$

By combining equation (D.3.1) and (D.3.9), the characteristic undraind shear strength is instead estimated with equation (D.3.10), which takes into account that the characteristic shear strength should increase with depth.

$$s_{u.c}(L) = b\left(\frac{(a+b'd)}{N_{KT}}\right) exp(-k_N\ \alpha_r(L)\ Q_r(L) - k_n\ \alpha_\delta(L)\ Q_\delta(L) - 0.5\ Q(L)^2) \tag{D.3.10}$$

The regression parameters are determined from equation (D.3.11) and (D.3.12)

$$b' = \frac{n\sum(x_i\ y_i) - (\sum x_i)\ (\sum y_i)}{n\sum(x^2) - (\sum x_i)^2} \tag{D.3.11}$$

$$a = \frac{1}{n}\ (\sum y_i - b'\sum x_i) \tag{D.3.12}$$

where

x_i	The depth measurement belonging to y_i	$[\text{m}]$
y_i	The value of $(q_t - \sigma_{v0})_i$	$[\text{kPa}]$
n	Number of measurements of x_i	$[-]$

From Project 2, there are 3722 measurement of the depth with a belonging value of corrected cone resistance and belonging vertical overburden stress. Table D.3.1 shows the seven first rows of the table used for calculating the regression parameters along with the sum of each column for the 3722 measurements.

Table D.3.1: Seven first measurements of depth and numerator of "$q_t - \sigma_{v0}$" used to calculate the regression parameters along with the sum of each row for the 3722 measurements.

d_i	$(q_t - \sigma_{v0})_i$				
x_i	y_i	x_iy_i	x_i^2	y_i^2	
[m]	**[kPa]**	**[kPa · m]**	**[m²]**	**[kPa²]**	
10.21	929.79	9489.71	104.17	864508	
10.22	908.45	9281.9	104.39	825279.9	
10.23	890.95	9113.73	104.64	793796.9	
10.24	889.42	9107.87	104.86	791072.8	
10.25	892.25	9146.65	105.09	796113.7	
10.26	890.55	9139.03	105.31	793084.8	
10.27	891.12	9154.61	105.54	794086.9	
…	…	…	…	…	
196451	21113135	1.3E+09	13036289	1.40035E+11	Sum

The regression parameters are calculated from equation (D.3.11), (D.3.12) and the 3722 measurements. The values are:

$$a = 2011\ \text{kPa},\ b' = 69\,\frac{ton}{\text{m}^2\text{s}^2}$$

It should be noted that if a different value of N_{KT} is used compared to 17.1, which has been shown in Table 5.1, the belonging bias would accordingly change for the model. The change in N_{KT} is thereby compensated by the bias and the value of characteristic shear strength is therefore not affected by the chosen value of the cone factors.

Appendix E Example of calculations

This appendix presents some of the calculations in detail from chapter 4 and 5.

Appendix E.1 Calculation of the cone factors

The first value of all the cone factors are here calculated for Table 4.2. The triaxial test is conducted in the depth of 17 m for Project 1, and the CPT measurement, 8 cm above and under this dept, are determined. The 8 cm above and under the depth of the triaxial test, corresponds to the interval Δa, which is 16 cm in height. The CPT data within Δa at the depth of 17 m is shown in the Table E.1.1. Further the belonging hydrostatic pressure, vertical overburden stress and the determined shear strength is also shown.

Table E.1.1: CPT measurements within Δa at the depth of 17 m, along with the belonging hydrostatic pressure, vertical overburden stress and the determined shear strength.

Nr.	q_c [kPa]	q_t [kPa]	u_2 [kPa]	u_0 [kPa]	σ_{v0} [kPa]	s_u [kPa]
1	2590	2890	729	170	327	105
2	2480	2825	714			
3	2490	2844	704			
4	2580	2906	695			
5	2770	3003	689			
6	2850	3106	684			
7	2990	3251	685			
8	3130	3370	695			
9	3370	3464	713			
Average	2806	3073	701			

It is seen that 9 measurements are inside the interval Δa. By taking the average of the cone resistance, corrected cone resistance and the pore pressure, the values for inserting into equation (1,2), (1,4), (1,5) and (1,6) are determined. The calculations of the one factors are respectatively shown in the following four equations:

$$s_u = \frac{q_c - \sigma_{v0}}{N_K} \quad \Rightarrow \quad N_K = \frac{q_c - \sigma_{v0}}{s_u} = \frac{2806\text{ kPa} - 327\text{ kPa}}{105\text{ kPa}} = 23.6$$

$$s_u = \frac{q_t - \sigma_{v0}}{N_{KT}} \quad \Rightarrow \quad N_{KT} = \frac{q_t - \sigma_{v0}}{s_u} = \frac{3073\text{ kPa} - 327\text{ kPa}}{105\text{ kPa}} = 26.2$$

$$s_u = \frac{q_e}{N_{ke}} = \frac{q_t - u_2}{N_{ke}} \quad \Rightarrow \quad N_{ke} = \frac{q_t - u_2}{s_u} = \frac{3073\text{ kPa} - 701\text{ kPa}}{105\text{ kPa}} = 22.6$$

$$s_u = \frac{\Delta u}{N_{\Delta u}} = \frac{u_2 - u_0}{N_{\Delta u}} \quad \Rightarrow \quad N_{\Delta u} = \frac{u_2 - u_0}{s_u} = \frac{701\text{ kPa} - 170\text{ kPa}}{105\text{ kPa}} = 5.1$$

This process is hereby repeated with new values of the measured CPT data, to calculate the rest of the cone factors for Table 4.2.

Appendix E.2 Calculation of undrained shear strength with different values of N_K

The following calculations shows, how to calculate the undrained shear strength when a representative cone factor has been chosen. Further it is seen that the determination of a correct cone factor is important, since it can have a great influence on the estimated undrained shear strength. The example is carried out with equation (1,2) and the CPT data from Table E.1.1, which is taken from the depth on 17 m in Project 1.

From Table 4.2 it is seen that the interval of N_K is determined to be in the interval of 7-27.2. The representable value of N_K is within this interval, so three values are chosen to investigate, what the estimated undrained shear strength will become. The values for N_K are randomly chosen to be 7, 17 and 27 and the undrained shear strength is hereby calculated in the following three equations. Note that the used values of the cone resistance and vertical overburden stress, is taken from Table E.1.1.

$$s_u = \frac{q_c - \sigma_{v0}}{N_K} = \frac{2806 - 327}{7} = 323\ \mathrm{kPa}$$

$$s_u = \frac{q_c - \sigma_{v0}}{N_K} = \frac{2806 - 327}{17} = 133\ \mathrm{kPa}$$

$$s_u = \frac{q_c - \sigma_{v0}}{N_K} = \frac{2806 - 327}{27} = 84\ \mathrm{kPa}$$

From the three equations it is seen that the derived undrained shear strength is relying a lot on the chosen value of N_K. It is therefore not an easy assignment to determine a representative value of the cone factors, since the derived undrained shear strength can deviate a lot depending on the chosen value.

Appendix E.3 Calculation of the reduction factor Γ

In Appendix D.2 it has been determined that the correlation length, D, is 0.5 m. By also knowing the length of the pile, the reduction factor can be estimated for the coefficient of variation for the undrained shear strength. This calculation example is assuming that the pile length, L, is equal to 20 m. From equation (D.2.4), the normalized field correlation parameter, b_c, can be determined:

$$b_c = \frac{L}{D} = \frac{20\text{ m}}{0.5\text{ m}} = 40$$

The variance reduction factor, Γ^2 is calculated by combining equation (D.2.1) and (D.2.5)

$$\Gamma^2(b_c) = \frac{2}{b_c}\int_0^{b_c}\left(1-\frac{\tau}{b_c}\right)\rho_{f_p}(\tau)\,d\tau$$

$$\Downarrow$$

$$\Gamma^2(b_c) = \frac{2}{b_c}\int_0^{b_c}\left(1-\frac{\tau}{b_c}\right)\exp\left(-\frac{|\tau|}{D}\right)d\tau \quad = \quad \frac{2}{40}\int_0^{40}\left(1-\frac{\tau}{40}\right)\exp\left(-\frac{|\tau|}{0.5}\right)d\tau = 0.025$$

The reduction factor Γ is determined as the square root of the variance reduction factor:

$$\Gamma = \sqrt{\Gamma^2} = \sqrt{0.025} = 0.157$$

It is seen that the reduction factor for the coefficient of variation, V_h, is significant. This is caused by the great value of the correlation parameter, b_c. If the pile had been shorter, the reduction would be less, since the correlation parameter, b_c, would be decreased.

Appendix E.4 Calculation of the characteristic undrained shear strength

An example of estimating the characteristic shear strength is here shown for a 20 m long pile. The data which is known on beforehand is shown in Table E.4.1. The calculation of the reduction factor, Γ, for a 20 m long pile is shown in Appendix E.3 and all the following equations are taken from Appendix D.3.

Table E.4.1: Prior known values to estimate the characteristic undrained shear strength for a 20 m pile

V_Δ	0.40	[-]
V_h	0.20	[-]
Γ	0.157	[-]
Quantile	5.00	[%]
b	1.00	[-]
N_{KT}	17.1	[-]
d	0.50	[m]
L	20.0	[m]
a	2011	[kPa]
b'	69.0	$\left[\frac{ton}{\text{m}^2\text{s}^2}\right]$

First the reduced coefficient of variation for the physical uncertainty is determined:

$$V_{h,red} = V_h\,\Gamma = 0.2 \cdot 0.157 = 0.031$$

The calculation of the Q_i and α_i values are hereafter calculated:

$$Q_r = \sqrt{ln(V_{h.red}^2 + 1)} = \sqrt{ln(0.031^2 + 1)} = 0.031$$

$$Q_\delta = \sqrt{ln(V_\Delta^2 + 1)} = \sqrt{ln(0.4^2 + 1)} = 0.385$$

$$V = \sqrt{V_\Delta^2 + V_{h.red}^2} = \sqrt{0.4^2 + 0.031^2} = 0.401$$

$$Q = \sqrt{ln(V^2 + 1)} = \sqrt{ln(0.401^2 + 1)} = 0.386$$

$$\alpha_r = \frac{Q_r}{Q} = \frac{0.031}{0.386} = 0.081$$

$$\alpha_\delta = \frac{Q_\delta}{Q} = \frac{0.385}{0.386} = 0.997$$

Hereafter the characteristic quantile factors are determined through a student-t test by using a 5 % quantile. First quantile factor is using the number of data from the CPT measurements and second equation is using the number of triaxial test used to derive the model uncertainty:

$$\mathrm{k}_N = \mathrm{t}_{\mathrm{v,p}} \sqrt{1 + \frac{1}{\mathrm{N}}} = \mathrm{t}_{3722-1,\ 0.95} \sqrt{1 + \frac{1}{3722}} = 1.65$$

$$\mathrm{k}_n = \mathrm{t}_{\mathrm{v,p}} \sqrt{1 + \frac{1}{\mathrm{n}}} = \mathrm{t}_{21-1,\ 0.95} \sqrt{1 + \frac{1}{21}} = 1.77$$

Hereby all the factors are known to estimate the characteristic undrained shear strength. The characteristic value is here calculated for the depth of 0.5 m into the Søvind Marl.

$$s_{u.c}(d, L) = b\left(\frac{(a + b'd)}{N_{KT}}\right) exp(-k_N\,\alpha_r(L)\,Q_r(L) - k_n\,\alpha_\delta(L)\,Q_\delta(L) - 0.5\,Q(L)^2)$$

⇓

$$s_{u.c}(d, L) = 1.00\left(\frac{\left(2011\ \mathrm{kPa} + 69\ \frac{ton}{\mathrm{m^2 s^2}} \cdot 0.5\ \mathrm{m}\right)}{17.1}\right) exp(-1.65 \cdot 0.081 \cdot 0.031 - 1.77 \cdot 0.997 \cdot 0.385$$
$$- 0.5 \cdot 0.386^2) = 120\ \mathrm{kPa} \cdot 0.47 = 56\ \mathrm{kPa}$$